Adriano Gonçalves Schommer

MODELING AND SIMULATION OF A TOURING RACECAR SUPPORTED BY EXPERIMENTAL DATA

Dissertação submetida ao Programa de Pós-Graduação em Engenharia Mecânica da Universidade Federal de Santa Catarina para a obtenção do Grau de Mestre em Engenharia Mecânica.
Orientador: Prof. Jonny Carlos da Silva, Dr. Eng.
Coorientador: Prof. Rodrigo de Souza Vieira, Dr. Eng.

Florianópolis
2018

Ficha de identificação da obra elaborada pelo autor,
através do Programa de Geração Automática da Biblioteca Universitária da UFSC.

Schommer, Adriano
MODELING AND SIMULATION OF TOURING RACECAR SUPPORTED BY EXPERIMENTAL DATA / Adriano Schommer ; orientador, Jonny Carlos da Silva, coorientador, Rodrigo de Souza Vieira, 2018.
137 p.

Dissertação (mestrado) - Universidade Federal de Santa Catarina, Centro Tecnológico, Programa de Pós Graduação em Engenharia Mecânica, Florianópolis, 2018.

Inclui referências.

1. Engenharia Mecânica. I. Carlos da Silva, Jonny . II. de Souza Vieira, Rodrigo. III. Universidade Federal de Santa Catarina. Programa de Pós-Graduação em Engenharia Mecânica. IV. Título.

Adriano Gonçalves Schommer

MODELING AND SIMULATION OF A TOURING RACECAR SUPPORTED BY EXPERIMENTAL DATA

Esta Dissertação foi julgada adequada para obtenção do Título de "Mestre em Engenharia Mecânica", e aprovada em sua forma final pelo Programa de Pós-Graduação em Engenharia Mecânica.

Florianópolis, 01 de Março de 2018.

_____

Prof. Jonny Carlos da Silva, Dr. Eng.
Coordenador do curso

_____

Prof. Jonny Carlos da Silva, Dr. Eng. – Orientador
Universidade Federal de Santa Catarina

_____

Prof. Rodrigo de Souza Vieira, Dr. Eng. – Coorientador
Universidade Federal de Santa Catarina

Banca Examinadora:

_____

Prof. Lauro Cesar Nicolazzi, Dr. Eng
Universidade Federal de Santa Catarina

_____

Prof. André Ogliari, Dr. Eng
Universidade Federal de Santa Catarina

_____

Prof. Henrique Simas, Dr. Eng
Universidade Federal de Santa Catarina

Dedico este trabalho aos meus pais
João e Lucila Schommer.

AGRADECIMENTOS

Muitas pessoas foram fundamentais para a conclusão deste trabalho. Agradeço à minha família, torcedores assíduos. Eng. João Schommer, Lucila e Betânia Schommer. Engª. Ludmila Nesi, companheira e incentivadora. Agradeço à UFSC e ao PosMEC, em especial aos Prof. Jonny e Rodrigo, excelentes orientadores. Agradeço à UFSM, em especial ao Prof. Mario Martins, ao Eng. Fernando Leal, ao futuro engenheiro Cassio Freitas e à equipe Formula UFSM. Agradeço à CAPES pelo suporte financeiro e, por fim, agradeço à equipe RZ Motorsport e à empresa JL Racing Products, em especial aos Eng. Ramon, Kevin, Jorge, Rodolfo e Robson.

"[...] it's about people, then money; it's about people, then machine. Not the other way around. So focus about people."

(Claude Rouelle)

RESUMO

Para pilotos e engenheiros de corrida, a introdução de um novo circuito no calendário de corridas traz muitos desafios e expectativas. Configurar o veículo para novas condições e o processo de aprender o traçado do circuito são tópicos importantes a serem tratados. O foco deste trabalho reside na inclusão de um novo circuito no campeonato conhecido como *Brasileiro de Marcas*: um campeonato profissional de competição automobilística que utiliza veículos semelhantes a sedans originais de fábrica. O problema tratado está relacionado aos poucos dados disponíveis sobre o Circuito dos Cristais – MG, recentemente inaugurado no estado de Minas Gerais, e o curto tempo para preparar os pilotos durante o final de semana de corrida. Esse trabalho tem o objetivo de demonstrar como a análise de dados e simulações de tempo de volta podem ajudar uma equipe a melhorar o desempenho na competição. Para atingir o objetivo, técnicas de pilotagem e indicadores de performance de dois pilotos profissionais foram comparados e discutidos com base em dados coletados no circuito. Simulações de tempo de volta foram realizadas por meio de um modelo simples do veículo, porém com os parâmetros de entrada derivados de simulações estocásticas. Precisamente, o método Monte Carlo foi utilizado para estimar o coeficiente de arrasto, a eficiência do trem de força e o coeficiente de atrito pneu/solo com base em dados coletados do sistema de aquisição de dados de um Toyota Corolla 2016 de competição. Dois tipos de dados foram utilizados neste trabalho: *dados de treinamento*, coletados no Circuito Ayrton Senna – GO, utilizados para estimar os parâmetros, e *dados de teste*, provenientes do Circuito dos Cristais – MG, utilizados para validar as simulações. Ambos os circuitos foram parametrizados com ajuda de um software de desenho assistido por computador (CAD).

Palavras-chave: Simulação de tempo de volta, método Monte Carlo, aquisição de dados, análise de dados, validação, parametrização, circuito.

ABSTRACT

For drivers and race engineers, a new circuit included to the racing calendar brings many challenges and expectations. How to setup a racecar and the process of learning the racing line are important topics to be addressed. This work focuses on data analysis techniques and lap time simulations to deal with the introduction of a new circuit to the Brazilian touring car championship known as *Brasileiro de Marcas*: a professional racing category of silhouette racecars resembling compact sedans. The problem addressed relates to the scarce data available from the Cristais Circuit – MG, recently built at Minas Gerais state, and the short time to prepare drivers during the race event. This work aims to demonstrate how data analysis and lap time simulations can help an entry-level racing team to improve performance. To accomplish with the objective, driving techniques and key performance indicators of two professional drivers were compared and discussed supported by data acquired at the racetrack. Lap time simulations were also carried with the help of a simple vehicle model with input parameters derived from stochastic simulations. Precisely, Monte Carlo method was used to estimate drag coefficient, drivetrain efficiency and tire/road coefficient of friction support by data acquired from a 2016 Toyota Corolla. Two sets of data were acquired for this work: training data, from Ayrton Senna Circuit - GO, at Goiás state - used to estimate the parameters, and Cristais Circuit – MG, used to validate the vehicle model. The parameterization of the circuits was performed via a computer-aided design software.

Keywords: Data acquisition, motorsport, Monte Carlo, validation, circuit parameterization.

LIST OF FIGURES

Figure 2.1 : Longitudinal load transfer. Adapted from Milliken & Milliken (1995). 8
Figure 2.2 : Tire friction circle concept. Adapted from Milliken & Milliken (1995). 10
Figure 2.3 : G-G diagram of a racecar. Adapted from Milliken & Milliken (1995). 11
Figure 2.4 : Speed effects on G-G diagram of a high downforce vehicle. Adapted from Milliken & Milliken (1995) and Brayshaw (2004). 13
Figure 2.5 : Corner phases and its corresponding G-G diagram areas. Adapted from Bentley (2011). 14
Figure 2.6 : G-G diagram for two different cornering maneuvers. Adapted from Milliken & Milliken (1995) and Segers (2014). 16
Figure 2.7 : The late apex approach. Adapted from Bentley (2011) and Segers (2014). 18
Figure 2.8 : The early apex approach. Adapted from Bentley (2011) and Segers (2014). 19
Figure 2.9 : Cornering sequence. Adapted from Bentley (2011) and Segers (2014). 20
Figure 2.10 : Vital signals analysis page in MoTeC i2® analysis software. 22
Figure 2.11 : Onboard camera overlay in AiM Race Studio Analysis® software. 22
Figure 3.1 : Mathematical models (RAYCHAUDHURI, 2008). 28
Figure 3.2 : Case-based modeling. Adapted from Raychaudhuri (2008). 29
Figure 3.3 : LHS examples with $d = 2$ dimensions and $p = 10$ points. Adapted from Viana (2013) 31
Figure 3.4 : Comparison of two models against experimental data. Adapted from Jachner & Boogaart (2007) 36
Figure 3.5 : Measures of two sets of data. Noisy and varying speed datasets are considered in comparison to the reference data. Adapted from Jachner & Boogaart (2007). 38
Figure 3.6 : Measures of two sets of data. Shifted and shifted + scaled datasets are considered in comparison to the reference data. Adapted from Jachner & Boogaart (2007). 39
Figure 4.1 : Overview of the method used to simulate the speed profile of the racecar. 41
Figure 4.2 : 2016 Toyota Corolla competing at *Brasileiro de Marcas* championship (BARROS, 2016). 42
Figure 4.3 : Right hand vehicle coordinate system. 44
Figure 4.4 : G-G diagram modeling of the vehicle in function of speed. 45
Figure 4.5 : Internal variables of a mass component in the multiport software AMESim®. 46
Figure 4.6 : Vehicle model. 46
Figure 4.7 : Powertrain model. 47

Figure 4.8 : Minimum braking distance longer than the distance to corner apex. 50
Figure 4.9 : Minimum braking distance shorter than the distance to corner apex. 51
Figure 4.10 : Histogram of engine speed at Ayrton Senna Circuit. 53
Figure 4.11 : Engine speed [rpm] versus vehicle speed [km/h]. 54
Figure 4.12 : Calculation of the frontal area with the help of a CAD software. 56
Figure 4.13 : Circuit parameterization based on a CAD software and GPS logged data. Ayrton Senna Circuit – GO, Brazil. 57
Figure 4.14 : Rolling mean method of circuit parameterization. 58
Figure 4.15 : Circuit parameterization with the help of a CAD software and driver's expertise to determine the racing line. Cristais Circuit – MG, Brazil...58
Figure 4.16 : DoE study for the target accuracy of Ayrton Senna Circuit – GO simulations. a) Speed profile of models 1, 2 and 3. b) Residual values between model 1 and 3. 60
Figure 4.17 : Pareto diagram of the input parameters. Effects of each parameter on simulation error is presented. 62
Figure 4.18 : Density distribution of drag coefficient along the Monte Carlo optimization process and its effects on model error. 65
Figure 4.19 : Density distribution of friction coefficient along the Monte Carlo optimization process and its effects on model error. 66
Figure 4.20 : Density distribution of drivetrain efficiency along the Monte Carlo optimization process and its effects on model error. 67
Figure 5.1 : Cristais Circuit has 17 corners indicated by the squared boxes, split into six sectors, indicated by balloons. 70
Figure 5.2 : G-G diagram and GPS plot of drivers A and B at sector 1. 71
Figure 5.3 : Data comparison of a qualifying lap of two professional drivers in Sector 1. a) time variance - Δ time, b) vehicle speed. Driver A is 0.198 seconds faster than Driver B 73
Figure 5.4 : Longitudinal acceleration data of sector 1. 73
Figure 5.5 : Gear chart of sector 1. 74
Figure 5.6 : Engine speed data of sector 1. 74
Figure 5.7 : Throttle percentage data of sector 1. 75
Figure 5.8 : Metrics of sector 1. a) average grip factors, b) steering angle and throttle position. Higher grip factors indicate more tire potential is being used. 76
Figure 5.9 : G-G diagram and GPS plot of drivers A and B racing line. 77
Figure 5.10 : Data comparison of a qualifying lap of two professional drivers in Sector 1. a) time variance - Δ time, b) vehicle speed. Driver B is 0.169 seconds faster than Driver A. 78
Figure 5.11 : Longitudinal acceleration data of sector 6. 79
Figure 5.12 : Lateral acceleration data of sector 6. 79
Figure 5.13 : Gear chart of sector 6. 80
Figure 5.14 : Throttle position data of sector 6. 80
Figure 5.15 : Metrics of sector 6. 81

Figure 6.1 : Reference points for Ayrton Senna Circuit – GO, Brazil. 82
Figure 6.2 : a) Speed profile comparison between experimental and simulated data. b) Residual values. 83
Figure 6.3 : Comparison of gear shifting strategies: simulated data against the strategy adopted in a flying lap at qualifying session. 85
Figure 6.4 : Reference points for Cristais Circuit – MG, Brazil. 86
Figure 6.5 : a) Speed profile comparison between experimental and simulated data. b) Residual values. 87
Figure 6.6 : Comparison of gear shifting strategies. Logged data versus simulation. 89

LIST OF TABLES

Table 4.1 : Gear ratios allowed for the racecars. 51
Table 4.2 : Drivetrain efficiency as function of gear ratio and engine speed for a FWD production sedan. (IRIMESCU; MIHON; PĂDURE, 2011). 52
Table 4.3 : Typical values of drag coefficient for a touring racecar. 55
Table 4.4 : Design of experiments setup to determine target accuracy of the model. 59
Table 4.5 : Design of experiments setup to investigate simulation errors. 61
Table 4.6 : Design of experiments setup to determine target model accuracy. ..63
Table 4.7 : Summary of estimated parameters via Monte Carlo optimization and the literature review. 67
Table 5.1 : Sectors time, in seconds, of two flying laps of the qualifying session at Cristais Circuit. Two professional drivers are compared. Δ time is the difference between Driver A and B, and ideal lap is composed by the best sectors of both drivers. 70
Table 5.2 : Signal gating thresholds for grip factors. 76
Table 6.1 : Target and actual deviance measures for training data. 84
Table 6.2 : Deviance measures for test and training data. 88

LIST OF ABBREVIATIONS AND ACRONYMS

ASME	American Society of Mechanical Engineers
AWD	All-Wheel-Drive
C.G	Center of Gravity
CAD	Computer-aided design
DoE	Design of Experiments
FWD	Front-Wheel-Drive
GF	Grip Factor
KPI	Key performance indicators
LHS	Latin Hypercube Sampling
LMP1	Le Mans Prototype 1
MAE	Mean absolute error
MSE	Mean squared error
NASCAR	National Association of Stock Car Auto Racing
OLHS	Optimized Latin Hypercube Sampling
OLHS	Optimized Latin Hypercube Sampling
PDF	Probability density function
RMSE	Root mean squared error
RWD	Rear-Wheel-Drive
SSE	Sum of squared errors
WOT	Wide open throttle

TABLE OF CONTENTS

1 INTRODUCTION 1
1.1 Problem statement 3
1.2 Objectives 4
1.3 Research contributions 4
1.4 Thesis outline 5
2 MAN AND MACHINE: THE RACECAR 7
2.1 Introduction 7
2.2 Front and rear-wheel-drive dynamics 7
2.3 G-G diagram 10
2.4 The phases of a corner 13
2.4.1 Phase 1: Pure braking 14
2.4.2 Phase 2: Trail braking 15
2.4.3 Phase 3: Pure cornering 16
2.4.4 Phase 4: Combined cornering and throttle 16
2.4.5 Phase 5: Full throttle 17
2.5 Racing lines 17
2.5.1 Corner leading to a long straight – the late apex line 17
2.5.2 Fast corner or leading to a short straight - The early apex line . 19
2.5.3 Cornering sequences “S bends” 20
2.6 Data analysis in motorsports 21
2.6.1 Vehicle performance 23
2.6.2 Driver´s performance 25
3 MODELING AND SIMULATION METHODS 28
3.1 Introduction 28
3.2 Monte Carlo method 28
3.2.2 Latin Hypercube Sampling 30
3.3 Modeling – general considerations 32
3.4 Lap time simulations – an overview 33
3.5 Verification and validation 34
3.6 Accuracy metrics and criteria for simulation validation 35
4 MATERIALS AND METHODS 41
4.1 Introduction 41
4.2 The racecar 42
4.3 Vehicle model 44
4.3.1 Thrust force 47
4.3.2 Braking force 48
4.3.3 Drag force 49
4.3.4 Rolling resistance 49
4.3.5 Driver´s model for braking strategy 50

4.4 Vehicle parameters 51
4.4.1 Drivetrain 51
4.4.2 Effective Tire Rolling Radius 53
4.4.3 Aerodynamic drag 55
4.5 Circuit model 56
4.6 Target accuracy 59
4.7 Parameter estimation 60
4.7.1 Design exploration 61
4.7.2 Monte Carlo parameter estimation 63
5 DATA ANALYSIS 69
5.1 Introduction 69
5.2 Cristais Circuit – MG, Brazil. 69
5.2.2 Sector 1 71
5.2.3 Sectors 2 to 5 77
5.2.4 Sector 6 77
6 SIMULATION RESULTS AND DISCUSSION 82
6.1 Introduction 82
6.2 Training data: Ayrton Senna Circuit – GO, Brazil. 82
6.2.1 Gear shifting strategy 85
6.3 Test data: Cristais Circuit – MG, Brazil. 86
6.3.1 Gear shifting strategy 88
7 CONCLUSIONS 90
7.1.1 Recommendations for future work 94
REFERENCES 96
APPENDIX A 101

1 INTRODUCTION

Due to cost reduction over the last years, the use of data acquisition systems became a popular tool in many racing categories, including small racing classes. In fact, the problem has shifted from the cost of hardware to the cost of hiring personnel to make use of data (PARKER; HARGRAVE, 2016). This is strengthened by the increased amount of logged channels, and the short time available between test runs during the race weekend (VADURI; LAW, 2000). In order to quickly extracting meaningful information from data, a race engineer has to anticipate where and what to search for, which points out the importance of race team preparation before the race event. In this way, the question to solve is what should be learned beforehand a race event.

Mitchell *et al.* (2000) extensively covered the process of learning a new circuit with the help of data acquisition, and from a driver technique viewpoint, Mitchell *et al.* (2004) presents a comprehensive review on driving books about racing lines. More specifically, Smith (1996) discusses about how the speed characteristic of a corner influences the line taken by the driver in order to improve performance. Shortly, he defines that slow corners will call for a late apex "slow in, fast out" approach, while fast corners will anticipate the apex.

Before modern data acquisition systems, drivers and stopwatch were the main source of data for racing engineers (SMITH, 1996). Data gathering started in the late of 60's with an analogue tachometer of the engine speed that could record the maximum engine speed. Because it indicated to the crew whether the driver had being damaging the engine by exceeding the revolution limit, this instrument was known as "telltale" tachometer (SMITH, 1996).

Its most common configuration is composed by two needles. The main needle displays instantaneous engine speed and pushes the telltale needle that holds the maximum engine speed. Further developments created a functionality to help drivers to control gear-shifting points, in which the telltale needle resets itself after a few seconds. In this way, the driver did not have to keep his eyes at the tachometer at exact time of upshifting (FARRINGDON, 2017).

In Brazil, one of the first modern data acquisition systems was used in the 1994 season of Formula Chevrolet with the drivers Ciro Alperti Jr. and Max Wilson. The system was a STACK® datalogger composed by 14 channels recording engine temperatures and pressures,

engine and wheel speed, throttle position, longitudinal and lateral accelerations. Although recorded channels were similar of those currently used in entry-level classes of motorsport, data analysis packages and computers were rudimentary, making data analysis much slower than it is nowadays (PERDOMO, 2017).

From the race engineer standpoint, speed profile of a circuit is a valuable clue to setup a racecar. It reveals important aspects of a circuit such as the ratio between fast and slow corners, average and range of speed, which are meaningful to compromise the setup between mechanical and aerodynamic grip (SEGERS, 2014). In addition, vehicle gear ratio and driver gear-shifting strategy are important process to deal with, since often a given corner offers more than one option of gear to be engaged, and it is not always obviously realized which option improves lap time (SMITH, 1996; MAGGIO *et al.*, 2003). So far, this introduction emphasizes the importance of data acquisition in motor racing. In this way, the question to solve is what should be learned beforehand a race event.

In the past years, different vehicle dynamics models have been developed. In a broad range of goals and levels of detail, they vary from simple linear models to high degree of freedom non-linear multi-body systems (YANG *et al.*, 2013). Regardless its complexity level, a simulation model is always going to be an approximation of the physical phenomena it is trying to represent (KUTLUAY; WINNER, 2014). Thus, how accurate a model represents a real system is a natural concern.

Some papers approach validation by comparing simulation results of a proposed model with commercial packages (e.g. ADAMS/Car) such as in (SAGLAM; UNLOSOY, 2011; ZHANG *et al.*, 2015; VADDI; KUMAR, 2015). In this validation approach, virtually any suitable vehicle with a determined set of known input parameters could be used to benchmark a proposed model. Although it has been reported as an effective validation approach, most of the real-life problems rely on the lack of data to populate a given vehicle model (CALLEA, 2004; TRAUB *et al.*, 2016).

On this topic, there is a tradeoff between model complexity and feasibility to acquire reliable input parameters for a model. This matter is especially important for small budget racing teams, because measuring vehicle parameters involves testing and tests cost money.

Lap time simulation packages are generally proprietary or focus on high-level racing categories. However, there are commercial simulations packages using simple models that require basic input

parameters. OptimumG®, for example, provides the OptimumLap®, a free software for lap time simulation, which uses a simple point-mass vehicle model claiming errors within 10% compared with experimental data (OPTIMUMG, 2017b). The drawback of OptimumLap® is that it is not open source, which means the software code is proprietary and cannot be accessed neither edited.

1.1 Problem statement

The context of this research lies on the Brazilian touring car championship known as *Brasileiro de Marcas*: a professional racing category of specified production sedans with identical tires, chassis and engine build. This work focus on data analysis techniques and lap time simulations to deal with the introduction of a new circuit to the calendar. The problem addressed is related to the challenges derived from scarce data available to setup racecars, and the short time to prepare drivers during the race event.

In professional racing categories, lap time difference between competitors is within tens of a second. Every improvement on the vehicle dynamics counts, which includes driver and team preparation. The challenge of racing a new circuit highlights the importance of quickly accessing precise information from vehicle data and feedback from drivers, since there is no reference from past events. Speed profile of a circuit plays a major role. Some corners have greater effects on lap time than others do, and the driving technique is strongly related to corner characteristics.

Even though lap time simulation is a well-established engineering tool, it is rarely used by entry motorsport categories. Accurate vehicle models are complex, which involves many input parameters not easily measurable, and/or simulation packages are expensive. However, when it comes to speed profile for circuit recognition, overall vehicle dynamics instead of detailed vehicle behavior is an effective approach. It reduces the need of complexity of the vehicle model at cost of accuracy and lack of details to explore vehicle parameters.

The simplest model available is a single-point of mass with a constant coefficient of friction between tire and road. Although it has been referred in the literature, the use of such simple models to generate speed profile of a circuit (Segers, 2014; Rouelle, 2014), results from simulations and how consistent these models are for various circuits were not discussed. Furthermore, the usefulness of such data for circuit recognition, and a method to populate such models with logged data

have not been addressed. In other words, could a small racing team benefit from such simulations? This is the main motivation for this work

The Brazilian motorsport scenario currently has three main professional categories: *Brasileiro de Marcas, Brasileiro de Turismo*, and *Stock Car*. Hierarchically, the first is an entry-level professional category because *Brasileiro de Turismo* gives access to the major class Stock Car. Compared to Stock Car racing teams, *Brasileiro de Marcas* and *Brasileiro de Turismo* are considered small budget categories.

1.2 Objectives

This work aims to demonstrate how data acquisition and lap time simulation together can help a small budget racing team to improve its driver's performance in a new and unknown circuit. To accomplish with the objective, the following key-points are addressed:

- Collect data from race events;
- Investigate key performance indicators of drivers from data;
- Investigate driving techniques according to circuit characteristics and its effects on lap time;
- Develop a vehicle model capable to simulate speed profile of a new circuit;
- Develop a method to populate the vehicle model with estimated parameters from logged data;
- Develop a model to parameterize a racing line in a new circuit;

1.3 Research contributions

Motorsport data is highly protected by racing teams. The main contribution of this dissertation is to incorporate to the literature a discussion on how a small budget racing team can use simulations and data analysis to improve its driver's performance.

This work provides a method to access overall vehicle parameters from data gathered at race events. Model parameters were estimated via a Monte Carlo optimization process using a cost function to evaluate simulation results with real data. The method was applied to a point-mass vehicle model using AMESim® software in order to simulate the speed profile of a circuit. Results were discussed in terms of

repeatability of the simulation for different circuits and the usefulness of the data to tackle a new circuit.

1.4 Thesis outline

The present dissertation is divided into six chapters: Introduction, literature review, materials and methods, results, discussion of results and summary/conclusions. An overview of the thesis outline follows:

Chapter 2 reviews the literature on driving techniques and racecar performance. First, front and rear-wheel-drive dynamics are discussed. After, the G-G diagram is presented followed by a discussion on cornering phases and racing lines. This chapter is enclosed with a brief presentation about data analysis in motorsports.

Chapter 3 composes the second part of the literature review. It addresses the state of the art of vehicle parameter estimation and lap time simulations, which includes a discussion on validation procedures.

Chapter 4 presents materials first. The racecar used for this work is introduced, as well as the data acquisition system and the circuits from which data were logged. After, methods are exposed in topics of vehicle model and assumptions, circuit and vehicle parameterization.

Chapter 5 focuses on data analysis. How data acquired at the race event help drivers to improve performance is presented and discussed.

Chapter 6 discusses simulation results in comparison to experimental data from the race event, focusing on the speed profile and gear shifting strategies of two Brazilian circuits.

Chapter 7 closes this work. It summarizes and presents conclusions of previously topics.

2 MAN AND MACHINE: THE RACECAR

> *When driving the limit, you are actually dealing with three different limits: the car, the track, and yourself (the driver). You must recognize and maximize each if you are to go faster* (BENTLEY, 2011).

2.1 Introduction

Back into the fifties, driving techniques had already been discussed in the literature (MITCHELL; SCHROER; GRISEZ, 2004). Since then, aerodynamics, engine, tire and chassis technologies have progressed and many aspects have changed on how to drive a racecar. Out of the pits when a racecar is on track, vehicle dynamics is not only the vehicle itself; it is an interaction between racecar, circuit and driver (BENTLEY, 2011). In order to improve performance, a racing team needs to tackle them all. A fast car cannot make a slow driver go fast and the opposite applies.

This chapter aims to discuss fundamental knowledge about motor racing. Firstly, the interaction between driver and racecar is discussed in the context of front and rear-wheel-drive configurations. Following, it presents the concept of performance envelope of a racecar, the so-called G-G diagram. Finally, racing lines and data analysis techniques are shown.

2.2 Front and rear-wheel-drive dynamics

A driver controls its racecar by throttle, braking, gear shifting and steering inputs. Improvements on lap time imply more time on throttle and less time on braking and coasting, which is the transition time between throttle and brake inputs. How the driver controls his racecar is known as driving technique. Besides, to drive a racecar at its limit implies different techniques according to the racecar particularities. This section discusses main characteristics of front and rear-wheel-drive because the object of this study is a front-wheel-drive (FWD) racecar, opposed to the popular rear-wheel-drive (RWD) racecar.

Engine torque and power accelerates a vehicle in function of driveline ratio and traction available at the tires. This longitudinal acceleration transfers loads from the car front end to its rear end, which

directs influences the tire traction capability (MILLIKEN; MILLIKEN, 1995).

Figure 2.1 illustrates this phenomenon. Whenever there is a forward acceleration (a_x), an inertial force (F) is developed. The moment about the C.G height (h) transfer load from the front tire to the rear tires (Δw_x) in function of (a) and (b), which are the distance of the C.G to the front and rear axle respectively.

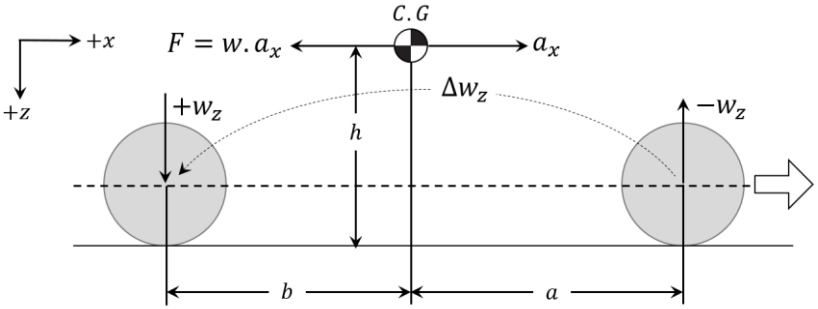

Figure 2.1: Longitudinal load transfer. Adapted from Milliken & Milliken (1995).

A rear-wheel-drive vehicle will benefit from this longitudinal load transfer due to an increased load on rear axle, which translates into more traction capability. The opposite is true for a front-wheel-drive vehicle, because forward acceleration subtracts vertical load from the driven wheels.

Indeed, in motorsport history FWD racecars have not been much popular. Most successful FWD racecars have competed in low power-to-weight ratio categories and in cases where directional stability was important, such as in slippery surfaces (MILLIKEN; MILLIKEN, 1995).

A recent attempt to compete in high level was the Nissan's 2015 GT-R LM NISMO, conceived to compete at the highest Le Mans racing class: the Le Mans Prototype 1 (LMP1), which has been essentially dominated by rear-wheel-drive solutions with temporary hybrid electric all-wheel-drive (AWD) configuration (COTTON, 2016). The project was considered disruptive because of the known dynamics limitations of a FWD configuration. In fact, the aim was to take aerodynamics advantages from LMP1 regulations, which were more compliant with front diffuser design (ORTIZ, 2015).

Aiming to increase traction at the driven wheels, FWD cars are commonly front weight biased, which means longitudinal position of the center of gravity (C.G.) is closer to front axle than rear axle of the vehicle. The tradeoff is a vehicle naturally understeer negotiating a corner at the limit of adhesion (MILLIKEN; MILLIKEN, 1995; ORTIZ, 2015). In addition, front weight bias negatively affects braking capability due to the overload of front brake discs, pads and due to the tire load sensitivity (ORTIZ, 2015). An increase in tire vertical load increases the tire adhesion on track surface, but not in a linear manner. In other words, an even load distribution on the tires produces more lateral and longitudinal forces than if it is unevenly distributed.

From a driver´s point of view, this natural tendency of a FWD to understeer is comfortable because easing off the throttle may bring the car back to control. However, an understeering car results in slow lap times because it is a stable condition. On this theme, Nowlan (2015) presents lap time simulations of two configurations of a LMP1 prototype: a FWD and RWD. The simulations confirms the FWD would have mid-corner understeer behavior resulting in slower lap times due to lower mid-corner and corner exit speeds.

One could conclude the overall concept of a FWD racecar is generally slower than a RWD. Milliken & Milliken (1995) complements: “Rear-wheel-drive is by far the most successful in racing. The combination of front-wheel steering and rear-wheel-drive gives the driver control over both end of the vehicle by steering by throttle.”

In FWD categories, vehicle setup needs to compensate the understeering tendency in order to have a competitive racecar. According to Milliken & Milliken (1995), it can be achieved by increasing the front axle adhesion, e.g. with bigger tires at the front axle, or reducing the rear axle adhesion by increasing lateral load transfer on the rear axle.

Another way of balancing an understeering vehicle is to increase rear brake bias to change the vehicle attitude and help the turn in phase of cornering. To exemplify, the key concept of the popular “hand-brake turn” rally maneuver is based on detraction of rear tires adhesion (MILLIKEN; MILLIKEN, 1995). Driving a FWD at the limits is no easy task. Bentley (2011) emphasizes the compromises to achieve balance of handling and performance, a fast car is only fast if it could be driven with confidence.

2.3 G-G diagram

G-G diagram is a plot of longitudinal acceleration (X-axis) against lateral acceleration (Y-axis) of a racecar, expressed in units of gravitational acceleration [G]. In motor racing, it is as a measure of the overall vehicle performance, a combination of driver, vehicle and road performances.

To understand the fundaments of the G-G diagram, the concepts of *tire friction circle* and *vehicle friction circle* need to be revisited. According Milliken & Milliken (1995), no matter how much slip angle and slip ratio a tire is subjected on, the maximum force it produces is limited by the vertical load times the tire/road coefficient of friction. Thus, the capacity of a tire to generate longitudinal, lateral or combined forces can be represented as a circle with constant radius for a given vertical load, camber angle, tread temperature and tire pressure. In fact, tire behavior is even more complex. Due to tire characteristics, the friction circle is often an ellipse but the main concept remains true.

In the *tire friction circle* illustrated by Figure 2.2, the limit of adhesion is represented by the radius (*R*) of the circle.

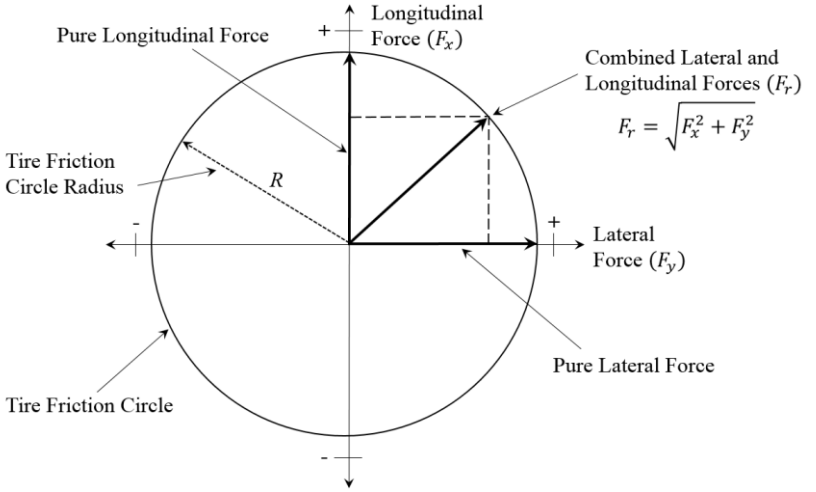

Figure 2.2: Tire friction circle concept. Adapted from Milliken & Milliken (1995).

The figure shows a resultant vector from two components, pure lateral and pure longitudinal forces. If the maximum tire capacity is used for pure longitudinal force, for example, there is no room to develop

lateral force. This phenomenon is defined by the equation below, in which the resultant total force (F_r) is the sum vector of lateral (F_y) and longitudinal (F_x) forces.

$$F_r = \sqrt{{F_x}^2 + {F_y}^2} \tag{2.1}$$

Tire capability to generate forces is independent of direction; it is a sum vector of both lateral and longitudinal forces limited by the maximum tire/road adhesion. Therefore, if tire load sensitivity is neglected, the tires could be lumped into only one *vehicle friction circle*, provided the vertical load is the total vehicle weight. Thus, the radius of a *vehicle friction circle* would be expressed as tire/road coefficient of friction times the vehicle weight (MILLIKEN; MILLIKEN, 1995).

In other words, *vehicle friction circle* is the ideal limit of adhesion of a racecar. It is considered ideal, impossible to reach, due to power limitations, load transfer and suspension effects, stability and brake balance. All these factors inhibit a vehicle to make use of maximum force available at the tires at the same time (MILLIKEN; MILLIKEN, 1995).

The *vehicle friction circle* is presented in Figure 2.3 (dashed line) in comparison to the *G-G diagram*, which is, in turn, measurable (black circles). LH and RH stands for left and right-hand respectively.

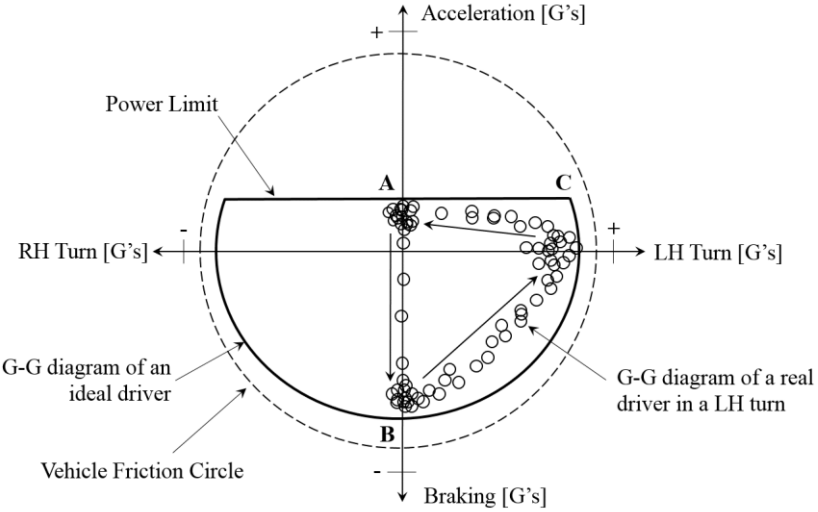

Figure 2.3: G-G diagram of a racecar. Adapted from Milliken & Milliken (1995).

Also presented in this diagram, the ideal G-G diagram (black line) represents the performance limit of the vehicle driven by an ideal driver. In other words, an ideal driver is capable to drive the vehicle hundred percent of the time at the limit. Although unachievable, the ideal G-G diagram provides a benchmark to the measured points. In this diagram, points A, B and C and the arrows indicate how acceleration is developed during a cornering maneuver.

The G-G diagram is the interaction of driver, racecar and track surface for a given maneuver. As an example, consider a vehicle accelerating in straight line, such as in drag racing. The peak of forward longitudinal acceleration depends on many factors such as driver throttle control, engine power, aerodynamic resistance, tire/road grip and so on. In this example, only the upper boundary of the G-G diagram is of interest, which in most cases is trimmed by the available engine power. In Figure 2.3, this power limit is seen in the flat plateau of the G-G diagram.

The other parts of the G-G diagram are explored in cornering maneuvers. Expanding the above example, consider a vehicle negotiating a left hand corner (Figure 2.3, points A, B, C). From wide open throttle (A), the driver brakes in a straight line exploring the lower part of the diagram (B); turn into the corner while brake pressure is reduced (transition B to C) until it reaches the corner apex (C), where the vehicle is momentarily in steady-state; then starts to accelerate the vehicle exiting the corner (transition C to A).

High downforce vehicles such as formula cars have the boundaries of the G-G diagram greatly affected by the speed (BRAYSHAW, 2004). Figure 2.4 presents a qualitative example of this phenomenon.

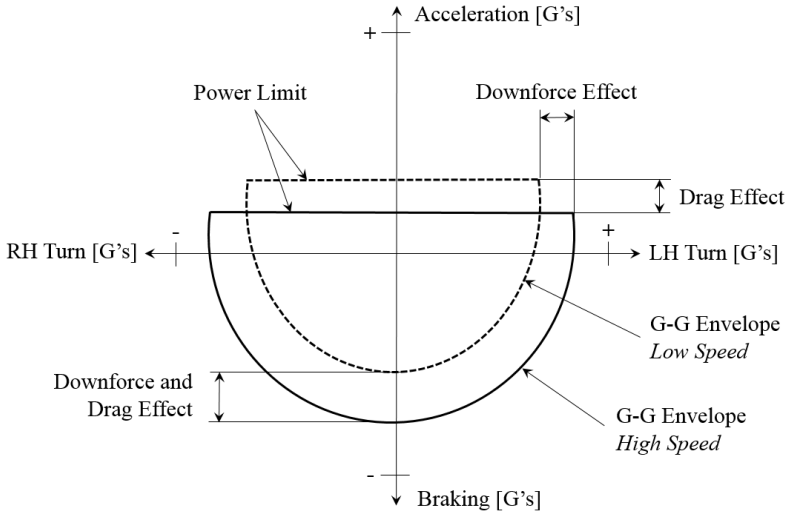

Figure 2.4: Speed effects on G-G diagram of a high downforce vehicle. Adapted from Milliken & Milliken (1995) and Brayshaw (2004).

As speed increases, cornering and braking ability are positively affected by aerodynamic forces, while forward acceleration is negatively affected by higher drag force. Because aerodynamic forces are changing with the square of velocity, higher speeds increase tire load and, in consequence, more tire forces are generated. This effect improves the cornering ability of a racecar, seen in the G-G diagram as a larger sideway envelope.

Downforce and drag forces also improve traction and braking ability; however, there is a conflicting effect on the G-G diagram. On the one hand, it improves braking because drag forces are contrary to forward movement, and downforce are generating more tire load. On the other hand, it reduces forward acceleration capability because increased drag is more significant than the improved traction for a power limited vehicle.

2.4 The phases of a corner

There are slightly different approaches to split a corner into phases. The approach considered in this work is presented in Figure 2.5.

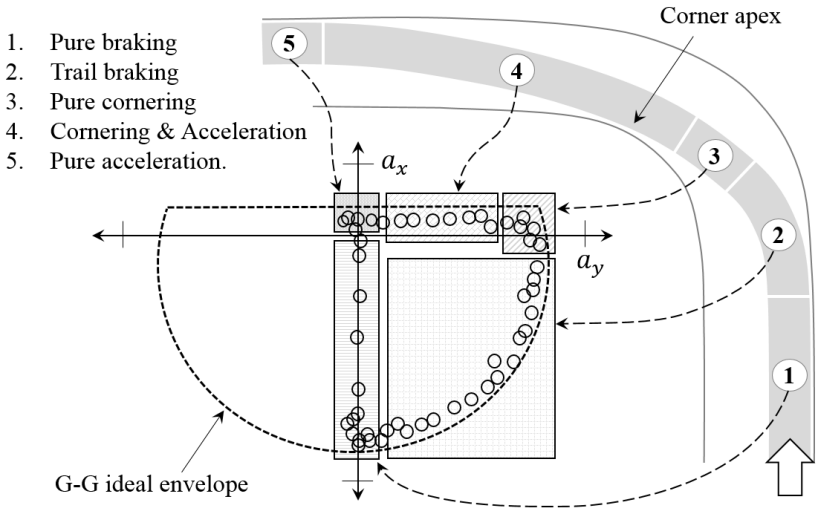

Figure 2.5: Corner phases and its corresponding G-G diagram areas. Adapted from Bentley (2011).

A macro view considers four phases: corner approach, corner entry, mid-corner and corner exit (SMITH, 1996; BENTLEY, 2011). It can be further detailed at the level of driver controls (BENTLEY, 2011), which is suitable to explore the G-G diagram (Figure 2.5) and considers five phases: 1. pure braking; 2. combined braking and cornering (trail braking); 3. pure cornering; 4. combined cornering and acceleration; and 5. pure acceleration.

2.4.1 Phase 1: Pure braking

According to Smith (1996), Sir Jackie Stewart (three-time Formula 1 world champion) once said the last thing a racing driver learns how to do really well is to use the brakes. The issues are related to how quick the driver hit the brakes, how much brake pressure is developed, and braking reference points. The following paragraphs address each one of them.

The less time a racecar spends braking, more time it spends on throttle, resulting in faster lap times (BENTLEY, 2011; SEGERS, 2014). Braking quickness and effort (rising and magnitude of brake pressure) are interrelated. To minimize the time wasted from wide open throttle (WOT) to braking phase, brake pressure must be built up as

quickly as possible as long as the wheels are prevented to lock (SEGERS, 2014).

In fact, it is a question of balance. As the driver brakes, load is transferred from the rear axle to the front axle, increasing tire adhesion. On the other hand, aerodynamic loads are being reduced with the square of velocity, decreasing tire adhesion. From a data analysis point of view, Segers (2014) suggests the differentiation of the longitudinal acceleration data channel as a measure of the braking quickness. As a rule of thumb, Segers considers fast braking as anything under 0.5 seconds to achieve the peak of negative longitudinal acceleration

Another side of braking has to do with choosing an appropriate reference braking point, to be the end of maximum braking instead of the common used start of braking point (BENTLEY, 2011). The basis of this affirmation lies on the effect of speed on the braking distance. The faster is the corner approach, sooner the driver should anticipate the start braking point to compensate the longer braking distance.

2.4.2 Phase 2: Trail braking

The overlap of braking and steering, the trail braking technique, started to be discussed in press only in the seventies (MITCHELL, 2004). At that time, the technique was controversial, since driving schools had been teaching braking and cornering as two separate phases. All the braking being done in a straight line to only then turn into the corner (BENTLEY, 2011). According to Mitchell (2004), only from the year 2000 trail braking was considered a standard technique.

From the driver´s point of view, trail braking is a tradeoff between braking and steering as the vehicle negotiates a corner (BENTLEY, 2011). The engineering side of trail braking has its base on the G-G diagram.

Figure 2.6 illustrates two G-G diagrams for the same cornering maneuver, the left diagram (a) illustrates braking and cornering in distinct phases, leaving unused tire potential indicated by the shadowed area. On the other way, the right diagram (b) shows braking and cornering overlapped, using full potential of the tires. This is the so-called trail braking technique.

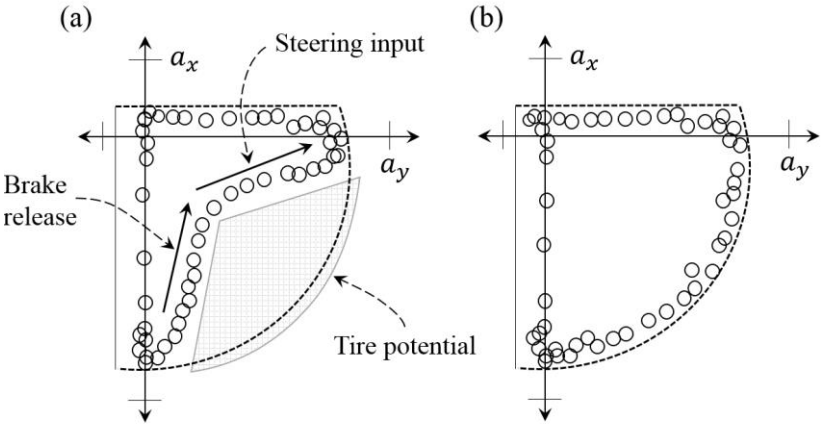

Figure 2.6: G-G diagram for two different cornering maneuvers. Adapted from Milliken & Milliken (1995) and Segers (2014).

From Figure 2.6-a, for a short period, the transition from braking to cornering is performed below the vehicle limit of adhesion. This waste of tire potential is directed translated into to waste of lap time. It happens because the vehicle cannot instantly change its trajectory from a straight line to a curved path (BENTLEY, 2011). Figure 2.6-b shows a smooth transition between braking and cornering at the vehicle limit of adhesion. As lateral acceleration increase, longitudinal acceleration decrease.

2.4.3 Phase 3: Pure cornering

The pure cornering phase is a very short period where the car is closer to its steady state. From the initial cornering maneuver, braking pressure is reduced to zero at some point before the corner apex. At this point, throttle is applied only to keep the vehicle at constant velocity (SMITH, 1996). It prevents external resistances such as aerodynamic drag, tire rolling resistance and driveline resistance to create a parasite longitudinal acceleration, reducing cornering capability from the G-G diagram.

2.4.4 Phase 4: Combined cornering and throttle

The success of the corner exit phase, including combined cornering and acceleration, is a consequence of the previously phases.

Its goal is to get on throttle as soon as possible without affecting car balance. The transition from pure cornering to WOT acceleration should be as smooth as possible (SMITH, 1996; BENTLEY, 2011). Too much steering input suddenly unloads the inner tires; too much steering angle slows the car down by scrubbing the tires; too much throttle input can cause wheel spin or detracts cornering capacity.

2.4.5 Phase 5: Full throttle

In the last cornering maneuver phase, the vehicle is at WOT without steering.

2.5 Racing lines

Early driving books considered a unique racing line for all drivers, while more recently books treat different racing lines for different drivers (MITCHELL, 2004). According to Smith (1996), there is, however, an optimum line through a corner, but it is a matter of circumstance, corner configuration, alongside the conditions of the circuit, vehicle and tires. For this reason, driving at the limit is frequently referred to as driving the "traction circle". (SMITH, 1996; MITCHELL, 2004; BENTLEY, 2011), another name for the *ideal G-G diagram*, which is the ultimate vehicle limit for a given operation condition (MILLIKEN; MILLIKEN, 1995).

Similar to other sports, motorsport is not an exact science. There is the human part of the equation. However, as shown there are many factors influencing the fastest line for a given corner, some fundamental concepts on professional driving techniques. The following sections discuss the basic concepts of racing lines.

2.5.1 Corner leading to a long straight – the late apex line

Late apex or the "slow in, fast out approach" sacrifices corner entry speed to favor corner exit speed by increasing the corner exit radius (SMITH, 1996). Because a racecar often spends most of its time on the straights at maximum acceleration (SEGERS, 2014), this racing line is used when there is a long straightaway following a corner.

The idea is to anticipate both braking and acceleration phases to carry on the exit speed advantage all the way down the straight. Since the distance travelled is function of speed, this advantage direct reflects in faster lap times. Bentley (2011) complements: "races are won on the straightaways, not in the corners".

The longer the straight, more substantial is the time advantage in comparison to the traditional geometric line (Figure 2.7). The limit of time gain is imposed by the vehicle acceleration rate, trimmed by engine power considering internal and external resistances, and/or gear ratio at highest gears.

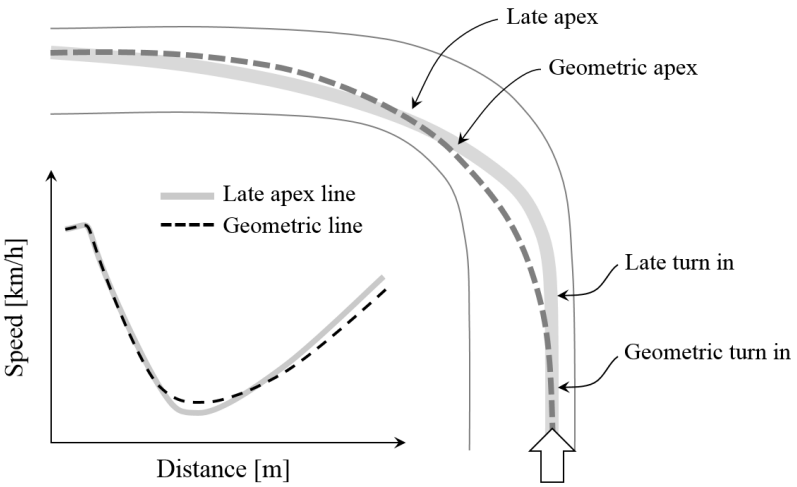

Figure 2.7: The late apex approach. Adapted from Bentley (2011) and Segers (2014).

Figure 2.7 illustrates the late apex approach in comparison with a tradition geometric line. The late apex racing line anticipates the braking zone; sharpens the turn in and takes a larger exit radius racing line. The travelled distance is also longer. Corners leading to long straightaways are the most important ones. For this reason, corner entry speed is sacrificed to gain corner exit speed.

According to Smith (1996), late apex is recommended for low and medium-speed corners. The concept of low, medium and high-speed is closely related to the racecar characteristics. A low-speed corner for a saloon racecar could be a medium-speed corner for a formula racecar, for example. This concept is based on a heuristic knowledge of the engineers and, to the knowledge of the author; there is no strict definition reported in the literature. However, according to Perdomo (2017, personal communication[1]), it is function of corner entry speed, corner radius and banking angle, which is the lateral inclination of the racetrack.

As a reference to the reader in this work, in which a low powered FWD racecar is the object of study, low-speed corners are considered those negotiated on first and second gears (lower than 110km/h). Medium-speed corners on third and fourth gears (110km/h – 160km/h); and high-speed corners are those negotiated on fifth to sixth gears (160km/h or higher).

For high-speed corners, higher exit speed provided by the late apex does not pays off the lower apex speed and the longer distance travelled. This happens due to the limited acceleration capacity at higher speeds, reduced by longer gear ratios and higher internal resistances (drive and powertrain efficiencies) and external resistances (tire rolling resistance and aerodynamic drag forces).

2.5.2 Fast corner or leading to a short straight - The early apex line

The early apex line is used in high-speed corners and in corners leading to a short straight (Figure 2.8).

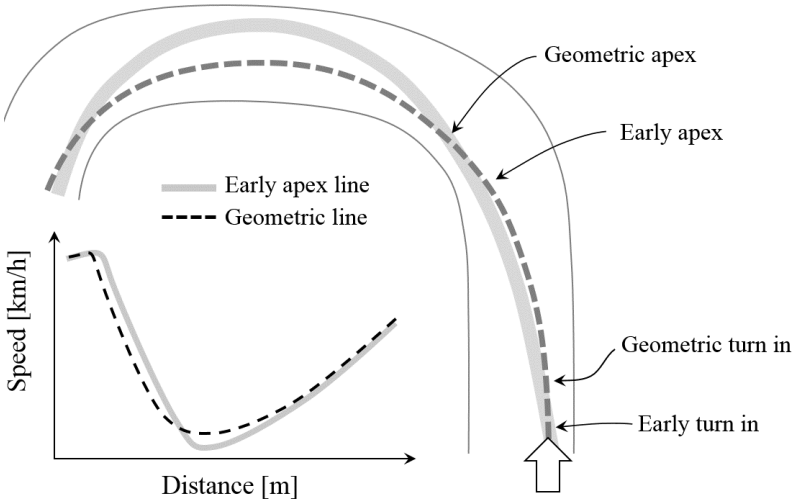

Figure 2.8: The early apex approach. Adapted from Bentley (2011) and Segers (2014).

[1] Personal communication with Rodolfo Perdomo, Eng. at Interlagos Circuit, 2017.

The faster the corner, the earlier is the apex (SMITH, 1996). For a corner leading to a short straight or to another corner, there is no advantage in preparing the corner exiting.

Back to the previous discussion, as the speed increases, the acceleration capability is reduced because it is no more limited by traction, but by power. Thus, taking a larger exit radius with a late apex approach does not help acceleration, because the limit factor is engine power, not tire adhesion. Therefore, all the speed carried through the corner and the shorter distance travelled compared with the late apex line is advantageous if the corner does not lead to a long straight.

2.5.3 Cornering sequences “S bends”

The racing line for corners in sequence should aim the exit speed by using the late apex approach, especially if it leads to a relative long straight (BENTLEY, 2011). In other words, the racing line should be considered as function of the last corner, preparing the exit phase.

Figure 2.9 shows a typical “S bend”, where the corner entry is taken by an early apex while the link curve is a preparation for opening the exit radius in the last corner.

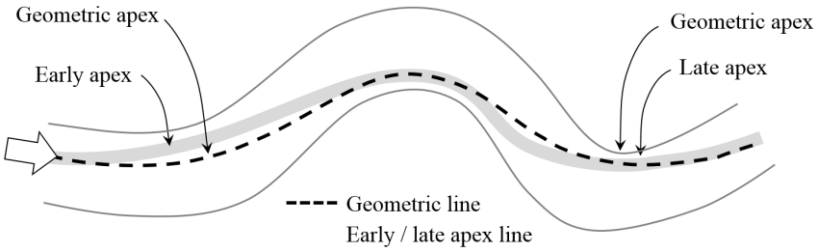

Figure 2.9: Cornering sequence. Adapted from Bentley (2011) and Segers (2014).

A racing line for an “S bend” cornering sequence should be planned to prepare the exit phase of the last corner. Early apex on the first corner; late apex on the last one.

2.6 Data analysis in motorsports

Data acquisition in a racecar has three main applications: analysis of *vital signals, driver activities* and *chassis parameters* (SEGERS, 2014):

Vital signals deals with racecar reliability; logged channels measure mainly temperatures, pressures and voltages, i.e. water radiator inlet/outlet temperatures; engine oil temperature and pressure; battery voltage and sensor readings. Vital signs analysis is performed in time domain because the engine could be running even if the vehicle is not moving.

Driver´s activities focus on driver controls. Measurements of steering angle, engaged gear, throttle position and brake pressure are considered basic logged channels. Instead of time domain, this analysis is performed in distance domain so events of different laps can be compared at the same circuit location.

Chassis parameters deal with vehicle performance. Accelerometer data, GPS data, tire pressure and temperature, ride height, suspension loads, displacements and velocities. Nowadays, virtually any parameter could be measured.

Sensor readings are recorded by a datalogger unit at various sampling rates according to the application. Suspension displacement measurements are logged at higher sampling rate than engine temperature, for example. Otherwise, details happening in a very short time interval, such as racetrack irregularities, are missed.

There are several companies providing complete solutions for data logging, including sensors, wiring harnesses, dataloggers and software packages specialized in motorsports data analysis. Most commercial data analysis packages provide several ways to display data. Most common ones are plots of data channel in time and distance domains; histograms; scatter XY plots and vehicle position at the circuit in map format. These packages allow to setup different screens for different analysis purposes.

As an example, Figure 2.10 demonstrates a customized page in MoTeC i2® software, used to analyze vehicle vital signals. The main window is a collection of temperatures and pressures plots in the time domain; the right side shows a scatter plot of the fuel pressure as function of lateral acceleration, and right below there is a track map with the vehicle position. The bottom part of the window displays a collection of alarm gauges, triggered at user-defined thresholds.

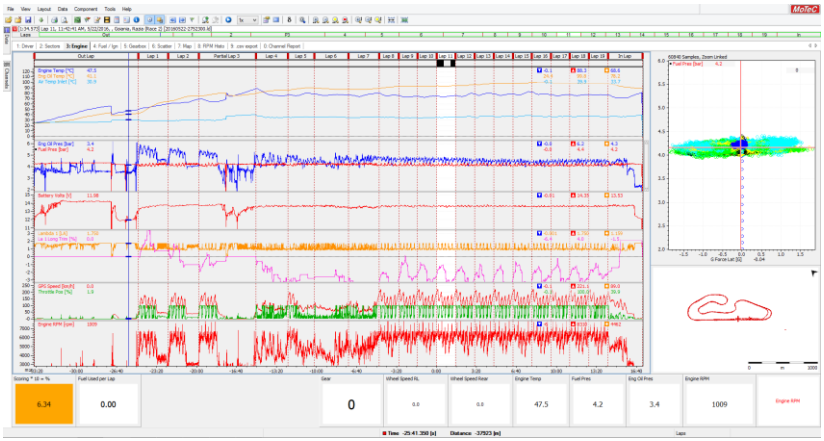

Figure 2.10: Vital signals analysis page in MoTeC i2® analysis software.

Besides, it is often possible to include videos overlays. Figure 2.11 presents an onboard video overlay performed in AiM Race Studio Analysis® software. On the left, longitudinal acceleration and vehicle speed are plotted in the distance domain; on the right, the onboard video is synchronized with logged data. As data cursor moves on the left, onboard video moves back and forward accordingly.

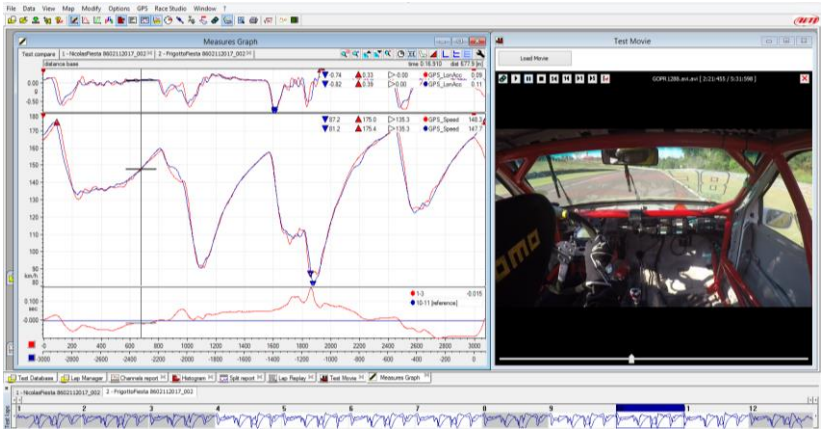

Figure 2.11: Onboard camera overlay in AiM Race Studio Analysis® software.

Segers (2014) emphasizes the great amount of sensors available. Therefore, engineers should always plan what they want to measure. Segers further states: “data analysis often provides as much questions as it provides answers”. Indeed, since 2000, when data acquisition systems became popular in NASCAR (National Association of Stock Car Auto Racing), the amount of collected data at race events and practice sessions was already greater than personnel resources to use it (VADURI; LAW, 2000).

2.6.1 Vehicle performance

There are various techniques to access vehicle performance and balance characteristics from data acquisition systems (VADURI; LAW, 2000; SEGERS, 2014; PARKER; HARGRAVE, 2016). The backside of data is that proper analysis is time consuming. As a result, according to Vaduri & Law (2000), many racing teams change springs, dampers, anti-roll bars, etc. purely on the driver´s feedback, without using data acquired from earlier runs. This is common practice, especially in small budget teams with limited personnel.

In cases feedback is provided by professional racing drivers, car balance seems to be more accurate. The problem lies when it comes to vehicle setup changes, for which the driver´s feedback solely could not be accurate enough to access small changes. This problem was even reported in more controlled environments, such as in passenger cars subjective evaluation of handling and steering feel, where disagreement between experts test drivers were reported (GÓMEZ *et al.*, 2015).

This scenario suggests the need of methods to quickly access vehicle performance at the racetrack. As an example, Vaduri & Law (2000) developed algorithms utilizing fuzzy logic with the aim to identify the vehicle balance. Their algorithm is capable to pin out understeer and oversteer events in actual data.

In recent years, aiming to cut costs in racing categories, more time is invested in vehicle simulations and driver simulators instead of actual track testing. Besides, time reduction at racetrack was not reacted by commercial analysis packages (e.g. in form of novel analysis solutions to reduce time spent by data engineers) (PARKER; HARGRAVE, 2016), which still motivates the development of alternatives data analysis packages and methods.

In respect to commercial data analysis packages, Segers (2014) proposes analysis techniques with the use of math channels to quickly access key performance indicators (KPI’s). He suggests the use of

metrics, where each metric is a single value per lap of a given statistical parameter. Metrics can be extracted from the entire distance or time over a complete lap or from specific locations at the circuit, such as a given corner or straight (SEGERS, 2014). Common metrics are average throttle position, average speed, percentage of the lap spent on brakes, etc.

The main advantage of metric use is the capacity to summarize large amounts of data in *run charts plots* (SEGERS, 2014). These plots display each metric as function of lap number and give a general overview of vehicle performance, where trends and improvements along runs can be more easily identified.

2.6.1.1 Grip factors

Based on the G-G diagram concept, Segers (2014) presents a technique to estimate grip levels of a racecar from accelerometer data, the so-called *grip factors* (GF). Lateral and longitudinal accelerations are used to create math channels of *overall grip* level, *braking grip*, *acceleration grip*, *cornering grip* and *aerodynamic grip*. Each math channel uses either combined acceleration or lateral and longitudinal accelerations depending on operation conditions. These math channels only store data within a predefined boundary, a technique known as signal gating (SEGERS, 2014). The following paragraphs describe the details of each grip factor.

Overall grip factor ($GF_{overall}$), defined by Equation 2.2, is the combined acceleration constrained by acceleration thresholds. Constraints are set to exclude data where the vehicle is power limited. As a result, data from straight-line acceleration are not included in the grip factor because the vehicle is power limited and instead of grip limited.

$$GF_{overall} = a_r \; for \; a_r > 1G \tag{2.2}$$

Combined acceleration, defined by Equation 2.3, is the resultant acceleration component (a_r) from longitudinal and lateral accelerations.

$$a_r = \sqrt{{a_x}^2 + {a_y}^2} \tag{2.3}$$

Braking grip factor ($GF_{braking}$) is defined by Equation 2.4. Negative longitudinal acceleration signal gating is triggered for values below *1G* to capture braking phase.

$$GF_{braking} = a_x \; for \; a_x < 1G \tag{2.4}$$

Acceleration grip factor, Equation 2.5, aims to record data only for acceleration phase. For this reason, constraints are set to trigger positive longitudinal acceleration and lateral acceleration within *0.5G*. Both criteria must be met at the same time.

$$GF_{acceleration} = a_x \; for \; a_x > 0 \; and \; |a_y| < \; 0.5G \tag{2.5}$$

Cornering grip factor, Equation 2.6, aims to collect data from cornering maneuvers. To do so, signal gating is triggered for lateral acceleration above *0.5G*.

$$GF_{cornering} = a_y \; for \; |a_y| > \; 0.5G \tag{2.6}$$

Aerodynamic grip factor is defined in a similar manner, except that thresholds are set to include speed dependency of aerodynamic forces on cornering maneuvers:

$$GF_{aero} = a_y \; for \; a_y > 1G \; and \; v_x > \; 120 \; km/h \tag{2.7}$$

where v_x is the vehicle speed.

The signal gating thresholds presented in this section are recommendations for a typical GT racecar; however, Segers (2014) emphasizes the importance of adjust this values according to the vehicle characteristics.

From the grip factor dataset, various *metrics* could be extracted, i.e. cumulative sum of the signals, maximum and average values. Segers (2014) recommends averaged values because the cumulative sum of signals in function of track distance is highly dependent on the distance signal accuracy, which is also affected by the racing line taken at a given lap. Besides, maximum values represent only a small percentage of the dataset and are prone to be affected by signal noise.

2.6.2 Driver´s performance

Nowadays, data gathering for driver´s training is spread from top to bottom level of motorsports. Even track-day drivers and karting championship have data analysis in their schedule (COSWORTH,

2016). The problem lies, again, in the time available to extract information.

Almost two decades ago, Mitchel (2000) had reported driving schools that were not often using data acquisition for training driving students due to limited time available during classes. According to him, the coach´s feedback may suffice to improve performance of a novice driver. However, as students get closer to instructor's performance, small improvements become less obvious and data logging becomes a crucial part of training.

In actual racing environment, data gathering is a basic requisite for performance improvements. It points out things the driver has not noticed and confirms others the driver has already figured out (BENTLEY, 2011).

Most of driver´s activities analysis is performed by comparing a given lap with a faster reference lap. Data overlay is a basic function of any quality data analysis package (SEGERS, 2014), and provides a direct measure of braking points, cornering speed, gear shifting, etc.

Although data overlay from laps of the same driver is meaningful, having a reference lap from another driver is desirable. Laps from the same driver are essential for driving consistency improvements along the runs, while comparing to another driver´s lap reveals different driving approaches.

To optimize the time spent in data analysis, Mitchell (2000) suggests the use of lap statistics to access overall performance before more in depth analysis. These lap statistics are sector times, average throttle position, average steering angle, average braking and minimum speed. In Mitchell (2000), lap statistics is presented in a tabulated form as an aid to training test drivers. According to concept Segers (2014), lap statistics is *metrics* and could be presented in *run charts* for a more visual presentation of data.

Important to highlight, although a racing driver should know how to properly interpret driver´s activity data (BENTLEY, 2011, SEGERS, 2014); a racing driver is not a data engineer. Thus, data amount presented to drivers should not be overwhelming. Small steps of improvements at time must be planned after each practice outing. Besides, more visual presentation of data such as track maps colored with throttle application sometimes gives more insights to the driver than data squiggly lines.

Driver's self-confidence should be also taken into account. Possible improvements on driving techniques should be tackled in conjunction with the driver understanding of data. In other words, a data

engineer must provide directions for the driver himself/herself see on data where he/she could improve and highlight progress along the race event. To knowledge of the author, currently there is no scientific methodology reported in literature for training racing drivers with data acquisition, even though various analysis techniques have been reported.

In the following chapter, an overview on lap time simulation is given. Methods for simulation such as Monte Carlo and Design of Experiments are presented with the aim to provide a background for the methodology proposed late on this work.

3 MODELING AND SIMULATION METHODS

> *Racecar simulation is a powerful tool, but it must always be cross-referenced by actual experience, hand calculations, and ultimately the stopwatch.* (NOWLAN, 2016).

3.1 Introduction

This chapter provides a background on modeling and simulation methods. First, Monte Carlo method is addressed focusing on the underlying reasoning and techniques for stochastic simulations. Secondly, general concepts of modeling are presented. Third section gives an overview of modeling strategies for lap time simulations based on the literature. After, a discussion on verification and validation of simulations is given. The enclosing section addresses accuracy metrics and accuracy criteria for simulations.

3.2 Monte Carlo method

Monte Carlo is a stochastic method that uses sampling random numbers to investigate a problem (SOLONEN, 2006). For Raychaudhuri (2008), "this method of simulation is very closely related to random experiments, experiments for which the specific result is not known in advance".

Monte Carlo simulations are applied to many areas of study, from natural and social sciences to engineering fields (RAYCHAUDHURI, 2008). Not surprisingly, there is no single Monte Carlo type of simulation (HARRISON, 2010). However, they do follow a pattern: systems are modeled as statistical distributions, often probability density functions (PDF's), from which input parameters are randomly sampled. Each set of the sampled parameters generates a set of output parameters used to solve numerical problems or to compute statistics of interest. (RAYCHAUDHURI, 2008; HARRISON, 2010).

Raychaudhuri (2008) presents a comparison between deterministic and stochastic models. Deterministic models evaluate mathematical expressions based on a set of input parameters (Figure 3.1).

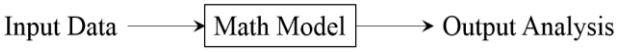

Figure 3.1: Mathematical models (RAYCHAUDHURI, 2008).

In cases where input data of deterministic models are composed of unique set of input parameters, influence of external factors are not being considered. Raychaudhuri (2008) highlights that “realistic models are subject to risk from the systematic variation of input parameters”. For this reason, many researches includes a baseline, a best and worst-case scenarios to accomplish with external variations of input parameters. This method is often referred to as case-based modeling (Figure 3.2).

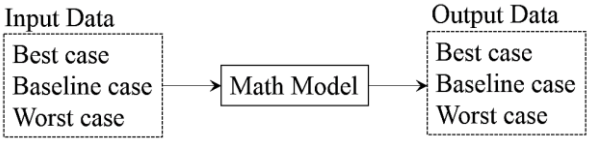

Figure 3.2: Case-based modeling. Adapted from Raychaudhuri (2008).

Raychaudhuri (2008) underlines that case-based modeling can have shortcomings. The identification of best/worst case scenarios might be difficult to perform and they may happen at different time for different parameters. This implies the need of more cases to include the combination of scenarios, which brings another disadvantage related to the management of various versions of input datasets. Monte Carlo method emerges as a handy tool for testing various combinations of input parameters and investigate its effects on model output (RAYCHAUDHURI, 2008).

Monte Carlo simulations became a popular tool for problems difficult to solve by analytical methods or for problems with costly, time-consuming or impractical experimentation (HARRISON, 2010). However, it also has disadvantages, mainly related to computational costs and the quality of results, which is related to the quality of the input parameters.

Raychaudhuri (2008) presents a general methodology typically used for Monte Carlo simulations. This methodology is composed of four steps: static model generation, input distribution identification, random variable generation, and analysis and decision making of the simulation outputs. Each step is briefly presented in the following paragraphs and further details are referred to Raychaudhuri (2008).

Static model generation addresses the underlying physics of the simulation. Mathematical expressions and relationships are developed. According to Raychaudhuri (2008), this step resembles the schema present in Figure 3.1.

Input distribution identification deals with the type of distribution each input parameter may have. According to Harrison (2010), common examples are: uniform, exponential, normal, and Poisson distributions. This step is supported by historical data of input parameters.

Random variable generation forms a set of input parameters for the deterministic model. It takes random samples from the distribution defined in the previously step. Raychaudhuri (2008) highlights that this is the core step of a Monte Carlo simulation. Random variable generation is further explored in the next section, where a method known as Latin Hypercube Sampling is presented.

Analysis and decision marking is performed after Monte Carlo simulations were run. Output parameters are statistically analyzed to provide confidence intervals of simulation results.

3.2.2 Latin Hypercube Sampling

Space-filling experimental designs aims to cover most of the input domain in cases where statistical assumptions about the relationship between input/output parameters of models may be scarce (VIANA, 2013). Most popular space-filling sampling methods are Latin Hypercube, orthogonal arrays and Hammersley designs (VIANA, 2013). This section focuses on the underlying concepts of Latin Hypercube Sampling (LHS) method and briefly overviews optimized forms of LHS.

LHS method was initially developed by McKay, Beckman and Conover (1979). Based on the Latin square experimental design, it attempts to mitigate the confounding effects of experimental factors without increasing the size of the experiment. LHS aims to represent each value of a variable in the samples, independently on their values importance (CHENG; DRUZDZEL, 2000).

Viana (2013) presents a formal definition of LHS, which is reproduced hereafter:

Let the p x d (points x dimension) matrix $X = \left[x_1\ x_2\ \ldots\ x_p\right]^T$ be the experimental design matrix. Each column represents a variable and each row $x_i = \left[x_i^{(1)}\ x_i^{(2)}\ \ldots\ x_i^{(d)}\right]$ represents a sample.

For example, let drag coefficient (C_d) and engine efficiency (η) be the two variables of interest (d = 2) for a sampling space of 10 points (p = 10). The dimensions of the design matrix X are 10 x 2:

$$X = \begin{matrix} \\ 1 \\ \vdots \\ 10 \end{matrix} \begin{matrix} C_d & \eta \\ \end{matrix} \begin{bmatrix} 0.45 & 0.88 \\ \vdots & \vdots \\ 0.41 & 0.91 \end{bmatrix}$$

where each row is a design sample x_i. For instance, $x_1 = [0.45 \quad 0.88]$ and $x_{10} = [0.41 \quad 0.91]$ are the first and last design samples of the above matrix *X*.

Aiming to assign values uniformly on the sampling space, LHS method divides each of *d* dimensions into *p* equal bins. For each bin, only one value is randomly assigned.

Because of the randomness, it could or could not be the optimum location for a good space filling sampling space (VIANA, 2013). Figure 3.3 illustrates this phenomenon.

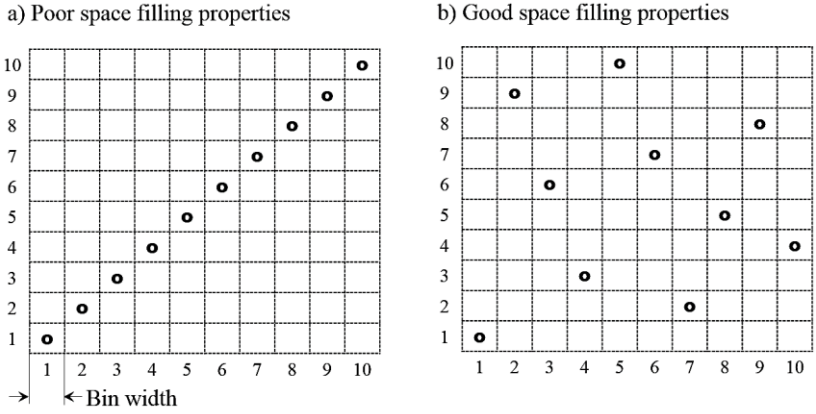

Figure 3.3: LHS examples with d = 2 dimensions and p = 10 points. Adapted from Viana (2013)

Figure 3.3 presents examples of a LHS design for two variables (d = 2). Regarding space filling properties (a) illustrates a poor design and (b) illustrates much better design, since data is uniformly spread along the design space. Viana (2013) underlines that although unlikely to happen, LHS can have poor space filling properties such as the extreme case shown in Figure 3.3-a.

In face of that, optimized forms of LHS were developed, often referred to as Optimized Latin Hypercube Sampling (OLHS). With the aim to improve space filling properties, focus is given to the optimization of point location on the design space. Generally, researches

addresses the optimization algorithm and the objective function to reduce computational costs, although only few addresses both at the same time (VIANA, 2013).

Far from being trivial, Viana (2013) states that the optimization of the LHS is a combinatorial optimization problem with search space of order $(p!)^d$. As an example, optimization of a LHS with d = 2 dimensions and p = 20 points would have to select the best design from more than 10^{36} possible designs. For d = 3, possible combinations would raise to more than 10^{55} (VIANA, 2013).

Detailed discussion about optimization algorithms of OLHS methods are beyond the scope of this work. To the interested reader, different approaches to optimize LHS methods are referred to Viana (2010) and Viana, Venter and Balabanov (2013).

3.3 Modeling – general considerations

When defining the model, Harrison (2010) emphasizes the importance of a careful analysis of the simulation aims. He suggests key points to be considered in defining a model:

What are the desired outputs of the simulation? Modeling assumptions and level of complexity of models depends on the specific applications of the simulations. Different questions are answered with different simulation results. To define a good model one should consider the aim of simulation results (HARRISON, 2010).

How accurate must the outputs be? Regarding the application, varying levels of accuracy are required. As an analogy with data acquisition in motorsports, engine temperature measurements may be gathered at 10 Hz with sufficient accuracy. On the other hand, due to the high-frequency nature of vehicle suspension systems, damper displacement may be logged at a frequency higher than 100 Hz (SEGERS, 2014).

How exactly the object can/must be modeled? This topic addresses the level of detail of the model and the available computational capabilities. According to Harrison (2010), although a phenomenon could be modeled down to the finest level of detail, computational cost would make the simulation unfeasible for some applications. In summary, although an object *can* be modeled in such detail, it does not mean it *must* be modeled that way.

How exactly input parameters are defined? As seen in Figure 3.1, mathematical models are feed with input data to generate outputs. A

simulation model is only feasible if its input parameters are measurable, which involves technological and economic factors.

To illustrate, Harrison (2010) states that the most accurate weather simulation would consider interactions down to subatomic level, which is beyond the actual computational capabilities and ability to measure input data. Instead, simulations use fluid dynamics and thermodynamics with input data being the weather conditions measured at many locations around the world.

The next section provides an overview of lap time simulations, where modeling strategies and its main application are discussed.

3.4 Lap time simulations – an overview

From an engineering standpoint, lap time simulation needs to model accurately the dynamic behavior of a racecar, predict lap times and have low computational costs to allow many configurations of a racecar to be tested within reasonable time (BRAYSHAL; HARRISON, 2005).

Lap time simulations follows into three categories: *steady state*, *quasi-steady state* (also referred to as *quasi-static* models) and *transient* models. Each modeling strategy are briefly described in the following paragraphs and are referred to Siegler, Deakin and Crolla (2000).

Steady state models assumes the vehicle is in permanent equilibrium and its derivatives with respect to time are zero. For steady state simulations, various iterations are needed in order to converge to the equilibrium state after a steering input at a constant forward velocity, for example. These models are incapable to simulate trail braking maneuvers, since velocity and lateral acceleration are changing simultaneously and thus are inherent time dependent.

Quasi-steady state models are similar of steady-state models except for the circuit parameterization strategy. Each corner is designed as a decreasing path of a series of constant radius turn. The aim of this strategy is to imitate an increasing steering towards the apex of the corner without solving transient equations. The vehicle limit of adhesion can be solved iteratively by steady-state equations for each segment of the corner or it can be accessed by an independently generated G-G diagram (BRAYSHAL; HARRISON, 2005).

Transient simulations involves numerical integration of equations of motion with respect to time (BRAYSHAL; HARRISON, 2005). Non-linear effects such as translational and rotational inertias, lateral and longitudinal weight transfer are considered.

Siegler, Deakin and Crolla (2000) compared a three-degree-of-freedom steady state, quasi-steady and transient models for case of a J-turn maneuver: at constant speed, and for a J-turn with combined braking and steering towards the corner (trail braking).

The three modeling strategies were found to be equivalent for the J-turn at constant speed. On the second case, however, the steady-state model was unsuitable to reproduce the transient maneuver in a realistic manner, since braking and steering were performed in two distinct phases.

Vehicle response from the quasi-steady state simulation was a good approximation of the transient simulations. Similar conclusions were found for a more complex seven-degree-of-freedom vehicle model in Brayshaw & Harrison (2005), where a complete lap was simulated and the effects of racing line and center of gravity location were investigated.

The next section presents the main concepts and literature recommendations on verification and validation of simulation models.

3.5 Verification and validation

Simulation environments, mathematical models and measurement tools are well established in the present days. However, there is a lack of methodological rigor on the validation procedures adopted by many vehicle dynamics simulations in the literature (KUTLUAY; WINNER, 2014).

Kutluay & Winner (2014) presents various definitions of *verification* and *validation*. In simple terms, they define *verification* as "building the model right" and *validation* as "building the right model".

For the American Institute of Aeronautics and Astronautics (1998 apud SARIN et al., 2003), regarding computational fluid dynamics, *verification* "is the process of determining that a model implementation accurately represents the developer's conceptual description of the model and the solution to the model".

From the same reference, *validation* is defined as "the process of determining the degree to which a model is an accurate representation of the real world from the perspective of the intended uses of the model".

Validation is related to the application of the model. A vehicle model valid for steady-state maneuvers, for example, may not be valid for ride comfort analysis. Kutluay & Winner (2014) state that a model is only valid within the design limits and the intended application and that

there will always be discrepancies between simulated and experimental data.

The fact that randomness are an inherent part of some physical phenomena, and the fact that measurements of parameters and data gathering of a system behavior are prone to random errors put in check a definitive validation of a model. In fact, Kutluay & Winner (2014) affirm that absolute validity of a model is refuted by many experts in the literature.

Although validation procedures exist, most of the applications of vehicle dynamics simulations rely only on visual comparison and subjective judgment of the results. In addition, often the development team of the model also decides subjectively whether the simulation is valid or not, which for Kutluay & Winner (2014) puts in question the credibility of these models.

On the other hand, many authors consider subjective assessments, such as *face validity*, and visual techniques as an accepted method for model validation (JACHNER; BOOGAART, 2007). Based on expert knowledge, these methods evaluate how feasible the model is, and how close measured and simulated data are. (RYKIEL, 1996 apud JACHNER; BOOGAART, 2007).

In conclusion, Kutluay & Winner (2014) point out that validation of vehicle dynamics simulation should consider the physical phenomena characteristics it aims to reproduce. This process includes planning the validation testing maneuvers, explicitly defining experimental procedures, accuracy criteria and validation metrics early in the design process.

From extensive review provided by Kutluay & Winner (2014), it is observed that little attention is given by the literature to accuracy criteria and validation metrics of simulation. This matter is aggravated regarding lap time simulations, where validation is barely addressed. The next section deals with this topic.

3.6 Accuracy metrics and criteria for simulation validation

Most of lap time simulations are validated by visual comparison with experimental data. Although accepted by some experts, it does not yield to a tangible measure to compare models across the literature. Aiming to provide insights on how validation of lap simulations can be supported by statistic metrics, this section presents common deviance measures for validation used in other research areas.

To this work, only the most common measures for absolute scaled time-series are presented: mean absolute error (MAE), mean squared error (MSE) and root mean squared error (RMSE).

The American Society of Mechanical Engineers (ASME) committee on verification and validation in computational solid mechanics (2004 apud SARIN et al., 2003) defines two steps for model validation:

1. Quantitatively comparing the computational and experimental results for the response of interest;
2. Determining whether there is an acceptable agreement between the model and the experiment for the intended use of the model.

The first step deals with *accuracy metrics* to evaluate discrepancies of measured and simulation data. The second step addresses *accuracy criteria* to accept or reject simulation results.

In Jachner & Boogaart (2007), various statistic measures are compared aiming to illustrate how they provide varying results evaluating common real-world problems. Although accuracy metrics are key for validating simulation results, Jachner & Boogaart (2007) point out that not only quantitative analysis are used, validation is commonly supported by expert knowledge to assess qualitatively the simulation accuracy.

For processes having different velocities, shifts in time or systematic differences, qualitative evaluation is especially important because exclusive use of quantitative analysis could lead to misleading conclusions (JACHNER; BOOGAART, 2007). Figure 3.4 illustrates this scenario.

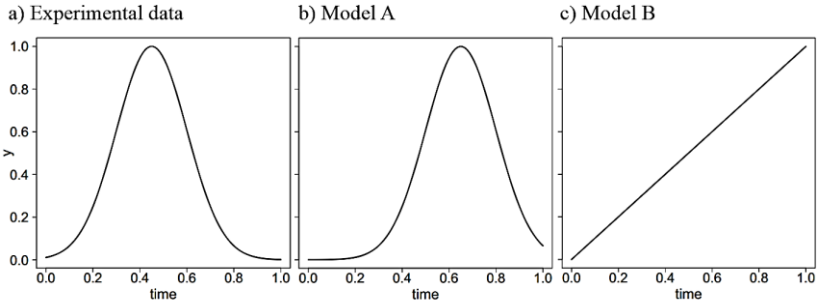

Figure 3.4: Comparison of two models against experimental data. Adapted from Jachner & Boogaart (2007)

In Figure 3.4, three plots are presented: experimental data (a) and simulation results of model A (b) and model B (c). Both models A and B aims to represent the phenomenon for which experimental data is presented.

In this simple example, humans would probably consider model A more accurate than model B. In contrast, a quantitative evaluation by the mean absolute error (MAE), defined by Equation 3.1, results in model B being more accurate than model A, which clearly underestimates the quality of model A (JACHNER; BOOGAART, 2007).

$$MAE = \frac{1}{n}\sum_{t=1}^{n} |y_t - \hat{y}_t| \tag{3.1}$$

At this point, some considerations must be addressed. Correct selection of accuracy metric is key for correct assessment of simulation discrepancies. According to Jachner & Boogaart (2007), the reason most people would choose model A instead of model B is that human decision is based on identification of data patterns instead of numerical values.

In this way, a robust metric should also include measures of data patterns. In some research areas, such as vehicle safety, this issue has already been addressed. Sarin et al. (2010), for example, developed a metric in which simulation errors were assessed by three independent measures associated with phase, magnitude and slope of the signal.

In contrast, validation of lap time simulations is mainly performed based on expert knowledge by visual comparison of datasets; see Callea (2004), Velenis & Tsiotras (2005), Simon et al. (2008) and Dal Bianco & Lot (2015) for example.

For time-series comparison, according to Jachner & Boogaart (2007), the most common deviance measures are: mean absolute error (MAE), defined by Equation 3.1, mean squared error (MSE), Equation 3.2, and root mean squared error (RMSE), Equation 3.3. In these equations, y_t is the experimental data and $\hat{y}_t$ is the simulation data at a given time, *t*.

$$MSE = \frac{1}{n}\sum_{t=1}^{n} (y_t - \hat{y}_t)^2 \tag{3.2}$$

$$RMSE = \sqrt{\frac{1}{n}\sum_{t=1}^{n} (y_t - \hat{y}_t)^2} \tag{3.3}$$

Various types of discrepancies can take place whenever two sets of data are compared. Depending on application, such discrepancies may be critical or not. For instance, relative differences between simulation and actual data may be more important than the magnitude of datasets (JACHNER; BOOGAART, 2007).

In statistics, many measures exists to access model accuracy. Chai & Draxler (2014) highlight that "statistics are just a collection of tools" and researches are in charge of the appropriate selection of these tools. Because deviance measures are defined differently, see Equations 3.1 to 3.3, they are expected to provide different results, which leads to the observation that sometimes multiple measures are required to access detailed error evaluation (CHAI; DRAXLER, 2014).

Two cases are illustrated in Figure 3.5: noisy data (a) and varying speed data (b), which is the closest case of lap time simulations. In this example, reference function is defined by $f(t) = \frac{3}{2}.sin(2t\pi) + 0.75$ and $g(t)$ are special functions to represent real-world data.

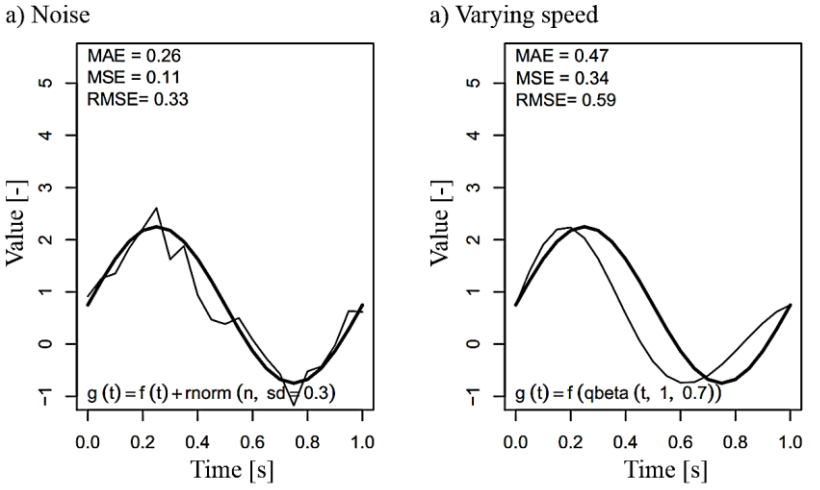

Figure 3.5: Measures of two sets of data. Noisy and varying speed datasets are considered in comparison to the reference data. Adapted from Jachner & Boogaart (2007).

From Figure 3.5, RMSE has higher magnitude on both cases (a) and (b) compared with MSE and MAE, which was expected for the following reasons:

1. Whenever a number is smaller than the unit, the magnitude of its square root is greater than that number, in this case MSE < 1 which leads to RMSE > MSE.
2. MAE attributes the same weight to all errors while RMSE attributes greater importance to errors with larger absolute values. In this way, RMSE is by definition never smaller than MAE (CHAI; DRAXLER, 2014).

From case (a) to case (b), all measures have risen in magnitude, which indicates an agreement on model error evaluation. However, MAE increased 80.7%; MSE, 309%; and RMSE increased 78.8%. Considering the magnitude of MSE was roughly 1/3 of MAE and RMSE in case (a), one can conclude MSE is less sensitive to noisy data than RMSE and MAE are.

Figure 3.6 illustrates another two cases: shifted datasets (a) and combined effects of shifted and scaled data (b).

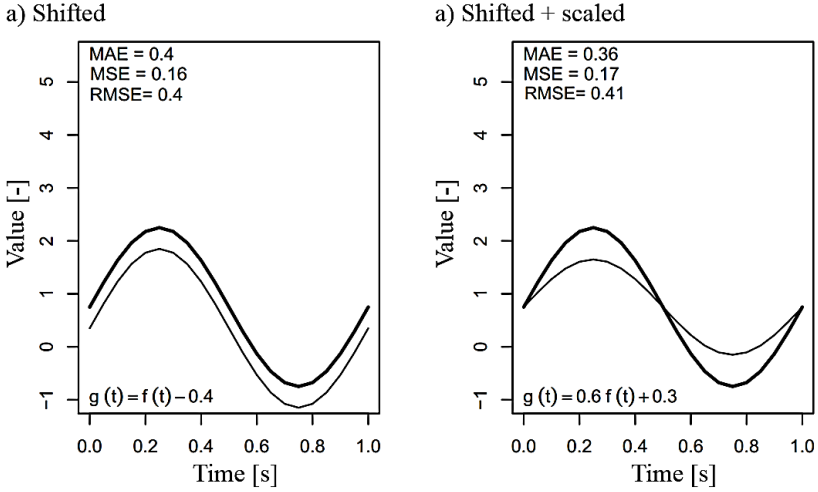

Figure 3.6: Measures of two sets of data. Shifted and shifted + scaled datasets are considered in comparison to the reference data. Adapted from Jachner & Boogaart (2007).

According to Figure 3.6, MAE and RMSE are similar for shifted data (a). In the case of shift and scaled data (b), RMSE magnitude slightly increases as MAE decreases 10%. MSE is almost insensitive to changes in cases (a) and (b) and remains about constant. Again, the three measures agreed on error evaluation.

In this section, common deviance measures were presented and discussed. As stated earlier, each measure emphasizes different aspects of error. For this reason, Chai & Draxler (2014) emphasizes that a combination of measures such as RMSE and MAE are often required to evaluate model performance.

The assessment of simulation error, presented in the results section, uses RMSE because it is more sensitive to absolute differences than MAE is. However, an extensive discussion about proper deviance measures for lap time simulations is beyond the scope of the present work.

The next chapter presents materials and methods used in this research. Focus is given to the vehicle parameters estimation with the help of Monte Carlo simulations.

4 MATERIALS AND METHODS

> *We should nevertheless always keep in mind that simulation is merely a tool and that it should be used as such. The results produced by the simulation software are as accurate as the accuracy of the modeled parameters.* (SEGERS, 2014).

4.1 Introduction

The Brazilian touring car championship *Brasileiro de Marcas*, started in 2011 as one of the major Brazilian racing categories. The championship promotes vehicle manufactures by racing silhouette racecars resembling compact sedans such as Toyota Corolla, Renault Fluence, Ford Focus and Chevrolet Cruze. Besides the marketing appeal, the championship aims to be a driver's competition instead of manufacture's competition. For this reason, technical rules provide little room for parts development; racecars share identical tubular spaceframe concept, powertrain and aerodynamic appendices. Thus, racing teams focus on driver performance, suspension and aerodynamic adjustments at race events.

In this chapter, materials and methods of this research are presented. Focused on the method, Figure 4.1 gives an overview of the speed profile simulation procedure adopted.

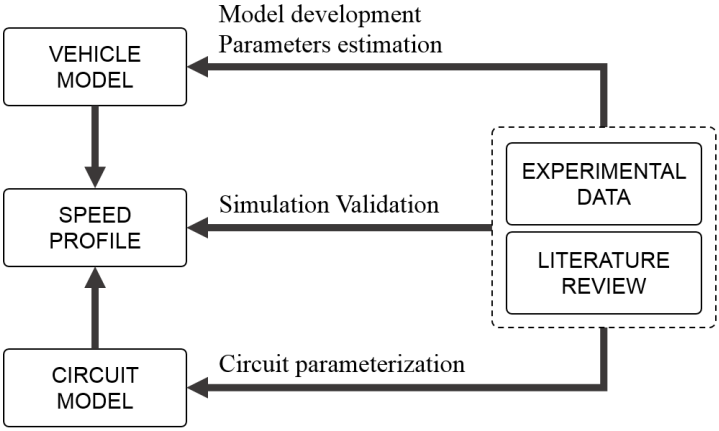

Figure 4.1: Overview of the method used to simulate the speed profile of the racecar.

To perform the simulations, a vehicle and a circuit model were developed. Experimental data from racetrack and literature review supported the model development and its assumptions; the input vehicle parameters estimation; simulation validation procedures; and the circuit parameterization.

In the following sections, the data acquisition system and the racecar from which data were acquired are first presented followed by a description of the coordinate system used in this work. Later, vehicle model and its assumption are exposed alongside vehicle and circuit parameterization.

4.2 The racecar

A 2016 Toyota Corolla competing at *Brasileiro de Marcas* championship was the source of experimental data for this research (Figure 4.2). Considering the rules do not allow unofficial tests, data available for this work comes exclusively from the previously race events and literature review.

Figure 4.2: 2016 Toyota Corolla competing at *Brasileiro de Marcas* championship (BARROS, 2016).

The 2016 season provided eight events held in seven different Brazilian circuits from which data were gathered. 2016 vehicles were

slightly modified from the previously years, with the most significant change being a lower limit for engine maximum speed. For this reason, only 2016 data were used in order to avoid diverged data on the parameter estimation process (discussed in section 4.7). Experimental data were divided into *training data* (from which the model input parameters were estimated) and *test data* (data used to test the validity of the model).

The data acquisition system of the racecar consists into a MoTeC SDL3 dashboard, which has 16 MB of logging memory and an integrated 3-axis accelerometer (± 5G) logged at 25 Hz. The dashboard also records data from an analogue steering angle sensor (25 Hz) and a GPS MoTeC L10 connected via RS-232 serial port (10 Hz). Although the GPS antenna is mounted externally, its aerodynamics effects are neglected due to the small size of the unit (48 mm x 41 mm x 14 mm). In addition, there are sensors logged from the MoTeC M400 ECU via CAN Bus communication at various sampling rates, mainly from the engine and gearbox. To the interest of this work, there are also hall effect sensors at the rear wheels (25 Hz), throttle position, and engine speed (20 Hz) measurements.

All vehicles of the championship are front-wheel-drive powered by a Berta TR4 engine. This is a Ford Duratec® based engine, naturally aspirated, 4 cylinders with a 2300 cm^3 of total displacement. Due to the nature of this specified racing class, engines are sealed to prevent modifications.

4.3 Vehicle model

Figure 4.3 presents the vehicle coordinates system used in this research.

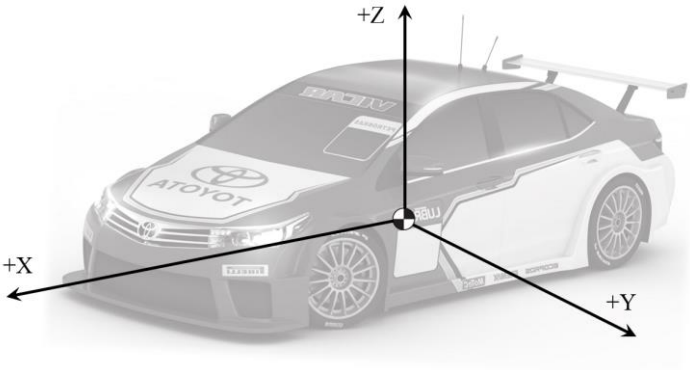

Figure 4.3: Right hand vehicle coordinate system.

Defined according to Sayers (1996), it is a right hand coordinate system with forward positive X-axis, Y positive to the left and Z positive upward, with its origin located on the vehicle center of gravity (C.G).

The velocity profile of the vehicle was simulated in this work based on the assumption of a point-mass being driven at the boundaries of the G-G diagram. The vehicle model consists of a point-mass reacting to external forces limited by its tire/road coefficient of friction (μ). This coefficient μ is assumed to limit both, lateral (a_y) and longitudinal (a_x) car accelerations. Furthermore, μ is considered constant, leading to the following assumptions:

1. The grip available at the racetrack does not change. In a real circuit, however, different locations of the racetrack may have varying levels of grip.
2. The constant coefficient of friction acts as the tires were operating at its optimum slip angle and slip ratios, thus generating maximum lateral and longitudinal forces.
3. Any changes in tire load neglects changes of the coefficient of friction. Again, a simplification because coefficient of friction is function of load. As load increases, μ also increases. Changes in tire load are mainly related to

aerodynamic lift and lateral/longitudinal load transfer, both neglected in this work.

Figure 4.4 summarizes the vehicle model assumptions by its G-G diagram.

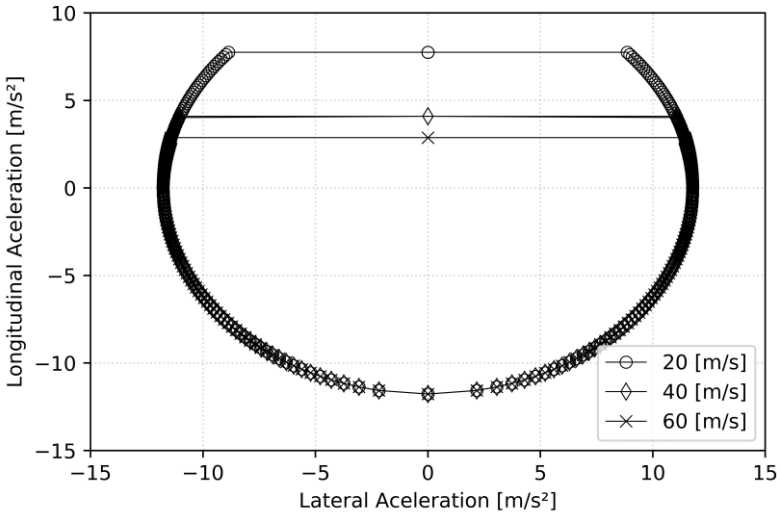

Figure 4.4: G-G diagram modeling of the vehicle in function of speed.

Because the coefficient of friction is constant, the G-G diagram has constant radius (Figure 4.4) except for the upper part of the diagram, which is trimmed by the engine power, dependent of speed because of external resistance forces such as aerodynamic drag.

Equation 4.1 express the assumed coefficient of friction (μ) as function of the vehicle maximum lateral acceleration.

$$\mu = \mu_y = \frac{F_y}{m.g} = \frac{a_y}{g} \tag{4.1}$$

In this equation,
μ – assumed coefficient of friction [-];
μ_y – lateral coefficient of friction [-];
F_y – lateral force generated by the tires [N];
m – overall mass of the vehicle [kg];
a_y – lateral acceleration [m/s²];
g – gravitational acceleration [m/s²].

According to Segers (2014), although simple, a point-mass vehicle model is capable to generate a velocity profile in a given circuit with satisfactory accuracy to draw conclusions about the characteristics of a circuit. In this research, vehicle model was implemented by the means of power flow in the AMESim® software. The principles behind the modeling process are explored in Figure 4.5, where a mass component in a multiport simulation environment is shown as well as its internal variables.

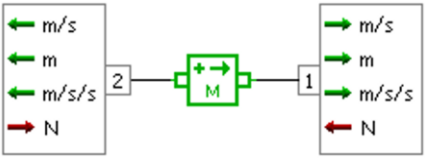

Figure 4.5: Internal variables of a mass component in the multiport software AMESim®.

The main concept of a multiport-domain simulation environment lies on the power flow between components, given by the product of flow and effort variables (SILVA, 2005). In the example above, the inputs (forces in both ports) are the effort variables and the outputs (velocity) are the flow variables. Based on the Second Newton's Law, this component gives also displacement and acceleration from the integration and derivative of the velocity output.

Figure 4.6 shows the vehicle model concept implemented in the multiport-domain software AMESim®:

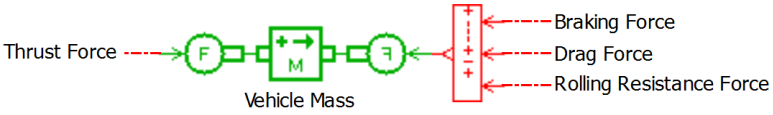

Figure 4.6: Vehicle model.

In this model, the equation of motion is defined as follows:

$$m.a_x = F_e - (F_b + F_d + F_r) \qquad (4.2)$$

where,
a_x – forward acceleration [m/s²];
F_e – thrust force [N];

F_b – braking force [N];
F_d – drag force [N];
F_r – rolling resistance force [N].

4.3.1 Thrust force

For a low powered vehicle, most part of the time longitudinal acceleration is limited by the engine and not by the tires (SEGERS, 2014). Based on this statement, this work considers that wheel spin does not occur when throttle is applied. This assumption allows designing a driver controller in such manner that thrust force from engine is always present, whenever forward acceleration is not limited by braking and/or trail braking on cornering maneuvers. In other words, the throttle either is off or applied in wide-open throttle (WOT).

The thrust force (F_e) is given by Equation 4.3, and the model implementation of the powertrain is shown in Figure 4.7

$$F_e = \frac{T.i_n}{R_R} \tag{4.3}$$

where,
T – engine torque [N.m];
i_n – gear ratio [-];
R_R – effective rolling radius of the tire [m].

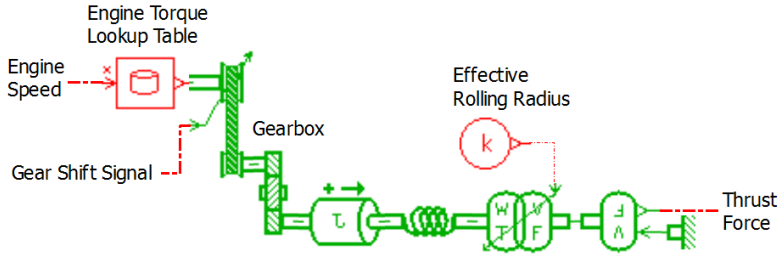

Figure 4.7: Powertrain model.

The powertrain model shown in Figure 4.7 is also a product of manipulation of effort and flow variables, embedded in the equations of each component. However, instead of translational mechanics presented before, the power is given by rotational mechanics where the effort variable is a torque [N.m] and flow variable is an angular velocity [rad/s].

In this model, engine torque is taken from a lookup table as function of engine speed. This torque is multiplied by a gear ratio according to the engaged gear on the gearbox and is transmitted to the traction wheels as power from the driveline torque (effort variable) and the wheel angular speed (flow variable). Finally, thrust force is derived from the effective rolling radius of the tires. Inertia and rigidity of the drivetrain components are necessarily included to respect the causality between physical components in the multiport environment, although their values are set negligible.

4.3.2 Braking force

According to the concept of tire friction circle, maximum braking force is achieved when braking in a straight line and must decrease as lateral force builds up. This phenomenon happens to accommodate the longitudinal and lateral forces to the available tire grip. In fact, grip is the maximum force available at the tires (F_t) and is function of lateral force (F_y) and braking force (F_b) vectors. When braking force is maximum, lateral force is zero and vice versa. Maximum tire force is calculated by Equation 4.4, lateral force by Equation 4.5 and the relation between these three forces is presented by Equation 4.6

$$F_t = m.g.\mu \tag{4.4}$$

$$F_y = \frac{m.{v_c}^2}{R} \tag{4.5}$$

$${F_t}^2 = {F_y}^2 + {F_b}^2 \;\therefore\; (m.g.\mu)^2 = \left(\frac{m.{v_c}^2}{R}\right)^2 + {F_b}^2 \tag{4.6}$$

where,
v_c – maximum cornering velocity [m/s];
R – cornering radius [m].

Isolating braking force (F_b) from Equation 4.6, its value is given by Equation 4.7 as function of lateral and total tire forces.

$$F_b = \sqrt{(m.g.\mu)^2 - \left(\frac{m.{v_c}^2}{R}\right)^2} \tag{4.7}$$

When a vehicle starts to negotiate a corner, lateral force starts to build up as braking force starts to decrease until it reaches zero at the apex of a corner. At this moment, only lateral force ($F_{y\,@apex}$) is acting on the tires and it takes all available force(F_t). Thus, the maximum speed that a vehicle could negotiate a given corner, in this paper called *maximum cornering velocity* (v_c), can be isolated from Equation 4.8 and defined by the coefficient of friction (μ), and the corner radius (R) such as:

$$F_{y\,@apex} = F_t \quad \therefore \quad \frac{m.{v_c}^2}{R} = m.g.\mu \xrightarrow{yields} v_c = \sqrt{g.\mu.R} \quad (4.8)$$

where, $F_{y\,@apex}$ is the lateral force at corner apex.

4.3.3 Drag force

Drag force is the only aerodynamic effect acting on this point-mass vehicle model. It is a vector force on X-axis in the negative direction (against thrust force) and its magnitude is calculated by the classic equation (KATZ, 1995):

$$F_d = \frac{1}{2}.\rho.C_d.A.v_x^2 \quad (4.9)$$

where,
ρ – air density [kg/m³];
C_d – drag coefficient of the car [-];
A – frontal area of the car [m²];
v_x– forward velocity [m/s].

4.3.4 Rolling resistance

According to Jazar (2008), a second order polynomial equation is adequate to fit experimental data of rolling resistance tests. This force is calculated by Equation 4.10 as function of a rolling resistance coefficient (u_r), given by Equation 4.11, and the vertical force applied on the tires. In this work, the vertical force will be the entire mass of the vehicle and is kept constant over the time:

$$F_r = u_r.m.g \quad (4.10)$$

$$u_r = u_0 + u_1.v_x^2 \quad (4.11)$$

where, $u_0\ [-]$ and $u_1\ \left[\frac{s^2}{m^2}\right]$ are experimental coefficients to fit rolling resistance data.

According to Jazar (2008), typical values are $u_0 = 0.015$ and $u_1 = 7e^{-6}$. As these values have been applied to passenger cars tires, they are used here due to the lack of modern racing tires parameters.

4.3.5 Driver´s model for braking strategy

Braking strategy stands for how the vehicle is controlled to optimize its braking capabilities in function of a circuit characteristic. When a driver is approaching to a corner, he brakes to reduce the vehicle speed at a certain distance from the corner apex. This distance (d) is function of the braking force, vehicle mass, forward vehicle speed (v_x) and the *maximum cornering velocity* (v_c). Equation 4.12 applies:

$$d = \frac{({v_x}^2 - v_c^2)}{2.F_b}.m \qquad (4.12)$$

Approaching a corner, this braking strategy yields to two different scenarios. The first scenario is illustrated in Figure 4.8:

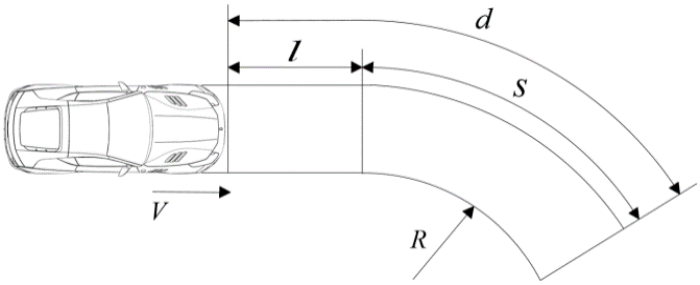

Figure 4.8: Minimum braking distance longer than the distance to corner apex.

Minimum braking distance (d) is longer than the distance (s) from the beginning of the corner (corner entry) to its apex. For this reason, the driver should anticipate the braking phase at a distance (l) before the corner entrance point. Otherwise, at corner apex the vehicle will exceed the tires limit of adhesion.

The second scenario is illustrated in Figure 4.9:

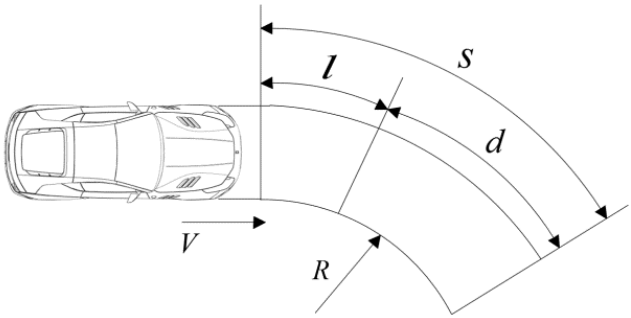

Figure 4.9: Minimum braking distance shorter than the distance to corner apex.

Minimum braking distance (d) is shorter than the distance (s) from the beginning of the corner to its apex. Therefore, the driver delays the braking phase by a distance (l) from the corner entrance.

4.4 Vehicle parameters

This section presents a literature review on typical vehicle parameters aiming to provide initial conditions for the parameter estimation process presented later in this section.

4.4.1 Drivetrain

Racecars of the *Brasileiro de Marcas* championship use a six speed sequential gearbox Xtrac® P426. Gear ratio changes are not allowed and the only set of gears available to the teams is presented below:

Table 4.1: Gear ratios allowed for the racecars.

Gear number	Gear Pair	Gear Ratio (i_n)
1st	13/39	$i_1 = 3.00$
2nd	15/30	$i_2 = 2.00$
3rd	14/22	$i_3 = 1.57$
4th	18/24	$i_4 = 1.33$
5th	19/23	$i_5 = 1.21$
6th	18/20	$i_6 = 1.11$
Final Ratio (bevel)	14/46	$i_f = 3.285$

Equation 4.13 defines gear ratio (i_n) presented in Table 1:

$$i_n = \frac{Z_{driven}}{Z_{drive}} \tag{4.13}$$

where,
Z_{driven} – number of teeth of driven gear [-];
Z_{drive} – number of teeth of drive gear [-].

To estimate transmission losses, Irimescu, Mihon and Pãdure (2011) conducted a study using a chassis dynamometer and FWD passenger car equipped with a manual gearbox. They concluded that drivetrain efficiency depends on both vehicle speed and gear ratio. Furthermore, drivetrain efficiency decreases as gear ratio decreases. Similar results were found by other researches such as in Changenet, Oviedo-Marlot and Velex (2006). The results of Irimescu, Mihon and Pãdure (2011) are summarized in Table 4.2:

Table 4.2: Drivetrain efficiency as function of gear ratio and engine speed for a FWD production sedan. (IRIMESCU; MIHON; PÃDURE, 2011).

Gear number	**Engine Speed (rpm)**	**Gear Ratio (i_n)**	**Efficiency (η)**
2nd	5500	$i_2 = 2.05$	$\eta \cong 91\%$
3rd	5500	$i_3 = 1.39$	$\eta \cong 89\%$
4th	5500	$i_4 = 1.03$	$\eta \cong 87\%$
5th	5500	$i_5 = 0.79$	$\eta \cong 72\%$

Aiming for accuracy, drivetrain efficiency should be modeled in function of gear ratio. However, to reduce the number of variables on the parameter estimation process, this study neglects gear ratio dependency and considers only an overall drivetrain efficiency. Because of a reasonable variety of slow and fast corners, Ayrton Senna Circuit was chosen as *training data* to provide a reasonable range of engine speeds. Figure 4.10 presents a histogram of a qualifying lap at Ayrton Senna Circuit, GO, Brazil.

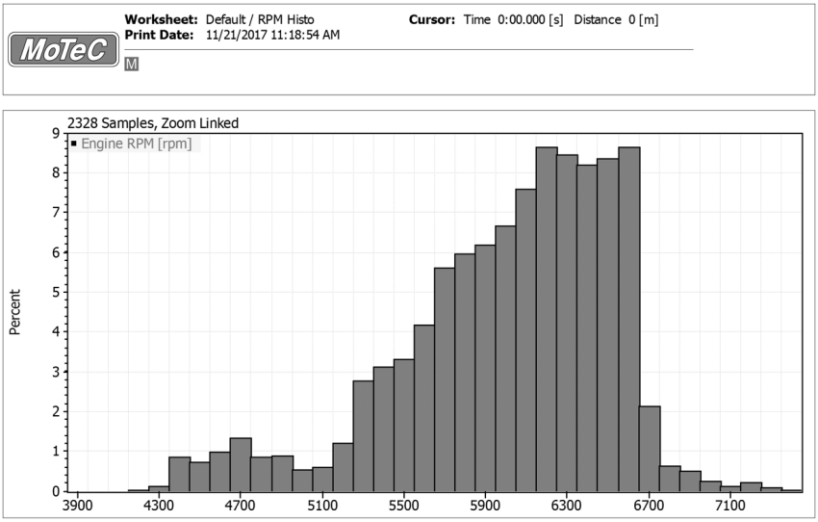

Figure 4.10: Histogram of engine speed at Ayrton Senna Circuit.

Engine speed is represented by bins and the Y-axis is the proportional time spent during the lap. Most part of the time, the engine operates between 5200 to 6700 rpm, which narrows the window for the overall efficiency estimation. Considering the engine speed is limited at circa 6670 rpm, the drivetrain overall efficiency of 80% was estimated as a baseline for the parameter estimation.

4.4.2 Effective Tire Rolling Radius

The effective rolling radius was calculated based on data gathered at previously race events. Figure 4.11 shows a scatter plot of the engine speed [rpm] versus vehicle speed [km/h] during a 25 laps race.

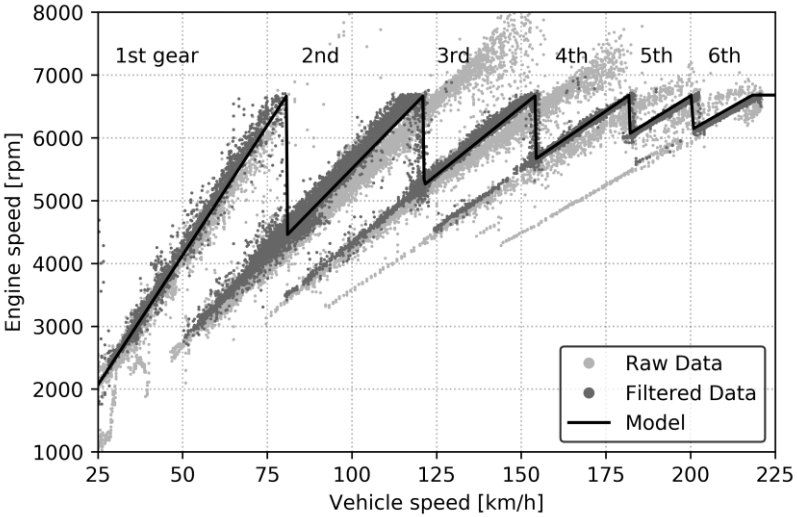

Figure 4.11: Engine speed [rpm] versus vehicle speed [km/h].

In this figure, the light grey scatter is the raw data from data acquisition system, the dark grey scatter is the filtered data for up shifting, and the black line shows the drivetrain model.

This plot gives six curves, one for each engaged gear. The inclination of each curve represents the total gear ratio. Theoretically, each scatter plot would fit a unique line. However, mainly due to wheel slip and lock up, the traces are sparse (SEGERS, 2014).

Figure 4.11 illustrates this fact; raw data gives different gear ratios due to wheel slip at braking. Therefore, to proper calculate the effective rolling radius, one needs first to acquire the effective gear ratio of the car for up shifting only. Raw data was filtered to exclude engine and vehicle speeds matching negative longitudinal acceleration (braking).

Finally, each gear ratio was fitted to the scatter traces by a linear polynomial regression and the effective rolling radius could be isolated using Equation 4.14 (JAZAR, 2008):

$$r_e = \frac{i_n \cdot i_f \cdot v_x}{\omega} \tag{4.14}$$

where,
ω – engine speed [rad/sec];
i_n – gear ratio [-];

i_f – final ratio [-].

4.4.3 Aerodynamic drag

As an initial guess for the parameter estimation, a literature survey was conducted to find typical values of C_d for a touring racecar. Table 4.3 summarizes the data collected.

Table 4.3: Typical values of drag coefficient for a touring racecar.

Vehicle model	Drag (C_d)	Reference
1995 BMW M3 FIA Supertouring	0.300 [1]	(KATZ, 1995)
1995 Dodge Neon Challenge	0.336 [1]	(KATZ, 1995)
2006 WRX Subaru STi	0.413 [1]	(MCBEATH, 2013)
2016 BTCC Subaru Levorg	0.441 [1]	(MCBEATH, 2016)
20XX Ford Focus TC2000	0.468 [2] *	(OPTIMUMG, 20XX)
20XX Ford Focus TC2000	0.568 [3] *	(OPTIMUMG, 20XX)

[1] wind tunnel data
[2] coast down test (rolling resistance calculated with an inertial unit data)
[3] coast down test (rolling resistance measured by a wheel force transducer)
* The authors of OptimumG (20XX) disclosure about the accuracy of the data since there was not sufficient runs to perform a statistical significance analysis.

According to Table 4.3, C_d varies from 0.30 up to 0.44 on wind tunnel tests, and achieves higher values for a TC2000 racecar instrumented with wheel force transducer and an inertial unit. Due to diverged C_d values (difference of 21%) encountered in OptimumG (20XX), initial guess of $C_d = 0.40$ was set based on wind tunnel tests only. However, TC2000 C_d coefficients were included in the design exploration (section 4.7.1) with the aim to consider the outliers found in the literature.

Another parameter affecting drag force is vehicle frontal area, in this work estimated with the help of a computer-aided design (CAD) software. This process is illustrated in Figure 4.12:

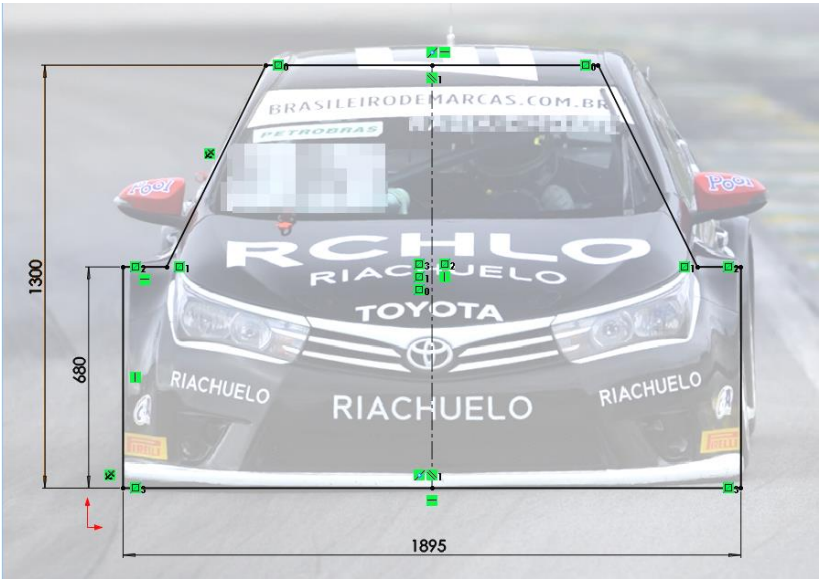

Figure 4.12: Calculation of the frontal area with the help of a CAD software.

Frontal area was computed with the help of sketch lines scaled by the front bumper width, which is specified by rules. From this approximation, a frontal area of A = 2.1 m² was calculated.

4.5 Circuit model

This section explains how the circuit parameterization was performed for the new circuit without previously logged data. Aiming to test the method, parameterization of the known Ayrton Senna Circuit – GO was performed first using a CAD software and GPS logged data.

GPS coordinates were exported to Google Earth® from which circuit map and the driver racing line could be overlaid. This process resulted in a scaled image (Figure 4.13) imported to a CAD software. Then, racing line was broken down into a series of arcs of constant radius and straight lines.

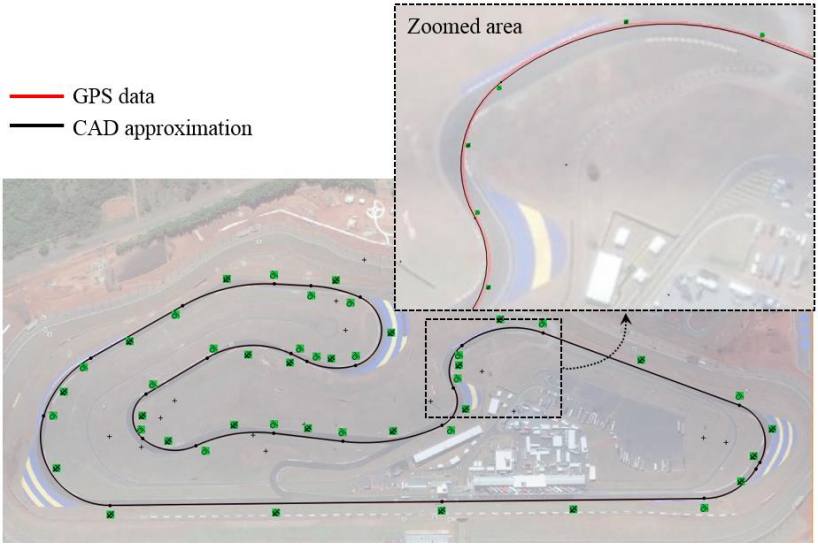

Figure 4.13: Circuit parameterization based on a CAD software and GPS logged data. Ayrton Senna Circuit – GO, Brazil.

Because circuit parameterization was given by a series of arc radius in function of distance, straight lines were set with an arbitrary radius large enough to not limit forward acceleration due to the tire limit of adhesion.

To simulate progressive steering increase towards corner apexes, corners are split into a series of decreasing arc radius (SIEGLER; DEAKIN; CROLLA, 2000). However, this is a time consuming process if performed manually in a CAD software. Aiming to reduce the number of sectors, a different approach was taken in this work: the racing line was split into coarse sectors of constant radius instead of decreasing radius. Then, with the help of Pandas library in Python, this data was up-sampled 16 times by a linear interpolation and further smoothed by a rolling mean function with a window size of 20 observations. The result of this process, named Rolling Mean Track Data, is compared with raw track data in Figure 4.14.

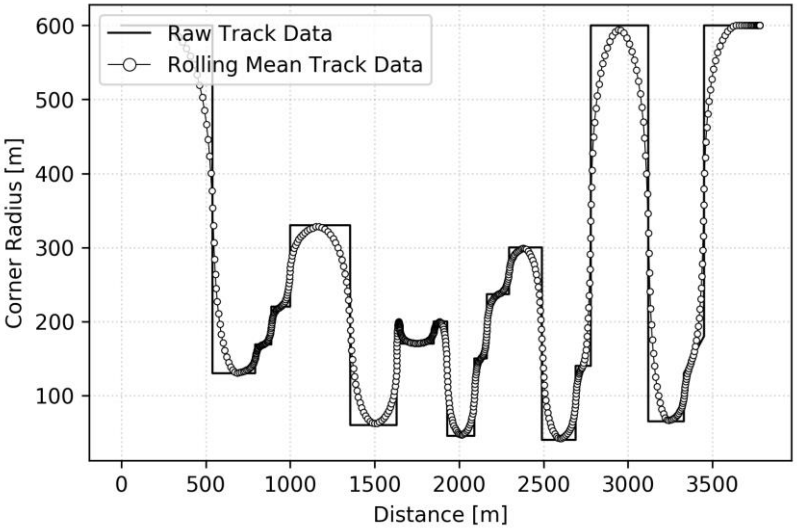

Figure 4.14: Rolling mean method of circuit parameterization.

Parameterization of the circuit was performed in two steps. Raw track data acquired from a CAD software and further data treatment in order to have a realistic progressive corner radius.

Figure 4.15 illustrates the circuit parameterization in CAD of the Cristais Circuit – MG, Brazil.

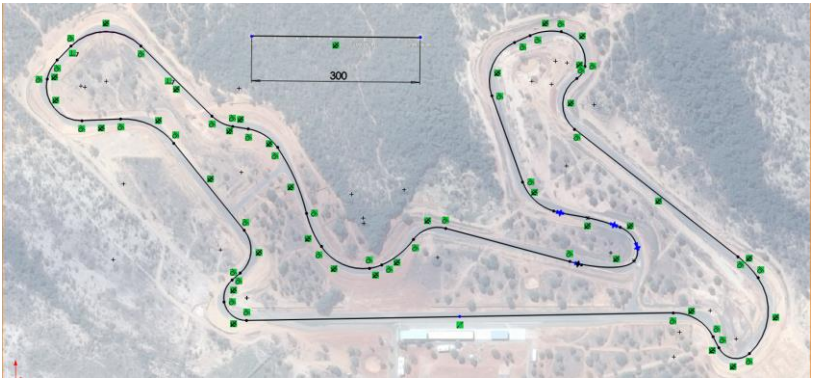

Figure 4.15: Circuit parameterization with the help of a CAD software and driver's expertise to determine the racing line. Cristais Circuit – MG, Brazil.

For the new circuit, the parameterization process was performed in a similar manner. The difference relies on the lack of GPS data to determine the driver racing line. Thus, the racing line was drawn with the help of driver's expertise.

4.6 Target accuracy

The first step in design exploration was to determine the target accuracy for the simulation results (presented in Chapter 6), in this work defined by the root mean squared error. As stated before, the aim of this model is to have an approximation of the speed profile of a new circuit. In this way, the model must output an overall speed profile independent of factors such as tire degradation and fuel consumption along the race. In a best-case scenario, it would output an average speed profile along the race.

Tire degradation is mostly related to tarmac characteristics, which is difficult to account for a new circuit. In this way, accuracy criteria was based on vehicle mass variation over the championship, which includes fuel consumed during the race and a handicap system imposed by the *Brasileiro de Marcas* championship rules.

The handicap system depends on the championship stands, and can possibly change a driver's handicap at each race event. The aim of the handicap system is to balance the performance of the competitors in order to equalize changes of winning. It specifies vehicle ballasts for the top eight drivers. The championship leader carries 80 kg of ballast; second place carries 70 kg, third place 60kg and so on.

Accuracy criteria were defined by a design of experiments (DoE) (ANTONY, 2014) with the aim to output the speed profile of a vehicle for a given circuit as function of the vehicle mass. The design of experiments setup is shown in Table 4.4.

Table 4.4: Design of experiments setup to determine target accuracy of the model.

Model Number	Description	m [kg]
1	Minimum Value	1090
2	Center Value (baseline)	1150
3	Maximum Value	1210

To explore the model sensitivity, a minimum vehicle mass specified by the rules, 1090 kg, was set as minimum value for the

experiment. To this minimum value, 80 kg of ballast and 40 kg of fuel was added totaling 1210 kg, which represents the maximum value of Table 4.4. Calculated by Equation 4.15, the target accuracy was defined by the root mean squared error (RMSE) between models 1 and 3:

$$RMSE = \sqrt{\frac{1}{n}\sum_{t=1}^{n}(y_1 - y_3)^2} \qquad (4.15)$$

where y_1 is the vehicle speed of model 1, y_3 is the vehicle speed of model 3, and t is the time step.

Figure 4.16 presents the results from the DoE study.

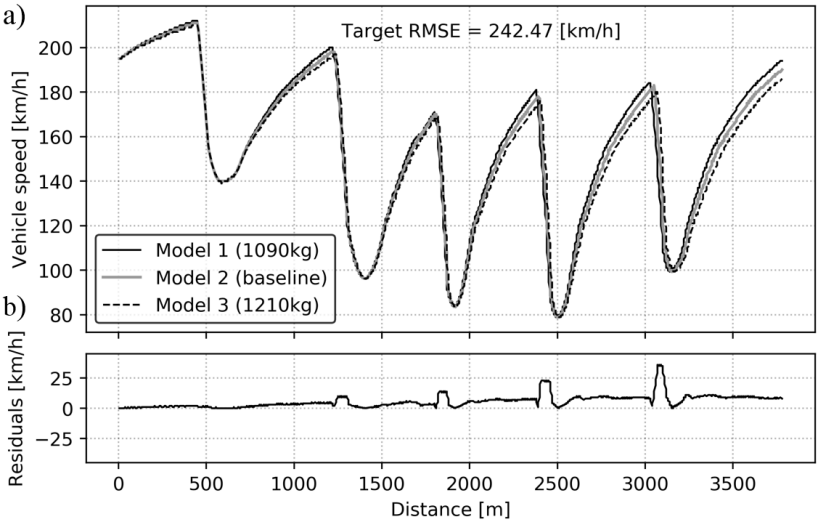

Figure 4.16: DoE study for the target accuracy of Ayrton Senna Circuit – GO simulations. a) Speed profile of models 1, 2 and 3. b) Residual values between model 1 and 3.

From the speed profile of models 1 and 3, the target accuracy RMSE = 242.47 km/h was calculated for the Ayrton Senna circuit simulations.

4.7 Parameter estimation

Validation can be performed by comparing results of simulation with data collected from field experiments. In this respect, additional

attention must be given to model input parameters (e.g. moments of inertia, aerodynamics coefficients, engine curves, tire parameterization) and naturally, such scenario requires a compromise between model complexity and feasibility to measure those input parameters. In fact, testing is difficult, some are too costly (e.g. tire testing), time consuming (e.g. endurance testing), or, in motorsport championships, unofficial circuit testing is often outlawed by rules.

To deal with lack of data, parameter estimation is an alternative to determinate unknown input parameters for vehicle dynamics models. A variety of techniques exists to accomplish this task (PRONZATO; WALTER, 1997). In this section, a parameter estimation using a Monte Carlo method is presented. This technique performs several simulations within a specified range of input parameters to evaluate the error between experimental and simulated data. To reduce computational cost, a design exploration analysis was firstly performed to find out which parameters have greater influence on model error. Then, these parameters were carried on to the Monte Carlo method.

4.7.1 Design exploration

According to Witten, Eibe and Mark (2011), a model with too many parameters relative to the number of training instances can become "too nonlinear". It means that the model could perfectly fit a *training data* due to its many degrees of freedom and not because the model correct represents the physical phenomena. Such a model will perform very well on *training data* but will perform poorly on *test data*. This phenomenon is known as overfitting, and can be minimized using structurally simpler models with fewer parameters (WITTEN; EIBE; MARK, 2011).

As an attempt to reduce model complexity, a design of experiments was performed aiming to investigate the effects of input parameters change on simulation error. Simulations were benchmarked by the baseline model of the accuracy criteria (Model 2 from Table 4.4). The design of experiments setup is shown in Table 4.5.

Table 4.5: Design of experiments setup to investigate simulation errors.

Parameter	Unit	Low Star Level	Low Level	Center Value	High Level	High Star Level
μ_0	[-]	0.05	0.010	0.015	0.020	0.025
μ_1	[s²/m²]	$5x10^{-6}$	$6x10^{-6}$	$7x10^{-6}$	$8x10^{-6}$	$9x10^{-6}$
C_d	[-]	0.20	0.30	0.40	0.50	0.60

u	[-]	1.00	1.20	1.40	1.60	1.80
η	[-]	0.70	0.75	0.80	0.85	0.90

The DoE study used in this research comprises a full factorial 2^N design matrix for the high and low levels and $2.N + 1$ extra runs for the other parameters. Where N is the number of parameters. In this work, $N = 5$, the DoE study ran $2^N + 2.N + 1 = 43$ simulations. Center values were assigned as the initial guesses taken from the literature survey presented in section 4.4, while high, low and star levels were set aiming to explore the outliers encountered on literature. Results of the DoE study are presented by a Pareto Diagram shown in Figure 4.17.

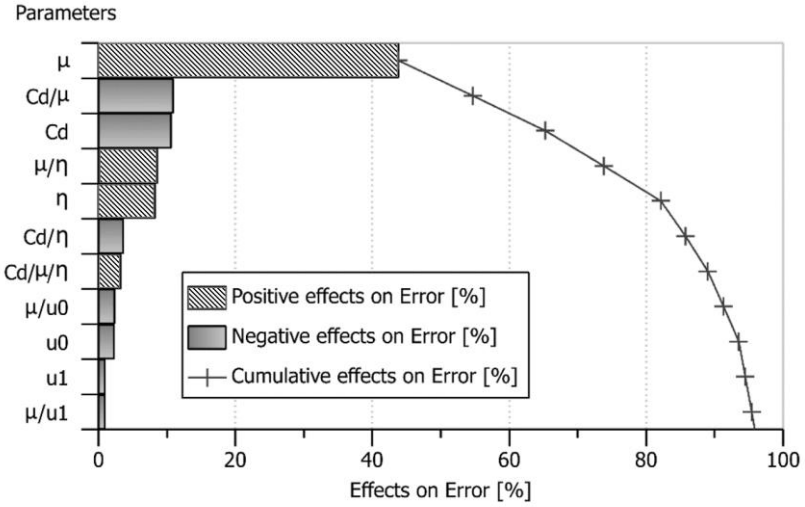

Figure 4.17: Pareto diagram of the input parameters. Effects of each parameter on simulation error is presented.

The effects of input parameters on simulation error is presented by the diagram above. Negative effects means that if a parameter decreases, model error also decreases (e.g. if C_d is reduced, model error also reduces). Positive effect error means that if a parameter increases, model error also increases (e.g. if u rises, the model error rises too).

From this diagram, some conclusions can be drawn. Coefficient of friction (u), driveline efficiency (η) and drag coefficient (C_d) account for more than 85% of effects on model error. Rolling resistance

coefficients μ_0 and μ_1 account for the other 15%. Following the recommendation of Witten, Eibe and Mark (2011) to avoid overfitting by using simpler models, rolling resistance coefficients were excluded from the parameter estimation process because they have much less influence on model error compared with the other parameters.

4.7.2 Monte Carlo parameter estimation

The parameter estimation was supported by the Monte Carlo method. In this process, simulations of the vehicle speed profile were performed with different values of drag coefficient (C_d), friction coefficient (μ) and the driveline efficient (η). The basic idea of the method was to run simulations enough to test many combinations of input parameters and its effects on simulation error.

Simulation error was evaluated by a cost function, calculating the sum of squared errors, similar to the DoE presented before (Equation 4.15). However, instead of calculating simulation error from a benchmark model, error was calculated against *training data*, which was taken from a flying lap of a qualifying session at Ayrton Senna Circuit – GO, Brazil.

The input parameters for these simulations came from pseudo-random values generated by an Optimized Latin Hypercube Sampling (OLHS) method. This method gives a uniform sampling and therefore, reduces the number of simulations needed in order to cover a high number of parameter combinations.

Table 4.6 shows input parameters for the experiments given by a target mean value and standard deviation of the samples.

Table 4.6: Design of experiments setup to determine target model accuracy.

Parameter	**Mean Value Target / Result**	**Standard Deviation Target / Result**
η	0.80 / 0.80	0.05 / 0.049
C_d	0.40 / 0.40	0.05 / 0.049
u	1.20 / 1.20	0.12 / 0.119

Table 4.6 presents target values and results of the OLHS method for a sampling space of $p = 1000$ combinations of parameters. The number of samples p was arbitrary chosen after an unsuccessful attempt to achieve the targets with $p = 300$ samplings. Even though $p = 1000$ samplings produced the desired outcome, a lower sampling space might

be more efficient, although this topic is not addressed in the present research.

Each combination of parameters generated by the OLHS method was carried on to run the Monte Carlo simulations. Each of the 1000 simulations contained a set of input parameters. Individual results were collected as function of the sum of squared errors. In this way, a parameter could be estimated based on its corresponding error (e.g. the estimated parameter would be a value resulting in the smallest error). However, when each isolated parameter is assigned based on its corresponding error, the error effect of other parameters are not being considered. Therefore, there is a risk that specific combinations of parameters are potentially overfitting the model, which results in misleading small errors.

To deal with this problem, the density of parameters values and its effects on model error were taken into account. Figure 4.18, Figure 4.19 and Figure 4.20 are scatter plots of the simulations performed by the Monte Carlo method. The density of each scatter plot is given by the size of each grey circle. The key point was assigning the estimated parameter to the minimum error given by the cloud boundary (dashed line).

Figure 4.18 presents the effects of drag coefficient on simulation error:

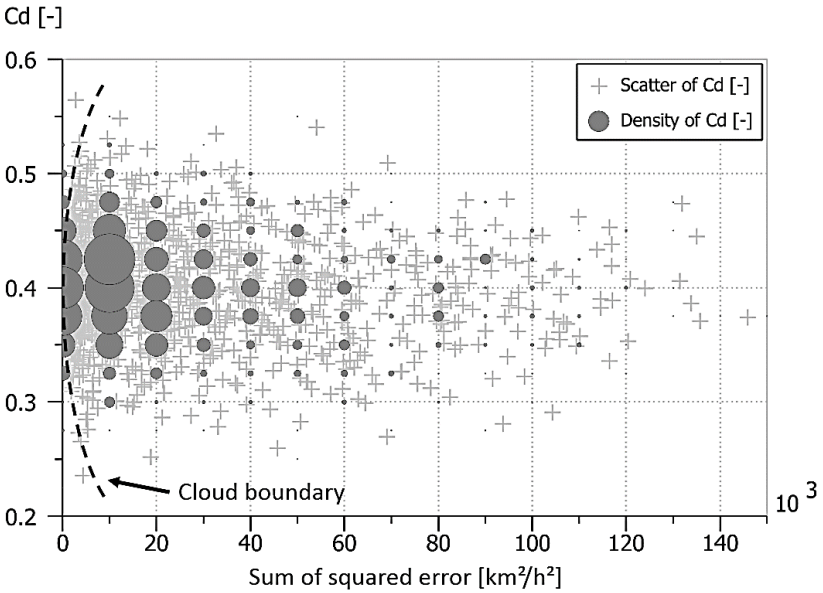

Figure 4.18: Density distribution of drag coefficient along the Monte Carlo optimization process and its effects on model error.

In Figure 4.18, not surprising small errors occurs where the biggest density of drag coefficient C_d are close to the literature typical values of $C_d \approx 0.40$. As this value diverges, model error increases. The sparse cloud of errors is probably due to random combinations of C_d, η and u that, as it can result in misleading small errors, it can also lead to misleading bigger errors.

Similar to Figure 4.18, Figure 4.19 presents the effects of the tire/road coefficient of friction on simulation error:

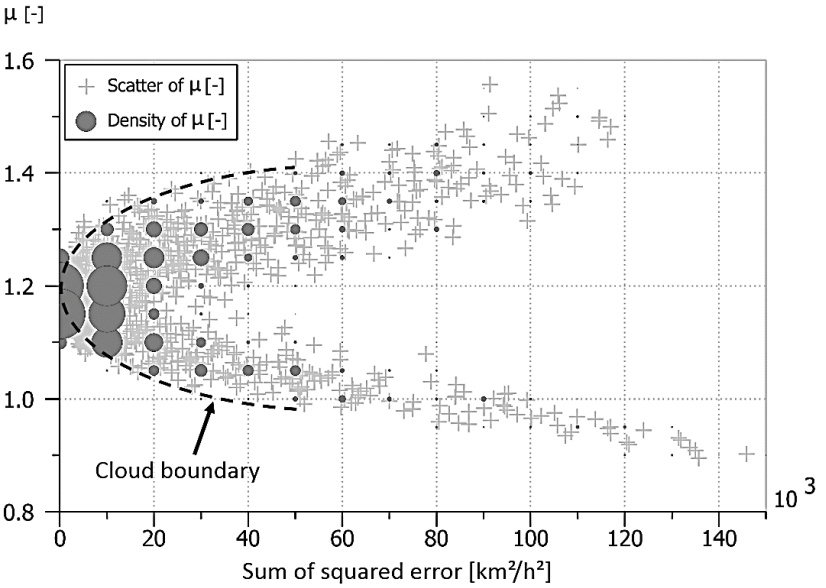

Figure 4.19: Density distribution of friction coefficient along the Monte Carlo optimization process and its effects on model error.

As expected, density distribution for small errors is concentrated in a smaller range of parameters (roughly, $1.15 < u < 1.25$). This fact was also shown in the Pareto diagram (Figure 4.17) where the friction coefficient alone takes more than 40% of effects on model error. In other words, this model is very sensible to changes in grip level of the circuit. This aspect can be a difficult issue to overcome while estimating a new circuit, since there is no chance to fine-tune grip level beforehand.

Finally, the effects of drivetrain efficiency on simulation error are presented in Figure 4.20:

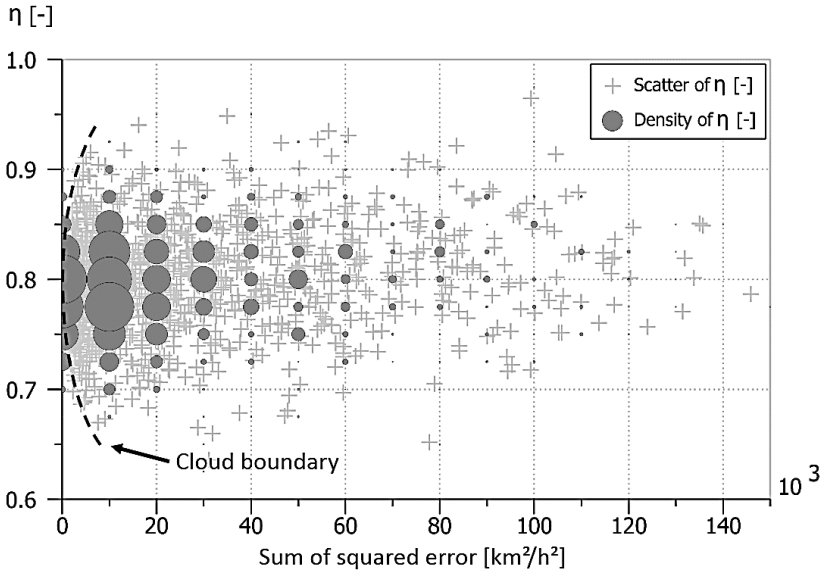

Figure 4.20: Density distribution of drivetrain efficiency along the Monte Carlo optimization process and its effects on model error.

According to Figure 4.20, drivetrain efficiency around 80% produces smaller effects on model error. As expected, this value is in accordance to the study conducted by Irimescu, Mihon and Pãdure (2011), therefore it was chosen as the estimated parameter for drivetrain efficiency. Table 4.7 summarizes the estimated parameter from the Monte Carlo method and from the literature review.

Table 4.7: Summary of estimated parameters via Monte Carlo optimization and the literature review.

Parameter	**Estimation Method**	
	Monte Carlo	**Literature review**
η	≈ 0.80	0.72 – 0.91
C_d	≈ 0.40	0.30 – 0.44
u	≈ 1.20	-

According to Table 4.7, simulation error was reduced when values of drivetrain efficient (η) and drag coefficient (C_d) were set close to the average values found in the literature review.

Regarding data acquired at the racetrack, this chapter focused on how vehicle model parameters were estimated with the help of a qualifying lap at Ayrton Senna Circuit – GO, Brazil.

The next chapter deals with another aspect of the data: how it is used to improve the driver performance during the race event. To accomplish with this aim, data from Cristais Circuit - MG, Brazil is presented in function of distance and is discussed based on the knowledge acquired along the race event.

5 DATA ANALYSIS

> *Every successful driver trail brakes at some corners. No successful driver trail brakes at every corner.* (SMITH, 1996)

5.1 Introduction

Data acquired at the racetrack has two main purposes in this work: estimate vehicle parameters, presented previously, and evaluate driver performance, addressed in this chapter. How data analysis supports improvements of lap time along the race event is the focus of the following sections.

As case of study, the dataset presented hereafter comprises two flying laps of the qualifying session at Cristais Circuit - MG. Vehicle speed, lateral and longitudinal accelerations, throttle position, and gear channels are presented and driver's activities are discussed supported by this data. After, G-G diagram is presented alongside the vehicle racetrack position from GPS data. This chapter also addresses the so-called Grip Factors, a metric developed by Segers (2014).

5.2 Cristais Circuit – MG, Brazil.

Racing a new circuit challenges drivers and racing teams regarding racecar setup and the learning process of a racing line. The case of study presented hereafter is supported by data acquired at the Cristais Circuit – MG, recently inaugurated at the time of writing.

Cristais Circuit was split into sectors with the aim to point out where in the racetrack time was being gained or lost. From the sectors, the *ideal lap* was calculated - an indicator of how much lap time could be improved, calculated by the sum of the best sectors from the laps being compared.

Although *ideal lap* is a widespread indicator, care must be taken on how it is performed. According to Segers (2014), the number of sectors directly influences the ideal lap time. More sectors result in faster ideal laps because different racing lines compromise different phases of a corner. The late apex approach, for example, tradeoffs corner entry to corner exit speed. If a circuit were split in too many sectors, ideal lap time would join different corner phases in an unrealistic manner.

To overcome this issue, Segers (2014) recommends starting/closing points of sectors at the straights. In this manner, all phases of a corner would be enclosed into the same sector, reducing unreal combination of corner phases from different laps.

In this work, Cristais Circuit was split into six sectors according to Figure 5.1. Sectors boundaries are given by the tick markers at the circuit, numbered according to the balloons. Corner numbering is given by the squared boxes. The following data analysis are excerpts from each of the six sectors.

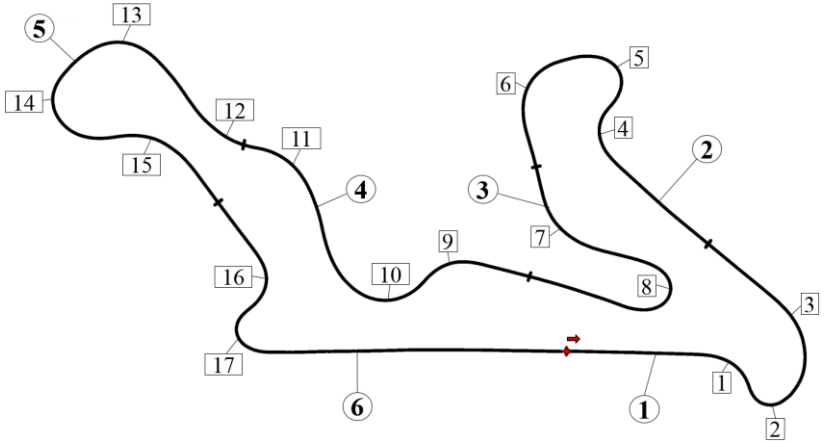

Figure 5.1: Cristais Circuit has 17 corners indicated by the squared boxes, split into six sectors, indicated by balloons.

Table 5.1 presents the dataset used hereafter for data analysis. Two professional drivers are compared along two flying laps at Cristais Circuit. S1 to S6 stands for sectors number, and time difference between drivers is given by the Δ time for each sector.

Table 5.1: Sectors time, in seconds, of two flying laps of the qualifying session at Cristais Circuit. Two professional drivers are compared. Δ time is the difference between Driver A and B, and ideal lap is composed by the best sectors of both drivers.

	S1	**S2**	**S3**	**S4**	**S5**	**S6**	**Total**
Driver A	20.846	21.110	18.669	17.645	22.337	23.709	124.316
Driver B	21.044	21.404	18.806	17.448	22.127	23.540	124.369
Δ time	-0.198	-0.294	-0.137	+0.197	+0.210	+0.196	-0.053
Ideal lap	20.846	21.110	18.669	17.448	22.127	23.540	123.740

According to the table, Driver A was faster in the first three sectors (S1 to S3), although lap time difference was only 0.053s between Driver A and B. The sum of the best sectors from the flying laps is given by the ideal lap time, which was 0.576s faster than the fastest lap achieved by Driver A.

5.2.2 Sector 1

Figure 5.2 presents the G-G diagram and the racing line taken by the drivers at sector 1.

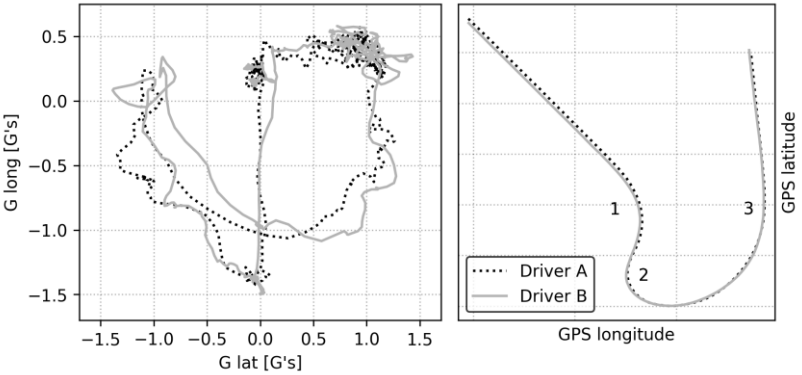

Figure 5.2: G-G diagram and GPS plot of drivers A and B at sector 1.

The aim of the G-G diagram in Figure 5.2 is to illustrate how drivers are exploring the performance envelope in a particular sector. In combination to the GPS plot, it illustrates how different racing lines cover different parts of the G-G diagram.

Forward acceleration explores the upper part of the diagram while the braking phase, the bottom. In a similar manner, right-hand corners explore the left side of the diagram (negative lateral acceleration), while left-hand corner, the right side (positive acceleration).

Sector 1 has three corners identified by numbers 1, 2 and 3 in the GPS plot. Corners 1 and 2 are low-speed corners linked together. Corner 3 is a medium-speed corner followed by a straight split into sectors 1 and 2.

Because corner 1 is linked to the low-speed corner 2, the exit phase is not as important as the entry phase, where time could be gained by trail braking into the corner (BENTLEY, 2011). On the opposite side,

the exit phase of corner 2 makes it the most important corner of sector 1. Every speed difference at corner exit is carried along the straightaway. This sector characteristic suggests late braking at corner 1 and a late apex approach at corner 2.

In the G-G diagram, positive lateral acceleration is assigned to the left-hand corners 2 and 3. At the entry phase of corner 1, there is a transition from the positive to negative longitudinal acceleration. This transition from forward acceleration to the pure braking phase is given by the vertical trace at the middle of the diagram.

From the pure braking phase, drivers trail brake towards the apex of corner 1, but Driver A has higher combined longitudinal and lateral accelerations (trail braking) than Driver B.

The transition from corner 1 to corner 2 is given by the traces going from the left to the right side of the plot. At the transition, Driver A explores more the vehicle performance than Driver B (data points of Driver A are closer to the boundary than those of driver B are). At the entry phase of corner 2, Driver B, in turn, explores more the vehicle (indicated in the diagram by the larger radius formed by the data points on the bottom right side of the plot).

The apex of left-hand corners 2 and 3 are plotted on the right side of the diagram. At the apex, the vehicle is at balanced throttle around 0 G's of longitudinal acceleration. The exit phase goes from the upper right side where maximum combined lateral and longitudinal acceleration takes place towards the central part of the diagram, which is the pure forward acceleration phase.

Figure 5.3 shows the first sector excerpt from the qualifying lap. Figure 5.3-a presents the time variance (Δ time) between Driver A and B, and Figure 5.3-b presents the vehicle speed plot.

Data channels are plotted against distance because driver activities must be compared at the same place of the racetrack. In a time-series, a point at the same time not necessarily means the drivers are at the same location of the racetrack due to lap time differences (SEGERS, 2014).

In the first sector, Driver A is 0.198 seconds faster than Driver B. The main sources of time difference are assigned to corners 1 and 2.

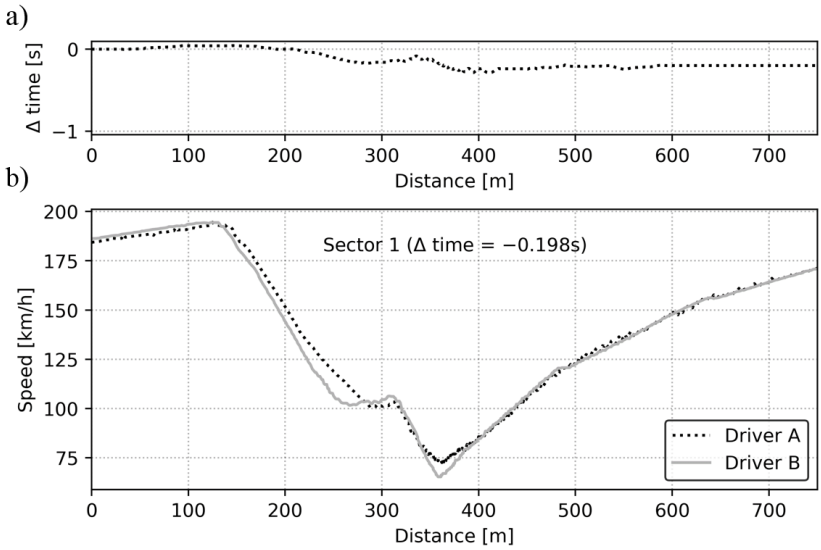

Figure 5.3: Data comparison of a qualifying lap of two professional drivers in Sector 1. a) time variance - Δ time, b) vehicle speed. Driver A is 0.198 seconds faster than Driver B

According to the inclination of the speed traces in Figure 5.3-b (~220 m to 300 m), Driver A trail brakes corner 1 and tradeoffs cornering exit speed for time gained along the braking phase (Figure 5.3-a), which is better explored in the longitudinal acceleration plot of Figure 5.4:

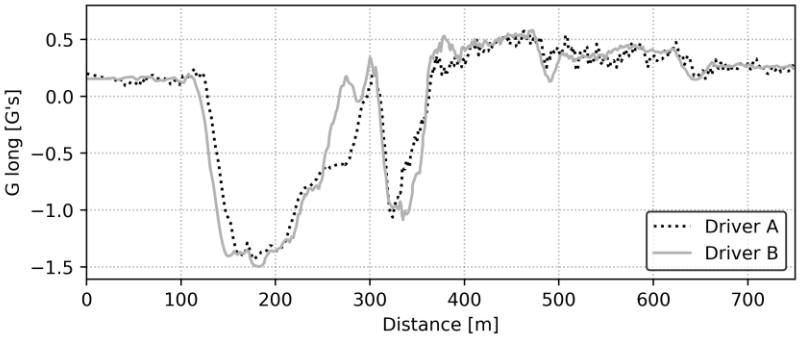

Figure 5.4: Longitudinal acceleration data of sector 1.

From the longitudinal acceleration plot above, in comparison with Driver B, Driver A brakes later for a longer distance and with less intensity, carrying more speed in the pure braking and trail braking phases of the corner (from ~110 m to ~300 m).

From Figure 5.3, cornering speed at corner 2 (~350 m) is another source of time difference, where Driver B had a lower minimum speed. Among the reasons, the use of first gear, shown in the gear chart of Figure 5.5 at ~310 m, contributes to it.

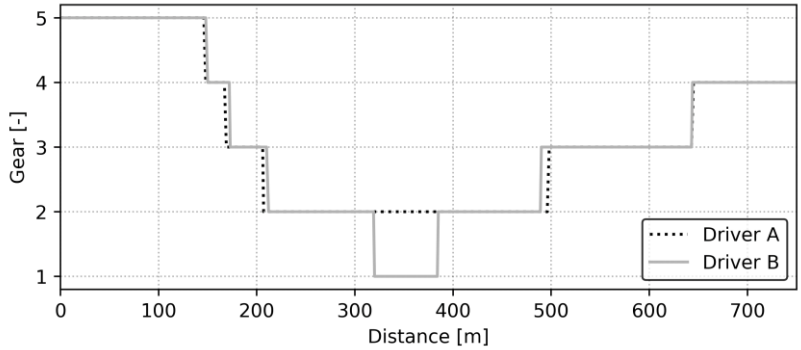

Figure 5.5: Gear chart of sector 1.

From the gear chart in the figure above, Driver A and B had different gear shifting strategies. Although the gearbox is sequential, lowering to first gear demands two extra driver inputs, one for downshift and another for upshift. It takes time and demands more attention because the high first gear ratio tends to upset vehicle balance raising the engine speed, observed in the engine speed plot of Figure 5.6.

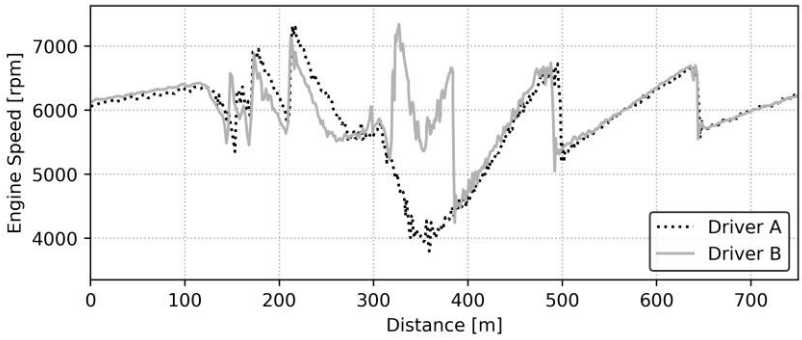

Figure 5.6: Engine speed data of sector 1.

From about 330 m in Figure 5.6, Driver B reaches much higher (> 2000 rpm) engine speed than Driver A. Besides the effects on vehicle balance, to make sure a gear reduction does not exceed the engine speed limit - over revolution, which could damage the engine, the driver must worry about blipping the throttle to match vehicle and engine speeds, a difficult task due to the rapidly raise of the engine speed in such high gear ratio. In fact, both drivers had exceeded the limit downshifting to the second gear at ~210 m, and Driver B downshifting to the first gear at 310 m.

Longitudinal acceleration and throttle position data, shown in Figure 5.4 and Figure 5.7 respectively, indicates that, although drivers A and B go off throttle at about the same place approaching corner 1 (~120 m), Driver B overlaps brake and throttle pedals, which is a characteristic of left-foot braking technique. Indeed, Driver B is a left-foot braking, while Driver A is a right-foot braking.

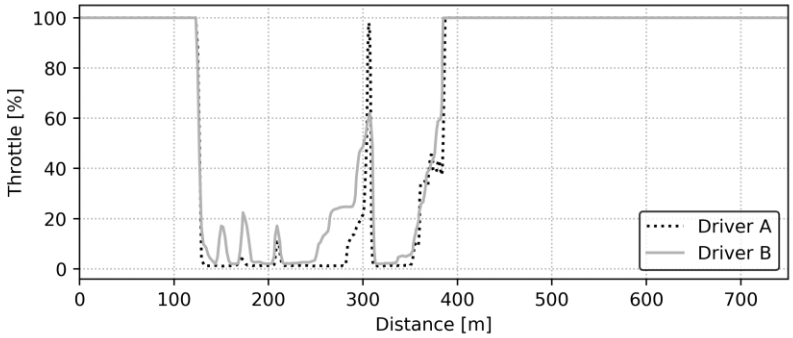

Figure 5.7: Throttle percentage data of sector 1.

Peaks of negative longitudinal acceleration (Figure 5.4), one at ~490 m and another at ~640 m, both close to gear shifting points, indicates Driver B reaches the engine speed limit twice, confirmed by the nosy plateau of the engine speed trace in Figure 5.6.

In this chapter, grip factors were calculated from the lateral and longitudinal accelerations. According to Segers (2014), thresholds of signal gating may vary from one racecar to another. For a low downforce racecar, for example, a high threshold may not gate the signal for the aerodynamic grip factor, or gate only a few data points, which are possible outliers. The opposite is also true: for a high downforce racecar, gating the signal too low reduces the sensibility of

the aero grip factor, for example. Table 5.2 presents the thresholds used to calculate grip factors in this chapter.

Table 5.2: Signal gating thresholds for grip factors.

Grip factor	G lateral	G longitudinal	G combined	Speed
Acceleration	< 1 G	> 0 G	-	-
Aerodynamic	> 0.8 G	-	-	120 km/h
Braking	-	< -1 G	-	-
Cornering	> 1 G	-	-	-
Overall	-	-	> 1 G	-

The values shown in Table 5.2 were slightly adjusted from a baseline proposed by of Segers (2014) for a touring racecar.

Figure 5.8 presents metrics of sector 1. Two bar plots are shown, a) average grip factors on the left side and b) average driver inputs on the right side. Although faster, Driver A surprisingly uses less tire grip than Driver B, which suggests sector time of Driver A could be improved.

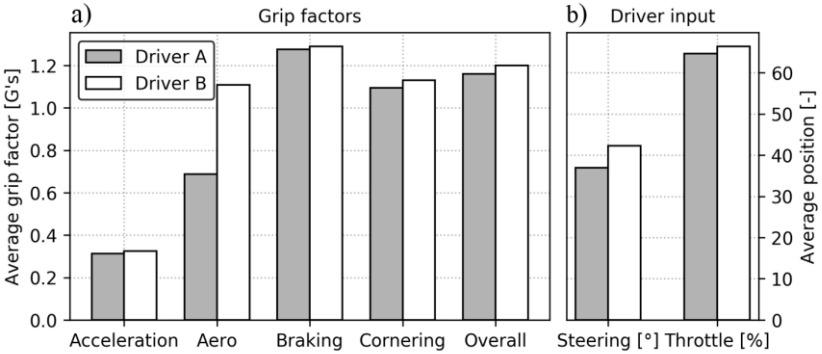

Figure 5.8: Metrics of sector 1. a) average grip factors, b) steering angle and throttle position. Higher grip factors indicate more tire potential is being used.

Aerodynamic was the main difference between grip factors, Driver B has 57% higher aero grip factor than Driver A. However, it is not necessarily a positive indicator because of a phenomenon known as *tire induced drag*, which increases tire rolling resistance by the increase of the tire slip angle (MILLIKEN & MILLIKEN, 1995). To further explain, both drivers are at WOT for the signal gating (v_x > 120km/h &

$|a_y|$ > 0.8G), which means the vehicle is being powered limited. Then, the higher lateral acceleration achieved by Driver B (Figure 5.3, from ~480 m to ~530 m) is a result of higher tire slip angle producing higher lateral forces. The key point is: tire rolling resistance is function of tire slip angle. More slip angle induces more tire rolling resistance, which is an external resistance working against the engine power.

From a driver point of view, Bentley (2011) points out two ways of increasing lateral acceleration, one negotiates a corner with higher speed; another is to tighten corner radius. Because Driver B was powered limited at corner 3, speed could not be increased. Then, the higher lateral acceleration only increased induced drag.

This analysis is in according to the higher average steering angle observed in Figure 5.8. On the same graph, higher average throttle position of Driver B is due to the low speed at the entry phase of corner 1. In Figure 5.3 (~250 m), Driver B had caught himself too slow and accelerates through corner 1.

5.2.3 Sectors 2 to 5

For the aim of this chapter, data analysis of sectors 2 to 5 are not essential. However, an interested reader is directed to Appendix A, where these sectors are fully covered.

5.2.4 Sector 6

Figure 5.9 presents the G-G diagram and the GPS plot of sector 5, comprised by the low-speed corners 16 and 17.

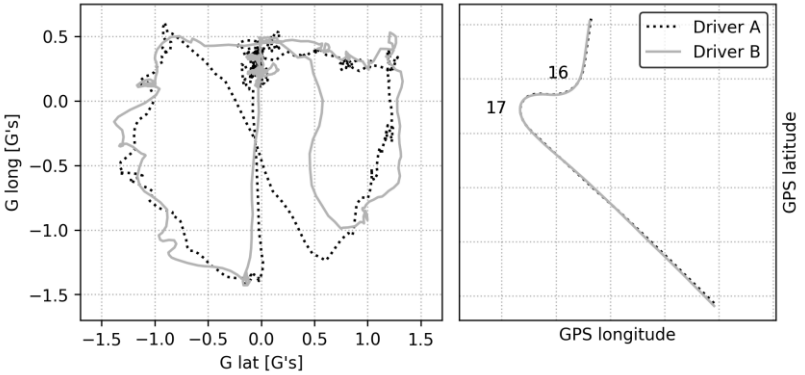

Figure 5.9: G-G diagram and GPS plot of drivers A and B racing line.

Corner 17 is the most important of the circuit because it leads to the longest straight of the circuit. The exit phase of this corner is crucial for time variance at sector 6.

According to the G-G diagram of Figure 5.9, Driver B has larger performance envelope compared with Driver A. At the transition from corner 16 to 17 (on the diagram, traces going from the upper left to the bottom right side of the plot), Driver B is closer to the performance envelope limits, especially at the upper part of the diagram and on the braking phase of corner 17 (descending trace at 0.5 G's).

In this sector, Driver B is 0.169 faster than Driver A. Figure 5.10 presents: a) time variance (Δ time) and b) vehicle speed.

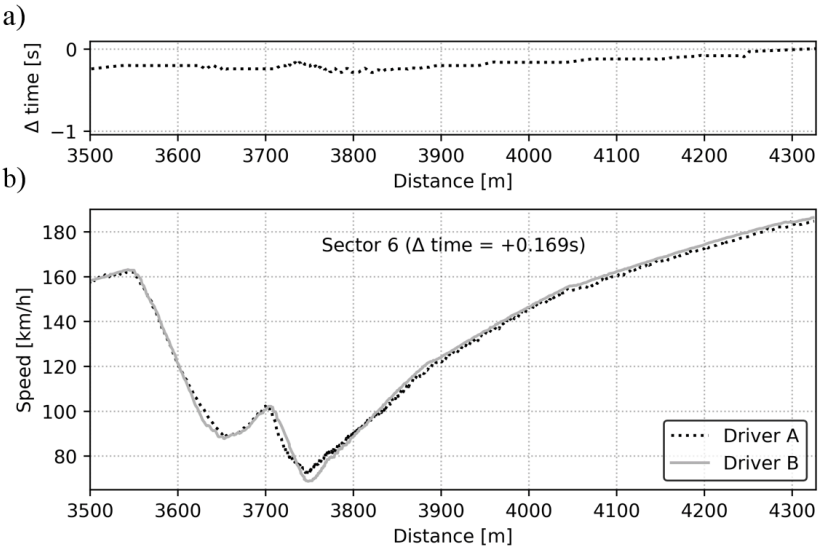

Figure 5.10: Data comparison of a qualifying lap of two professional drivers in Sector 1. a) time variance - Δ time, b) vehicle speed. Driver B is 0.169 seconds faster than Driver A.

Figure 5.10-b is a clear example of how important corner exit speed is. According to Table 5.1, at the beginning of sector 6 Driver B was 0.210 seconds slower than Driver A. After corner 17, time variance was progressively reduced to only 0.053 seconds at the finish line.

Longitudinal acceleration data of sector 6 is shown in Figure 5.11, and lateral acceleration shown in Figure 5.12.

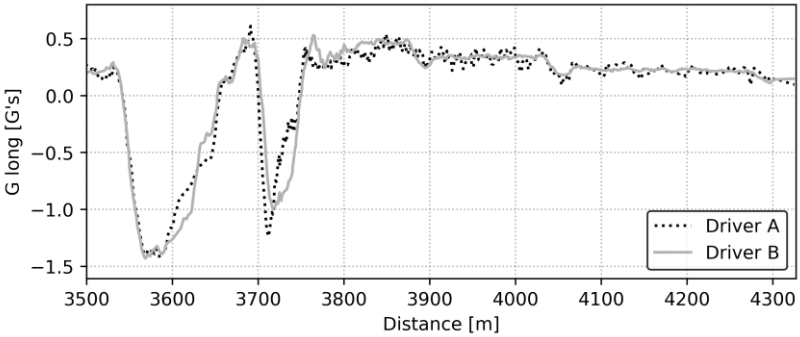

Figure 5.11: Longitudinal acceleration data of sector 6.

Corner 16 is negotiated in a similar manner. From Figure 5.11, at the pure braking phase, both drivers start braking at ~3540 m and reach the peak of deceleration at about the same place (~3560 m). Nevertheless, Driver B brakes for longer distance than Driver A at the trail braking phase (from ~3590 m to ~3630 m).

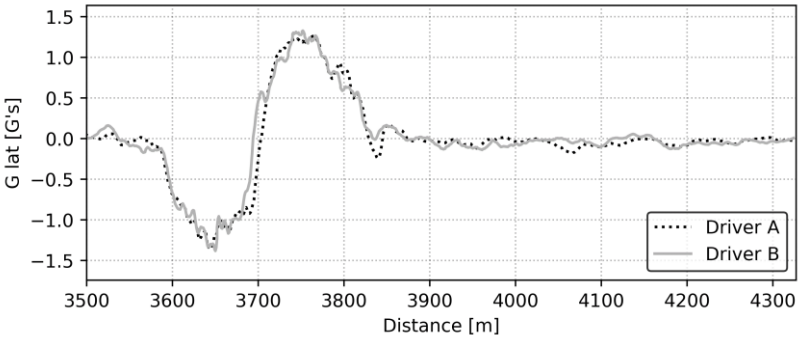

Figure 5.12: Lateral acceleration data of sector 6.

From the G lateral plot (Figure 5.12), both drivers reach similar lateral acceleration. However, because Driver B had braked for a longer distance than Driver A, Driver A is slightly faster as indicated by the speed plot in Figure 5.10-b.

The gear chart is shown in Figure 5.13, and the throttle position in Figure 5.14.

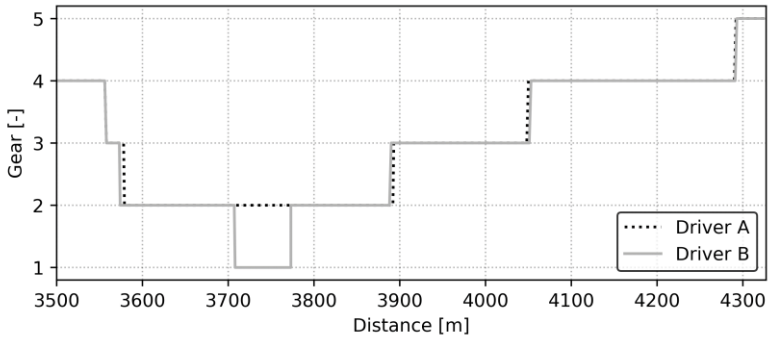

Figure 5.13: Gear chart of sector 6.

At Corner 17, drivers take different gear shifting strategies. Although both drivers late apex at this corner, Driver B engages first gear at ~3700 m while Driver A negotiates the corner in second gear.

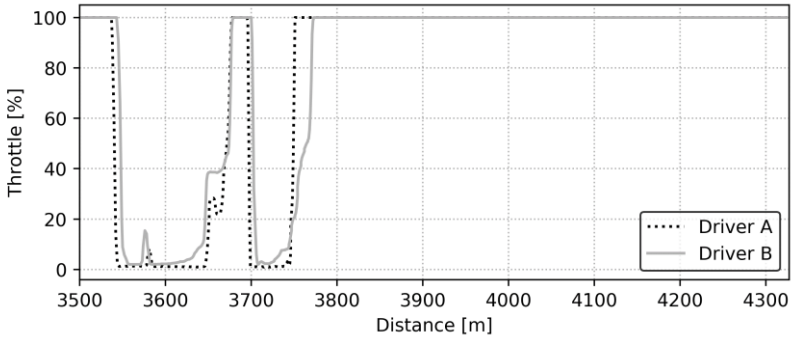

Figure 5.14: Throttle position data of sector 6.

Because of the higher gear ratio, to avoid wheel spin Driver B was more progressive on throttle application and reaches wide-open throttle at ~3770 m, 20 m after Driver A. However, from the longitudinal acceleration data, it is observed how the high gear ratio helps to overcome the acceleration inertia of the vehicle. The G longitudinal signal reaches higher values when compared with the signal of Driver A (~3750 m).

Figure 5.15 presents sector 6 metrics. Because this sector is composed by low speed corners, there was no signal gating for the aero grip factor.

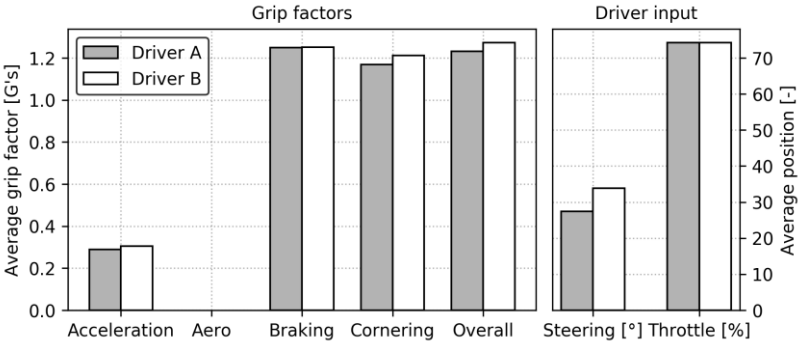

Figure 5.15: Metrics of sector 6.

The better acceleration of Driver B at the exit phase of corner 17 is announced by a slight higher acceleration grip factor, even though drivers have the same average throttle position. Driver B has slightly higher values of cornering and overall grip factors. Driver B also uses more steering angle than Driver A does.

In the next chapter, results of the simulation are presented and compared with experimental data. Besides Cristais Circuit, which is the focus of this work, Ayrton Senna circuit is also presented with the aim to compare the level of accuracy between *training* and *test data*.

6 SIMULATION RESULTS AND DISCUSSION

> *The results produced by the simulation software are as accurate as the accuracy of the modeled parameters.* (SEGERS, 2014)

6.1 Introduction

In this section, simulation results are present and discussed based on comparison to the experimental data from flying laps at the qualifying session. Two sets of data are used: *training data* from Ayrton Senna Circuit – GO, Brazil, and *test data* from Cristais Circuit – MG, Brazil.

For each circuit, a comparison of experimental with simulated speed profile are presented and discussed. Aiming to have a tangible measure, visual comparison is performed alongside the root mean squared error (RMSE) and residual values between datasets. Simulated gear shifting strategy is also presented and discussed.

6.2 Training data: Ayrton Senna Circuit – GO, Brazil.

Figure 6.1 indicates the circuit location of some points of interest for the discussion of results.

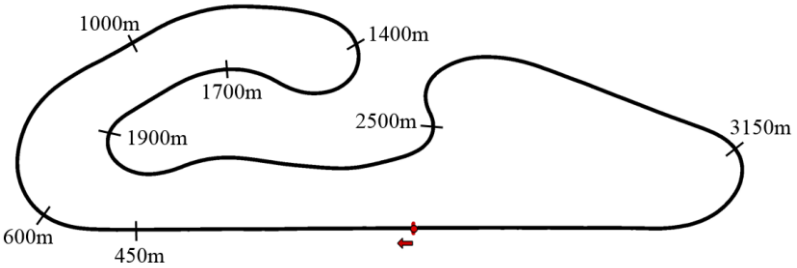

Figure 6.1: Reference points for Ayrton Senna Circuit – GO, Brazil.

Braking points and minimum speeds location are shown by the tick marks along the circuit. This figure aims to give a spatial reference for the speed plot shown in Figure 6.2.

Simulation predicted a lap time of 93.30 seconds at Ayrton Senna Circuit, while the real fastest lap time was 93.14 seconds. Figure 6.2

presents simulation results along with *training data* from Ayrton Senna Circuit – GO:

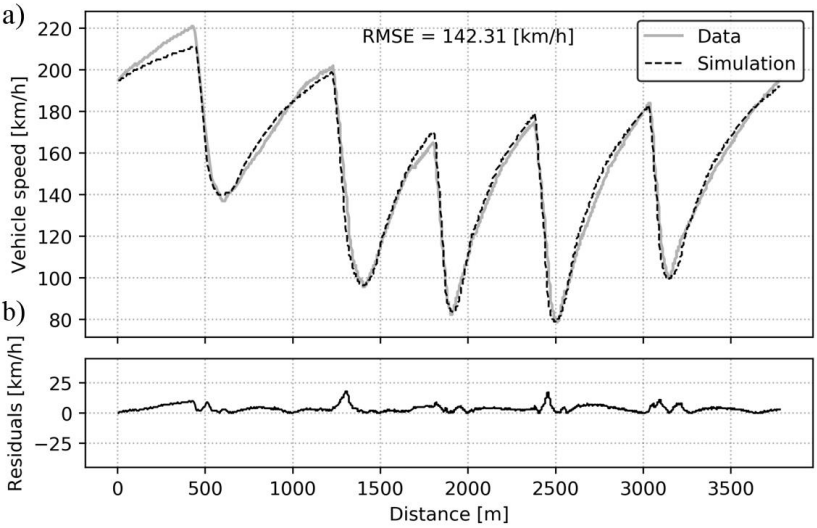

Figure 6.2: a) Speed profile comparison between experimental and simulated data. b) Residual values.

Composed by two subplots, the main plot of Figure 6.2 overlays simulation results with experimental data. The bottom plot provides residual values between datasets, which indicates where the error is more significant and is the first step for calculating the deviance measures MAE, MSE and RMSE.

The speed plot reveals differences between simulation and experimental data at the end of the main straight (< 450m). Predicted top speed was about 10km/h lower than actual data due to higher external resistances presented in the model.

At this location of the circuit (< 450m), speeds are above 200km/h, which emphasizes lack of aerodynamic fit of the model. Furthermore, rolling resistance, also function of speed, may be acting in combination to over detract engine power. As stated in Chapter 4, rolling resistance parameters were based on common values of passenger vehicles, which may be inadequate for a racing tire. If rolling resistance coefficients were set too low, the parameter estimation process may be biased to increase the drag coefficient aiming to reducing simulation error by counterbalance the external resistances.

This hypothesis is supported by the evidence that for speeds below 180 km/h, this effect is not much pronounced.

The vehicle model considers a constant coefficient of friction between road and tire. For this reason, at some points it was expected to over or underestimate the grip available along the circuit. For instance, at the exit phase of corner 1 (> 600m), simulation overestimates the grip resulting in higher acceleration than real data.

On the other hand, approaching the wide right hand turn at ~1000m, a crossover point between simulated and real speed trace is observed (Figure 6.2), i.e. simulation speed trace decreases and crosses the data trace. Two reasons are assigned: grip of the racetrack is underestimated, thus cornering speed is decreased; lack of aerodynamic and rolling resistance fit for speeds above 180km/h, also detracting cornering speed.

From ~1700m, simulation data in Figure 6.2 shows higher speeds than experimental data. At this location, the racecar is negotiating a left hand corner at wide-open throttle (WOT). Revisiting the model assumptions in Chapter 4 shows that the model considers rolling resistance only in function of speed and consequently treats a WOT corner as a simple straight line. However, rolling resistance is also function of tire slip angle; higher slip angle produces higher rolling resistance forces (MILLIKEN; MILLIKEN, 1995). Therefore, simulation overestimates the acceleration capability of the racecar because it is not considering the additional rolling resistance from the tire slip angle.

Residual values, seen in Figure 6.2-b, indicate differences around corner apexes, where speeds are minimum (600m, 1400m, 1900m, 2500m and 3150m). They were assigned to the rolling mean method for data treatment of circuit parameterization. Designed curvature profile is less sharp around corner apex than it should. In practice, it means the driver's steering input is more aggressive at corner apexes than the simulated one.

Residual values direct impact deviance measures, summarized in Table 6.1 in comparison with the target accuracy criteria presented in Section 4.6.

Table 6.1: Target and actual deviance measures for training data.

Deviance Measure	Unit	Target	Training Data	Difference [%]
RMSE	[km/h]	242.47	142.31	-41.3

Simulation results accomplished the target accuracy for the three proposed deviance measures. Actual MAE was 36% lower than the target; MSE, 65.6% lower and RMSE was 41.3% less than the target.

6.2.1 Gear shifting strategy

Derived from the speed profile, Figure 6.3 presents a gear chart for both simulated and experimental data.

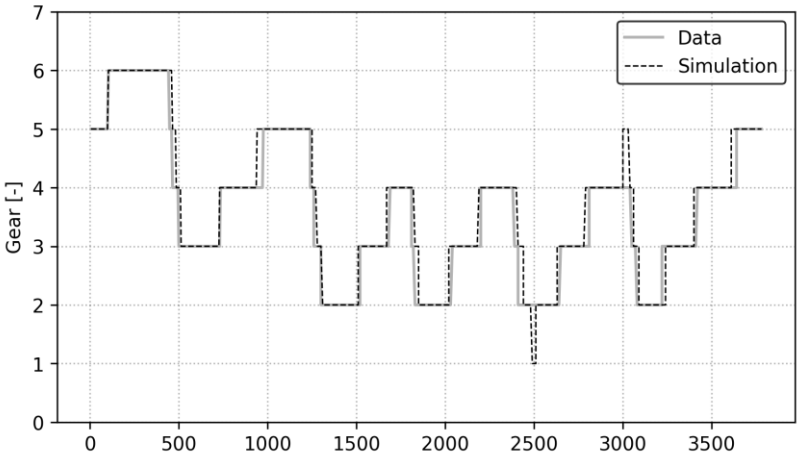

Figure 6.3: Comparison of gear shifting strategies: simulated data against the strategy adopted in a flying lap at qualifying session.

According to Figure 6.3, simulated gear chart follows similar strategy adopted in real life. It also illustrates two points where simulated gear shifting strategy diverged from experimental data: first gear engaged at 2500m and fifth gear at 3000m.

Simulated gear chart, in this work, points out where there is engine speed margin to change gears, but it does not take into account driver´s technique nor vehicle balance.

To exemplify, consider Figure 6.3 at 3000m. The racecar approaches braking point in fourth gear, very close to the engine speed limit. A driver could either shift to fifth gear, as in the simulation, or keep the racecar in fourth gear until it reaches the speed limiter at the braking phase, as in real data. Upshifting may increase vehicle speed at the braking point. However, a driver might also lose performance on the braking and corner exit phases in consequence. This particular corner

leads to the longest straight of the circuit, which highlights the importance of corner exit speed (BENTLEY, 2011).

Therefore, gear selection depends upon the corner it is being negotiated and driver's technique. For this reason, gear chart presented in this work is meant to be merely a clue for testing shifting strategies at the circuit. In fact, drivers could have different gear shifting strategies without penalties on lap time.

6.3 Test data: Cristais Circuit – MG, Brazil.

Figure 6.4 provides reference points for the speed plot on Figure 6.5, discussed in the following section.

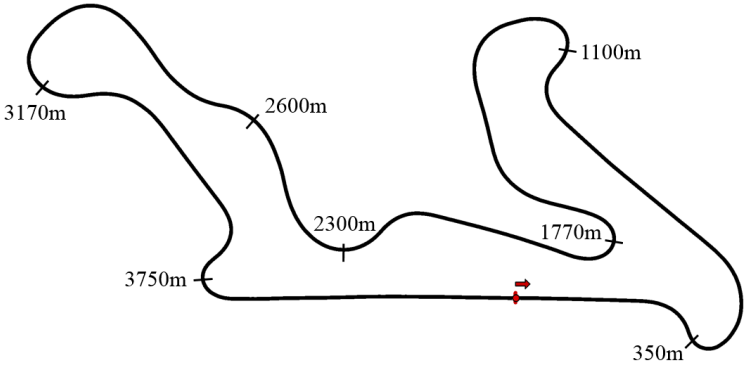

Figure 6.4: Reference points for Cristais Circuit – MG, Brazil.

For the sake of simplicity, not all corners are discussed in this section. Reference points for Cristais Circuit are composed by relevant low speed corner apexes (~80km/h).

At Cristais Circuit, simulated lap was 121.20 seconds long and the real lap time took 124.30 seconds, a difference of 2.6%. Figure 6.5 presents a comparison of simulated data with *test data* collected after the race event. Test data is a flying lap at the qualifying session at Cristais Circuit.

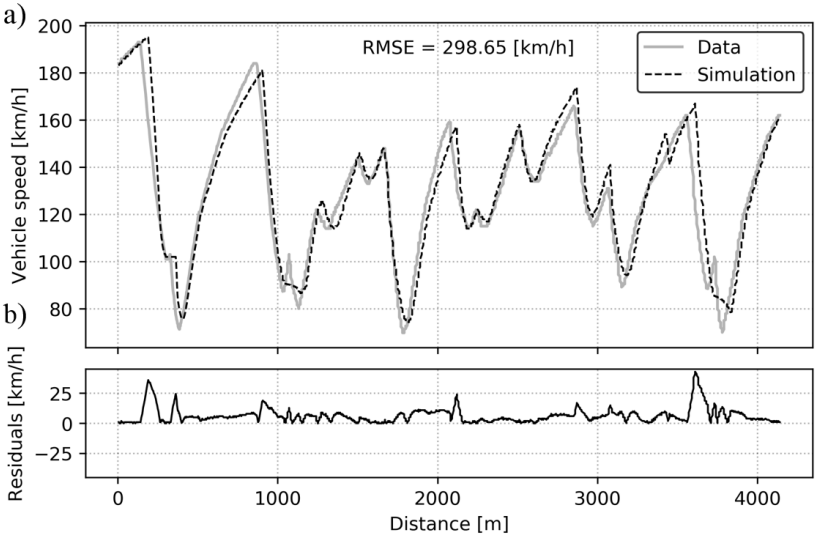

Figure 6.5: a) Speed profile comparison between experimental and simulated data. b) Residual values.

According to Figure 6.5, simulation follows the real speed profile of the circuit. Main characteristics such as cornering speeds and braking points were captured by the simulation. Main differences between datasets are observed on braking maneuvers and at the apex of slow corners (around 80km/h).

Alongside coefficient of friction, circuit parameterization was assigned as a source of errors, especially the rolling method of data treatment. According to the speed plot of Figure 6.5 (~1000m and ~3700m), designed curvature profile was incapable to capture correctly details of tight cornering sequences.

Because the tire/road coefficient of friction was estimated for the Ayrton Senna Circuit, differences were expected for Cristais Circuit in comparison with *test data.*

In fact, simulation overestimates the grip in almost all corners of Cristais Circuit (Figure 6.4 and Figure 6.5: 350m, 1100m, 1770m, 3170m and 3750m) and its preceding braking points.

In agreement, residual values in Figure 6.5 highlight data differences, from where deviance measures were calculated. Table 6.2 summarizes deviance measures of *test data* benchmarked by *training data*.

Table 6.2: Deviance measures for test and training data.

Deviance Measure	Unit	Training Data	Test Data	Difference [%]
MAE	[km/h]	3.69	6.34	+71.8
MSE	[km²/h²]	20251.23	89192.44	+340.4
RMSE	[km/h]	142.31	298.65	+109.9

At the time simulations were run, no previously logged data from Cristais Circuit was available to the racing team. Therefore, simulation accuracy criteria was not defined and deviance measures are presented aiming to incorporate reference values to the literature.

Lower accuracy was expected for *test data* in comparison with *training data* because model input parameters were not biased on the parameter estimation process. MAE was 71.8% higher than training data, MSE, 340.4% and RMSE, 109.9%.

From deviance measures, MSE is much more sensitive to data differences than MAE and RMSE, which could be a good indicator for small differences between datasets. On the other hand, the fact that MSE units are squared detracts the physical meaning of the measurement.

6.3.1 Gear shifting strategy

As stated before, gear chart gives an estimate on where the driver could possibly test a different shifting strategy, but does not arbitrary means that it improves lap time. At the race event, four gear-shifting strategies were tested. They were selected based on the driver's expertise while performing circuit recognition at the free practice sessions.

Figure 6.6 shows simulated gear shifting strategy in comparison to experimental data.

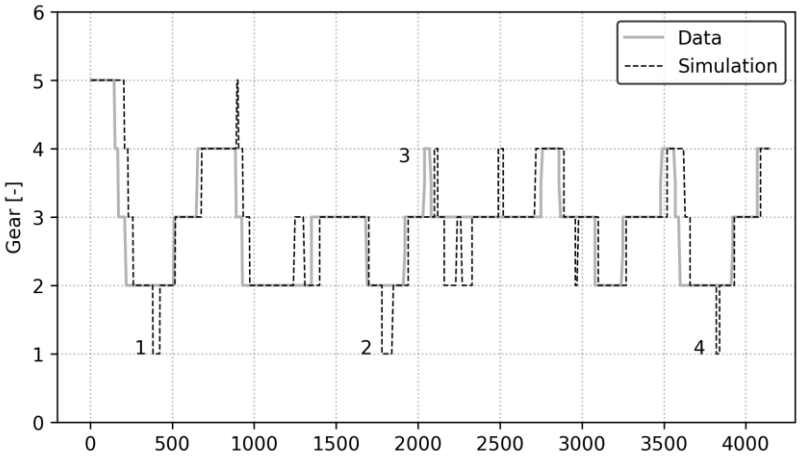

Figure 6.6: Comparison of gear shifting strategies. Logged data versus simulation.

In Figure 6.6, tests performed at the racetrack are marked by numbers 1 to 4.

Tests 1, 2 and 4 aimed to evaluate if the first gear would help on corner exit phase, where the vehicle is accelerating towards the straight. These tests did not improved lap time because the vehicle balance was negatively affected by the high gear ratio reduction.

Test 3 aimed to investigate if the engaged fourth gear would reduce lap time over the attempt to maintain the engine at the speed limiter before the corner entry. While engaging the fourth gear was 0.05 seconds quicker, laps keeping the third gear at the speed limiter were more consistent because drivers focused on the braking point without worrying about shifting to fourth gear.

Supported by subjective and objective evaluations, simulation results were presented and discussed in this chapter focused on the speed profile and gear shifting strategies.

The next chapter concludes this research. Previously chapters are briefly revisited and the main takeaways of this work is presented. Recommendations for future research are also addressed, followed by recommendations for novice data engineers.

7 CONCLUSIONS

As an object of study, modeling strategies were investigated aiming to simulate the speed profile of a new circuit. Because simulation accuracy is closely related to its input parameters, this research focused on vehicle parameters estimation with the help of a tool for stochastic simulations: the Monte Carlo method.

To this end, experimental data were acquired from a Toyota Corolla silhouette racecar, a front-wheel-drive competing at the Brazilian championship *Brasileiro de Marcas*. Data from two race events were used for this research: Ayrton Senna Circuit, a known racetrack in Goias state, and Cristais Circuit, a new racetrack in Minas Gerais state.

According to the literature, lap times comprise driver, vehicle, and racetrack performances. Each has its particular constraints including, but not limited to, driver's ability, vehicle setup, and racetrack conditions. In effect, overall performance is trimmed by which limit comes first: a talented driver, for example, cannot make a slow racecar goes faster (beyond the machine limit), neither achieve lap times of dry conditions while racing in the rain.

Conceptually, front-wheel-drive (FWD) racecars are slower than rear-wheel-drive configuration and are prone to understeer on throttle application, which is a stable condition. The FWD limit of performance is a tradeoff between the predictable behavior of an understeering vehicle with a front-weight biased setup, which improves traction but may suddenly oversteer on trail braking maneuvers. Thanks to the G-G diagram concept, lap time simulations presented in this work could reproduce the overall vehicle performance without the need of a complex vehicle model. It was possible because vehicle limits were lumped into a *performance envelope,* supported by experimental data.

Explaining further, maximizing performance is about exploring the tires limit of adhesion, often expressed by the vehicle friction circle. This concept lumps into a single diagram the grip available at the four tires in function of lateral and longitudinal accelerations. However, due to power limitations and tire load sensitivity, a real vehicle is incapable to use all the tire capability and reach the boundaries of the vehicle friction circle. Instead, the real interaction of driver, vehicle, and racetrack is better expressed by the vehicle performance envelope; the so-called G-G diagram, feasible to be measured with lateral and longitudinal acceleration signals.

From the literature, various types of lap time simulations were performed supported by the G-G diagram concept. From simple point-mass simulations to high degree-of-freedom, the more complex the vehicle model is, more detailed is the shape of the diagram and more vehicle parameters can be studied. To reduce computational costs, the diagram can be computed beforehand the simulations, used as a lookup table of the limit of adhesion in function of vehicle speed and curvature profile of the circuit, yet in this work the G-G the diagram was calculated online and the differences in terms of performance were not evaluated.

Lap time simulations fall into three categories: steady state, quasi-steady state and transient models. Outcomes of steady state models are only valid for steady state maneuvers. On the other hand, a circuit split into many steady state entities (quasi-steady state approach) can approximate a transient model with savings in computational cost.

In this work, quasi-steady state simulations were performed with the help of stochastic simulations aiming to parameterize the vehicle model. Combinations of input parameters were provided to a simple point-mass vehicle model by an Optimized Latin Hypercube Sampling algorithm. The set of inputs were evaluated by a cost function between simulations and logged data of the Brazilian circuit Ayrton Senna – GO.

The parameter estimation process was performed considering the impact of input parameters on simulation error. Coefficient of friction (u), driveline efficiency (η) and drag coefficient (C_d) accounted for more than 85% of effects on model error. Rolling resistance coefficients (μ_0, constant) and (μ_1, speed dependent) accounted for the other 15%.

For the Ayrton Senna Circuit, used as training data, drag coefficient was estimated about ($C_d \cong 0.40$), drivetrain efficiency ($\eta \cong 0.80$) and coefficient of friction of ($u \cong 1.20$). The parameters estimated were in accordance to the initial guesses taken from the literature, which suggests that for a simple model (e.g. point-mass vehicle model) typical values may suffice to simulate the speed profile of a racecar, although some error is certainly introduced to the simulations.

Parameterization of the circuit was performed with the help of a CAD environment, in which the racing line was drawn by a sequence of arcs of constant radius. For the Ayrton Senna Circuit – GO, the process was supported by GPS data acquired at the race event. As for the Cristais Circuit – MG, there was no logged data available and design of the racing line was supported by the expertise of two professional drivers.

Approximation of a quasi-steady state model is closely related to the number of sections a racing line is split. Joining small segments of a circuit provides smooth transitions between cornering maneuvers. For a new racetrack, CAD environment boosts the design of the racing line because drivers visually compare the line with the real circuit, which includes curbs and run-off areas. The drawback is that designing by straight lines and arcs of constant radius - instead of splines, provides coarse data points, which in this work were further processed by a rolling mean method to smooth raw data. However, errors were reported in the results section because the rolling mean method was not able to capture small cornering sequences. Parameterization of splines may be a better option aiming for accuracy.

This research also presented a case of study on how data is used by a small racing team to improve driver's performance. Flying laps of two professional drivers were compared at the Cristais Circuit – MG. Although different driving techniques were attempted by the drivers, lap time difference was within a tenth of a second.

In agreement with the literature, data analysis led to the conclusion that late apex technique is advantageous attempting a new circuit. During the learning process, the conservative approach of prioritizing corner exit instead of corner entry speed resulted in better sector times compared with the earlier apex approach.

Entry-level racing categories have limited time on track, which affects data analysis along the race event due to the short time available between free practices. To extract information quickly from data, this research used the so-called grip factor metrics, developed by Segers (2014), which condenses the G-G diagram into metrics using signal gating of lateral and longitudinal accelerations.

The concept of the G-G diagram elucidates why overlapping progressive steering and braking release towards the apex of a corner improves performance - trail braking. The magnitude of the sum of lateral and longitudinal acceleration vectors are greater compared with a single vector reaching the limit of grip.

Grip factors provided important insights to this research. Higher accelerations or higher grip factors does not necessarily imply better lap times. A driver could be overtightening a corner, resulting in higher lateral accelerations but higher rolling resistances acting against forward speed (i.e. tire scrub).

Results of lap time simulations were presented for Ayrton Senna and Cristais circuits. Speed profiles were overlaid with experimental data and evaluated by the RMSE deviance measure. Simulation error of

Ayrton Senna Circuit was expected to be lower in comparison to the Cristais Circuit because it was used as *training data* to estimate the parameters. Simulated lap time at Ayrton Senna circuit was 93.30 seconds, 0.16 seconds slower than the best lap time achieved during the race event. The RMSE was calculated in 142.3 km/h.

Cristais Circuit simulation was 0.10 seconds faster than the fastest lap time recorded. Compared with Ayrton Senna, RMSE increased 109.9%, which highlights that simulation error is underestimated whenever data is used to adjust parameters (i.e. training data).

Simulation of gear-shifting strategies with such simple model, on the other hand, indicates where there is engine speed margin to up or downshift, but does not point out if time is being gained or lost.

The aforementioned observations lead to the conclusions:

- Data analysis should consider the combination of vehicle, racetrack and driver performances. Tires and racetrack conditions changes constantly and the driver's confidence must be preserved, especially in challenging times such as competing in a new circuit;
- Late apex approach is advantageous on the learning process of the racing line;
- Grip Factor is valuable to extract information quickly from data, nevertheless should be used carefully as a performance indicator. Higher grip factors do not necessarily implies better lap times;
- Provided input parameters are reasonable, a point-mass vehicle model is capable to simulate the speed profile of a circuit;
- Deriving gear-shifting strategies from such simple model provides a clue whether the engine has speed margin to up or downshift but does not provide insights about time gained or lost;
- Estimating parameters with the help of stochastic simulations and data acquired at race events is capable to fine tune typical values from the literature for a specific racecar;
- If parameters were estimated with a given set of data (training data), simulation validation must be performed with a completely different set of data (test data), otherwise simulation accuracy is overestimated;

- Tire/road coefficient of friction, aerodynamic drag resistance and drivetrain efficiency account for about 85% of the effects on simulation error of a point-mass vehicle model.

7.1.1 Recommendations for future work

Along the years, few books about data analysis techniques have been written, among them, Segers (2014) has brought important knowledge from his experience from GT series and more recently DTM and Brazilian Stock Car. From a driver's perspective, Bentley (2011) presents an extensive guide of driving techniques, supported by years of experience as a driver himself and coaching drivers in many racing classes, including Indy Cars.

Literature about data analysis and driving techniques is extensive and currently up to date. On the other hand, *a methodology* for data analysis in motorsports is an important topic yet to be addressed, both to real and virtual race events. Driving simulators are playing a major part of driver's preparation, even in entry-level racing categories. Besides, a methodology to tackle data analysis in virtual racing environments is perhaps a more feasible alternative for future works.

Data analysis in motorsports is heavily supported by heuristic knowledge, and poorly documented in the literature. Tire mileage, racetrack condition and driver's feedback should always be considered by the data engineer. Trying to improve lap times with warn out tires or with an unconfident driver certainly becomes a frustrating experience.

Drivers are physical and mentally overloaded driving at the limit. Consequently, they have limited capacity to absorb information from data acquired right after test sessions. This work suggests some points to be considered in future researches:

- Data analysis should be objective and focused on the most important sources of time variance;
- Use of metrics possibly to attenuate data overload;
- Driving consistency should be tackled first. If a given corner is negotiated in a different manner every single lap, improvements are less likely to happen;
- Driver's activities: steering angle, throttle position, gear, brake pressure and vehicle speed, should be analyzed before other logged channels (regarding driver´s performance);
- A visual oriented analysis, such as onboard video comparisons, can help drivers to understand the improvements to be made.

In summary, concepts and techniques to improve driver performance exists and are well documented. How to use them effectively is the problem to be solved.

Another topic yet to be addressed deals with validation procedures for lap time simulations. Although visual comparison between simulation and experimental data is considered valid by many experts, the lack of tangible measures makes difficult to compare different methods. This work presented three deviance measures: mean absolute error (MAE), mean squared error (MSE), and root mean squared error (RMSE). Although RMSE is more sensitive to data outliers, there is no strong argument to use this deviance measure instead of the others. In fact, a robust metric could even have more than one deviance measure and it might include other types of evaluation such as dynamic time warping algorithms (DTW).

Finally, this work presented a method for estimating parameters using stochastic simulations. This method could be automated by the development of a software. Furthermore, provided output torque from a chassis dynamometer is available, it may be possible to estimate parameters solely from the data acquired at the racetrack. Using conservation of energy, external resistances can be calculated and fitted into a model. Future works could also compare different methods to estimate parameters. Drag coefficient, for example, estimated with the help of computational fluid dynamics (CFD), coast-down tests, and data from racetrack before mentioned.

REFERENCES

ANTONY, J. **Introduction to Industrial Experimentation**. In Design of Experiments for Engineers and Scientists. Elsevier, 2014.

BARROS, D. **Toyota Corolla.** Photograph. Available at: < http://www.brasileirodemarcas.com.br//>. Accessed in December, 2017.

BENTLEY, R. **Ultimate Speed Secrets: The complete guide to high-performance and race driving.** Motorbooks International, 2011.

BRAYSHAW, D. L.; HARRISON, M. F. **A quasi steady state approach to race car lap simulation in order to understand the effects of racing line and centre of gravity location.** Proceedings of the Institution of Mechanical Engineers, Part D: Journal of Automobile Engineering. v. 219, n. 6, p. 725–739, 2005.

BRAYSHAW, D. **The use of numerical optimisation to determine on-limit handling behaviour of race cars**. PhD Thesis, Cranfield University, UK, 2004.

CALLEA, G. **Race Car Tire Modeling: A Simplified Approach for Vehicle Dynamic Analysis and Real-Time Simulation**. SAE Technical Paper, n. 2004-01-3530, 2004.

CHAI, T.; DRAXLER, R. R. **Root mean square error (RMSE) or mean absolute error (MAE)?–Arguments against avoiding RMSE in the literature.** Geoscientific Model Development 7, no. 3: 1247-1250, 2014.

CHANGENET, C.; OVIEDO-MARLOT, X.; VELEX, **P. Power loss predictions in geared transmissions using thermal networks-applications to a six-speed manual gearbox**. Journal of Mechanical Design 128.3: 618-625, 2006.

CHENG, J.; DRUZDZEL, M. J. **Latin hypercube sampling in Bayesian networks.** In FLAIRS Conference, pp. 287-292. 2000.

COSWORTH. **Trace Engineering for Race Engineers.** Racecar Engineering. UK, v. 26, n. 8, p. 51-52, August, 2016.

COTTON, A. **Defense Mechanism**. Racecar Engineering. UK, v. 26, n. 5, p. 8-14, May, 2016.

FARRINGDON INSTRUMENTS. **Tachos.** Available at: < http://farringdoninstruments.com/tachos.html>. Accessed in December, 2017.

GÓMEZ, G.; NYBACKA, M.; BAKKER, E.; DRUGGE, L., **Findings from subjective evaluations and driver ratings of vehicle dynamics: steering and handling**. Vehicle System Dynamics: International Journal of Vehicle Mechanics and Mobility, 2015.

HARRISON, R. **Introduction to Monte Carlo Simulation.** AIP conference proceedings. Vol. 1204. No. 1. AIP, 2010.

IRIMESCU, A., MIHON, L., & PĂDURE, G. **Automotive transmission efficiency measurement using a chassis dynamometer.** International Journal of Automotive Technology, 2011.

JACHNER, S.; BOOGAART, K., G. **Statistical Methods for the Qualitative Assessment of Dynamic Models with Time Delay**. Journal of Statistical Software. v. 22, no. 8, 2007.

JAZAR, R.; N. **Vehicle Dynamics: Theory and Applications**. Springer US, Inc. 2008

KATZ, J. **Racecar Aerodynamics.** Cambridge. MA: Bentley, 1995.

KUTLUAY, E.; WINNER, H. **Validation of vehicle dynamics simulation models - a review.** Vehicle System Dynamics, v. 52, n. 2, p. 186–200, 2014.

LOT, R.; DAL BIANCO, N. **Lap time optimisation of a racing go-kart.** Vehicle System Dynamics. v. 3114, n. January, p. 1–21, 2015.

MAGGIO, F.; BIRAL, F.; LIO, M. DA. **How Gearbox Ratios Influence Lap Time and Driving Style. An Analysis Based on Time-Optimal Maneuvers.** SAE Technical Paper, n. 2003-32-0056, 2003.

MCBEATH, S. **Subaru touring car aerodynamic study**. Racecar Engineering. UK, v. 26, n. 5, p. 57-58, Sept, 2016.

MCBEATH, S. **Tale of the tape**. Racecar Engineering. UK, v. 23, n. 5, p. 45-46, May, 2013.

MCKAY, M. D.; BECKMAN, R. J.; CONOVER, W. J. **Comparison of three methods for selecting values of input variables in the analysis of output from a computer code**. Technometrics, v. 21(2), p. 239-245, 1979

MILLIKEN, W. F.; MILLIKEN, D. L. **Race car vehicle dynamics**. Warrendale, Society of Automotive Engineers, 1995.

MITCHELL, W. C.; SCHROER, R.; GRISEZ, D. B. **Driving the Traction Circle.** SAE Technical Paper, n. 2004-01-3545, 2004.

MITCHELL, W. C.; SCHROER, R.; GRISEZ, D. B. **Training Test Drivers with Data Acquisition.** SAE Technical Paper, n. 2000-01–3568, 2000.

NOWLAN, D. **L'Ouest inquest.** Racecar Engineering. UK, v. 25, n. 10, p. 62-25, October, 2015.

NOWLAN, D. **Simulate to Create.** Racecar Engineering. UK, v. 26, n. 1, p. 69-71, January, 2015.

OPTIMUMG. **Aerodynamics Analysis**. Technical Paper, 20XX. Available at: http://www.optimumg.com/docs/Aero_BertaReport.pdf . Accessed in May, 2017.

OPTIMUMG. **OptimumLap.** Available at: < http://www.optimumg.com/software/optimumlap/>. Accessed in December, 2017.

ORTIZ, M. **Can a front wheel drive compete at Le Mans?** Racecar Engineering. UK, v. 25, n. 7, p. 24-25, July, 2015.

PARKER, M. C.; HARGRAVE, G. K. **The development of a visualization tool for acquired motorsport data**. Proceedings of the Institution of Mechanical Engineers, Part P: Journal of Sports Engineering and Technology, v. 230, n. 4, p. 225–235, 2016.

PERDOMO, R. **Data acquisition in Brazilian motorsport classes.** Personal communication, Sao Paulo, 2017.

PRONZATO, L.; WALTER, E. **Identification of parametric models from experimental data.** Springer, Berlin, 1997.

RAYCHAUDHURI, S. I**ntroduction to Monte Carlo Simulation.** In Simulation Conference, 2008. WSC 2008. Winter, pp. 91-100. IEEE, 2008.

ROUELLE, C., **Applied Vehicle Dynamics Seminar.** OptimumG, Denver, USA. 3-day seminar at Cologne University of Applied Sciences. Cologne, Germany. Nov 10-12, 2014.

SAGLAM, F.; UNLUSOY, Y. S. **Identification of low order vehicle handling models from multibody vehicle dynamics models.** IEEE International Conference on Mechatronics, ICM 2011 - Proceedings, p. 96–101, 2011.

SARIN, H.; KOKKOLARAS, M.; HULBERT, G.; PAPALAMBROS, P.; BARBAT, S; YANG, R. **Comparing time histories for validation of simulation models: error measures and metrics.** Journal of dynamic systems, measurement, and control. v. 132, no. 6, 2010.

SAYERS, M. **Standard terminology for vehicle dynamics simulations.** The University of Michigan Transportation Research Institute (UMTRI), Technical Report. Feb, 1996.

SEGERS, J. **Analysis techniques for racecar data acquisition**. Warrendale, PA: SAE International, 2014.

SIEGLER, B.; DEAKIN, A.; & CROLLA, D. **Lap Time Simulation : Comparison of Steady State , Quasi- Static and Transient Racing Car Cornering Strategies.** Proceedings of the 2000 SAE Motorsports Engineering Conference & Exposition, 2000.

SIEGLER, B.; DEAKIN, A.; CROLLA, D. **Lap Time Simulation: Comparison of Steady State , Quasi- Static and Transient Racing Car Cornering Strategies.** Proceedings of the 2000 SAE Motorsports Engineering Conference & Exposition. v. 1, n. 724, 2000.

SILVA, J.C. **Virtual Environment for Dynamic Modelling of Multi-Domain Systems.** Proceedings of the 18th COBEM, 2005.

SIMON, B.; VITTORE, C.; MATTEO, M.; MARTINO, P. **Application of the "Optimal Maneuver Method" for Enhancing Racing Motorcycle Performance.** SAE International Journal of Passenger Cars Electronic and Electrical Systems. v. 1, n. 1, p. 1311–1318, 2008

SMITH, C. **Drive to Win**. Warrendale, PA: SAE International, 1996.

SOLONEN, A. M. **Monte Carlo Methods in Parameter Estimation of Nonlinear Models**. Master's thesis, Lappeenranta University Of Technology, 2006.

TRAUB, L.; BUTAKOV, V.; SIMPSON, R. **Parameter identification for a multi-body vehicle model.** IEEE Intelligent Vehicles Symposium, Proceedings, v. 2016–Aug, n. IV, p. 521–526, 2016.

VADDI, P. K.; KUMAR, C. S. **A non-linear vehicle dynamics model for accurate representation of suspension kinematics.** Proceedings of the Institution of Mechanical Engineers, Part C: Journal of Mechanical Engineering Science, v. 229, n. 6, p. 1002–1014, 2015.

VADURI, S.; LAW, E. H. **Development of an Expert System for the Analysis of Track Test Data.** SAE Technical Paper, n. 2000-01-1628, 2000.

VELENIS, E.; TSIOTRAS, P. **Optimal velocity profile generation for given acceleration limits; the half-car model case.** IEEE International Symposium on Industrial Electronics. v. I, p. 361–366, 2005.

VIANA, F. A. C. **Things you wanted to know about the Latin hypercube design and were afraid to ask**. 10th World Congress on Structural and Multidisciplinary Optimization, p. 1-9, 2013.

VIANA, F. A. C.; VENTER, G.; BALABANOV, V. **An algorithm for fast generation of optimal Latin hypercube designs.** International Journal for Numerical Methods in Engineering, Vol. 82, pp. 135-156, 2010

VÖLKL, T.; MUEHLMEIER, M.; WINNER, H. **Extended Steady State Lap Time Simulation for Analyzing Transient Vehicle Behavior**. SAE Technical Paper, n. 2013-01-0806, 2013.

WITTEN, I. H.; EIBE F. & MARK A. H. **Data Mining: Practical Machine Learning Tools and Techniques**, 2011.

YANG, S.; LU, Y.; LI, S. **An overview on vehicle dynamics.** International Journal of Dynamics and Control, v. 1, n. 4, p. 385–395, 2013.

ZHANG, Y.; WANG, L.; ZHANG, B.; ZHANG, N. **Vehicle Parameter Estimation Based on Full-Car Dynamic Testing.** SAE International Journal of Passenger Cars - Mechanical Systems, v. 8, n. 2, p. 2015-01–0636, 2015.

APPENDIX A

SECTOR 2

G-G diagram and GPS plot are presented in Figure A.1. Sector 2 is composed by corners 4, 5 and 6. Corners 4 and 5 are low-speed corners linked the medium-speed corner 6.

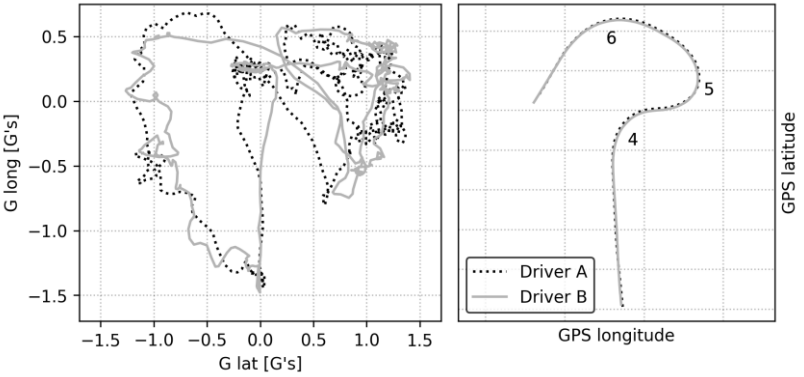

Figure A.1: G-G diagram and racing line of drivers A and B at sector 2.

From the G-G diagram, drivers explores the performance envelope in a similar manner, except for the exit phase of corner 4, and for the transition from corner 4 to 5. At corner 4, Driver A has better acceleration (higher G longitudinal values on the upper left part of the diagram). However, from corner 4 to 5, Driver B further explores the vehicle performance in comparison to Driver A (data points are closer to the boundary of the diagram than those of Driver A).

Figure A.2 presents a) the time variance and b) vehicle speed in sector 2.

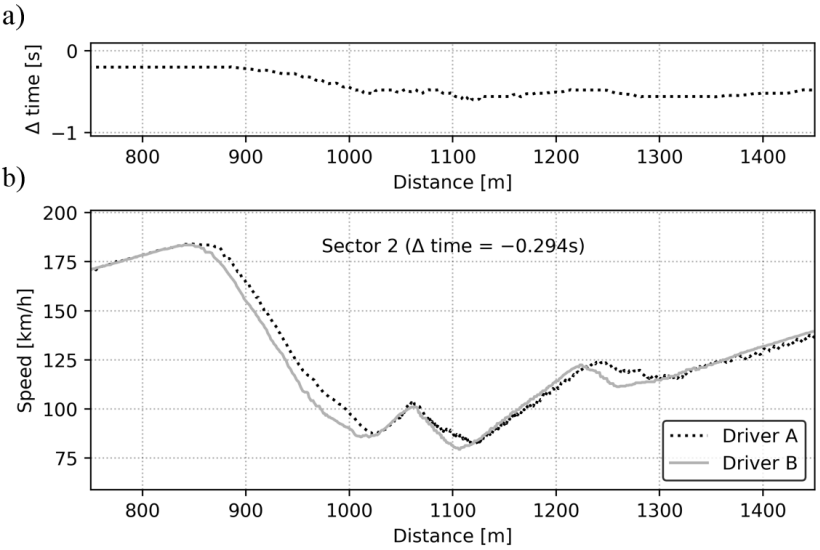

Figure A.2: Data comparison of a qualifying lap of two professional drivers in Sector 2. a) time variance - Δ time, b) vehicle speed. Driver A is 0.294s faster than Driver B.

According to the time variance (Figure A.2-a), Driver A is 0.294s faster than Driver B in sector 2. Driver B lost time mainly on the braking phase of corner 4, from ~840 m to ~1020 m, which is also indicated by the vehicle speed (Figure A.2-b).

G longitudinal data of sector 2 is presented in Figure A.3.

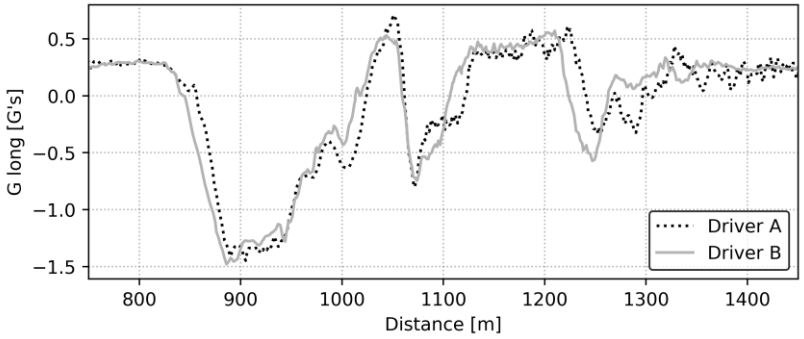

Figure A.3: Longitudinal acceleration data of sector 2.

From the G longitudinal data, Driver B starts the pure braking phase of corner 4 at ~840 m; 20 m before Driver B. The inclination of the longitudinal acceleration curve also reveals Driver B also brakes with less intensity.

Lateral acceleration data is presented in Figure A.4.

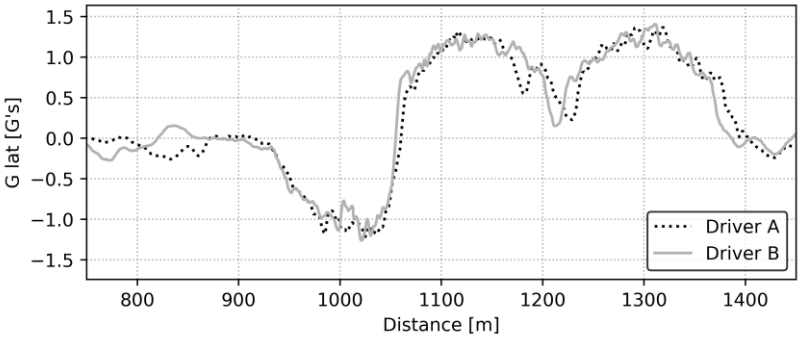

Figure A.4: Lateral acceleration data of sector 2.

Despite both drivers are negotiating corners 4, 5 and 6 at about the same magnitude of lateral acceleration, driver B has lower speed along the braking and trail braking phases, which indicates that Driver B takes a tighter racing line compared with Driver A. In fact, Driver B had tighten his racing line to take the inside portion of the racetrack with the aim to prepare the late apex at corner 5 (GPS plot of Figure A.1)

The late apex approach improves lap time when the following straight is long enough to trade off the time lost preparing corner exit at the braking and trail braking phases (SMITH, 1996; BENTLEY, 2011; SEGERS, 2014).

Despite the better acceleration indicated in the G long plot at ~1100 m (Figure A.3), and the earlier acceleration indicated by the throttle position in Figure A.5, the late apex taken by Driver B at corner 5 did not improved lap time because the following straight was too short to recover the time lost at the braking phase.

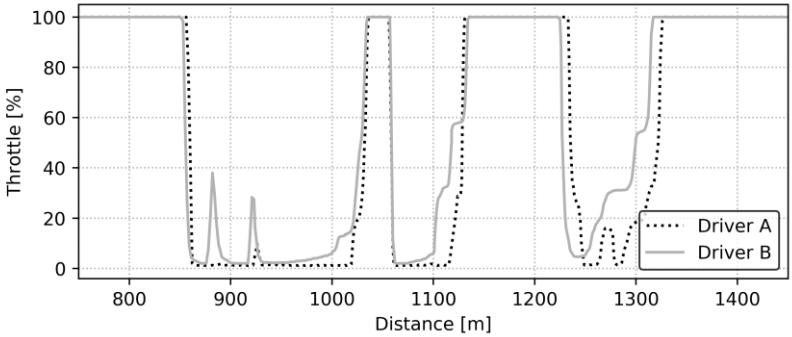

Figure A.5: Throttle position data of sector 2.

In the same way, at corner 6 (~1230 m) Driver B prepares the exit phase while Driver A trail brakes to achieve higher cornering speed. Again, because the following straight is too short, Driver A was faster.

Gear chart of sector 2 is presented in Figure A.6.

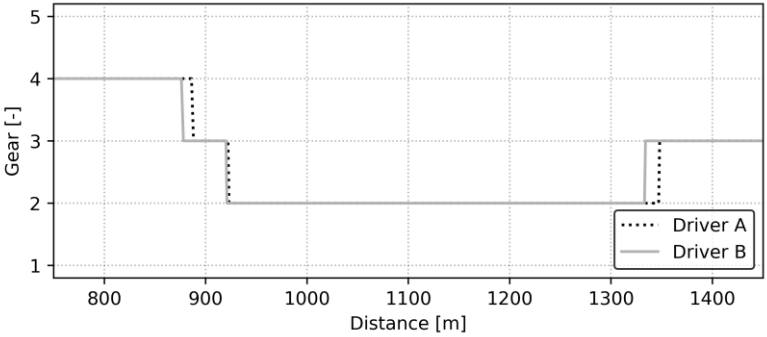

Figure A.6: Gear chart of sector 2.

According to this figure, although different approaches were taken to negotiate the corners of sector 2, similar gear shifting strategy was adopted by the drivers.

Figure A.6 presents metrics of sector 2.

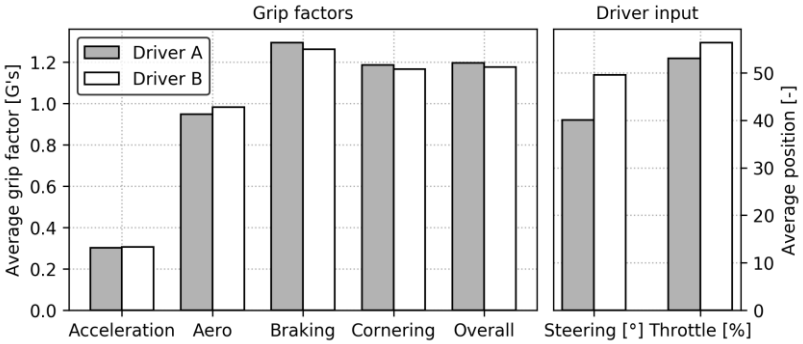

Figure A.7: Metrics of sector 2.

Driver A has consistently slightly higher grip factors except for the aero grip factor. From the right plot of the figure, Driver B uses 25% more steering angle and 5% more throttle.

SECTOR 3

G-G diagram and GPS plot are presented in Figure A.8. This sector is composed by two corners. Corner 7 is a medium-speed corner linked to corner 8, which is a low-speed corner followed by a short straight upon sector 4.

Corner 7 is on the right side of the G-G diagram. At this corner, Driver A trail brakes more at the entry phase while Driver B trail brakes more exiting the corner. Both driver reach similar lateral acceleration to negotiate the corner.

At the braking phase of corner 8, on the left side of the diagram, Driver B corrects the racing line to take the inside part of the racetrack, G lateral is then developed along what would be a pure braking phase (seen on the diagram as a vertical trace at ~ -0.5 G lateral). As a result, Driver B cannot reach maximum G longitudinal because part of the tires adhesion is being used for cornering. Overall, at corner 8 Driver A develops larger boundaries of the performance envelope than Driver B does.

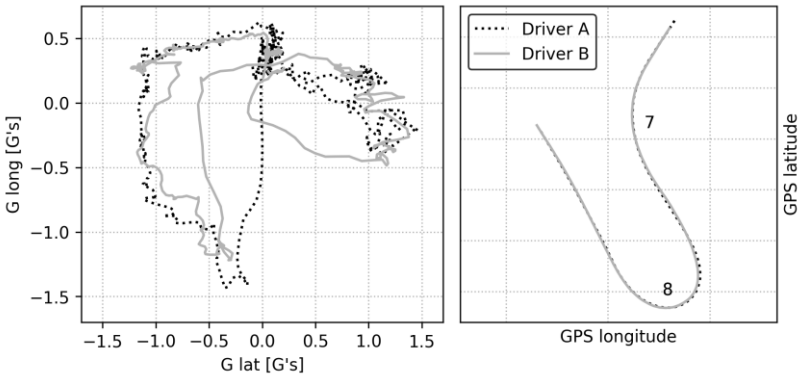

Figure A.8: G-G diagram and GPS coordinates of drivers A and B racing line.

Figure A.9 presents a) time variance and b) vehicle speed data of sector 3.

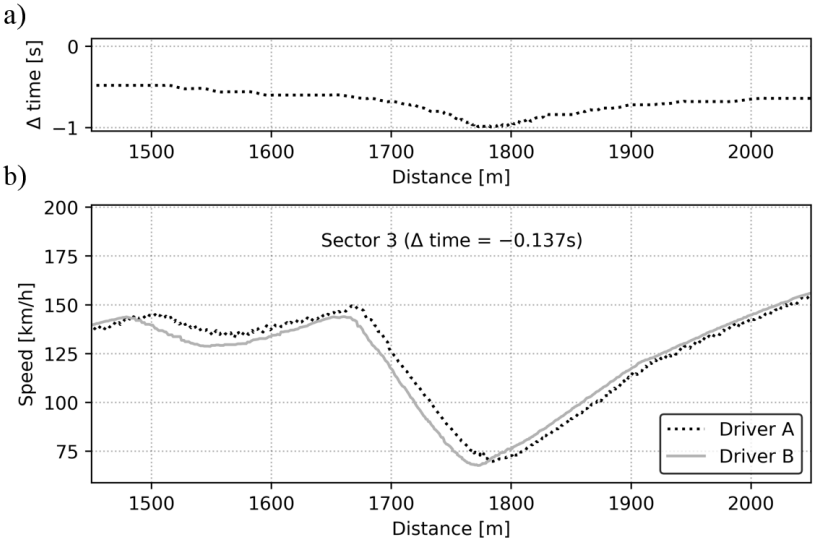

Figure A.9: Data comparison of a qualifying lap of two professional drivers in Sector 3. a) time variance - Δ time, b) vehicle speed. Driver A is 0.137s faster than Driver B.

According to the time variance (Figure A.9-a), Driver B loses time on both braking zones (~1470 m and ~ 1650 m). As a result, Driver

A is 0.137 seconds faster than Driver B in sector 3. The speed differences shown in Figure A.9-b also announces that different strategies were used to negotiate corners 7 and 6.

Longitudinal acceleration and lateral acceleration data are presented in Figure A.10 and Figure A.11 respectively.

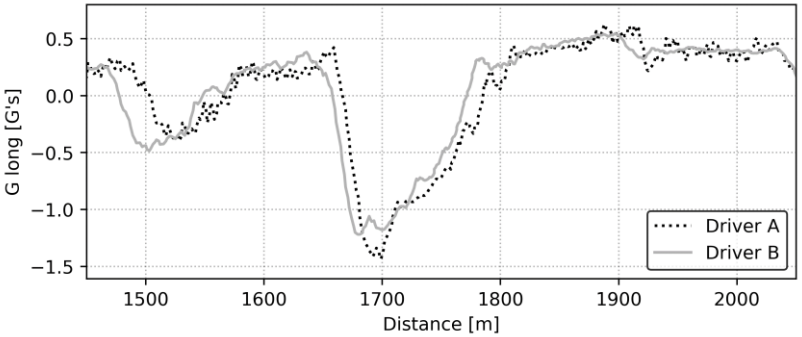

Figure A.10: Longitudinal acceleration data of sector 3.

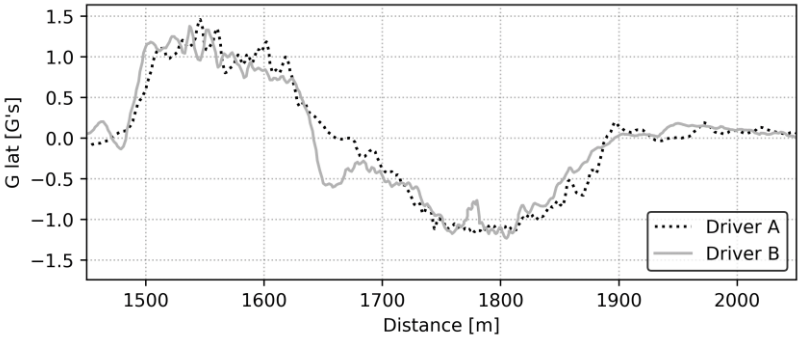

Figure A.11: Lateral acceleration data of sector 3.

According to the longitudinal acceleration data (Figure A.10), at corner 7 Driver B brakes at ~1470 m; 30 m before Driver A. At the same corner, lateral acceleration of both drivers are close in magnitude (Figure A.11), but Driver's B speed is 8.5 km/h lower at the apex (~1550 m). This indicates Driver B had tighten his racing line. In fact, throttle position shows a tentative to reaccelerate the vehicle earlier than Driver A does (~1550 m). However, tires were at the limit of adhesion resulting in power understeer. In response, Driver B backs off throttle right after in order to balance the vehicle at ~1560 m (Figure A.12).

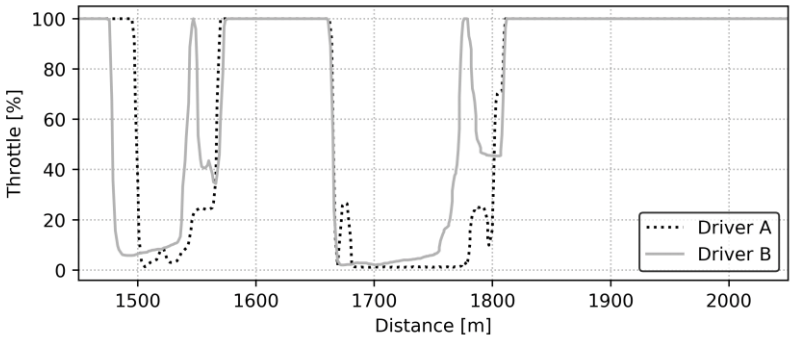

Figure A.12: Throttle position data of sector 3.

At corner 8, drivers chose different racing line approaches. Driver A takes a geometric line while Driver B takes a late apex. Because the following straight is 300 m long - ending at sector 4, time lost by Driver B at the braking phase is recovered along the straightaway.

Gear chart of sector 3 is shown in Figure A.13.

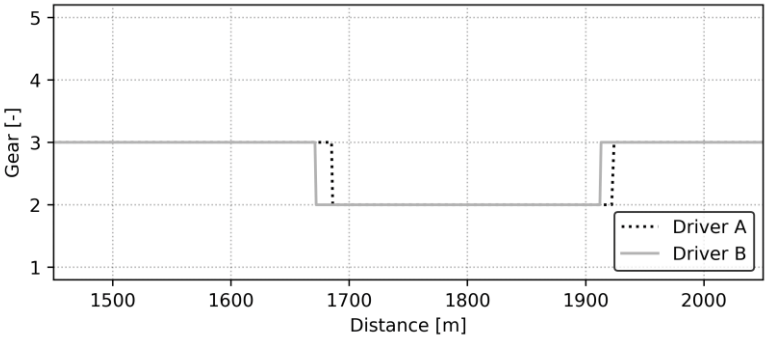

Figure A.13: Gear chart of sector 3.

From the gear chart above, similar gear shifting strategy was adopted again by both drivers.

Figure A.14 presents the metrics of sector 3. Except for the braking grip factor, which is 20% higher for Driver A, grip factors are close for both drivers.

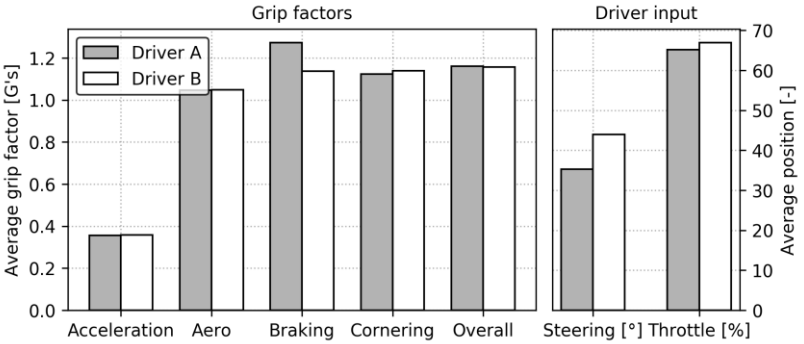

Figure A.14: Metrics of sector 3.

From the right side of the figure, the late apex approach of Driver B at corner 8 appears as a slight higher average throttle position. Driver B also uses 26% more steering angle, which is in accordance to the previously finding that a tighter racing line was taken.

SECTOR 4

Figure A.15 presents the G-G diagram and the GPS plot of sector 4, which encloses three medium-speed corners. Corners 9 and 10 form an "S" cornering sequence. Corner 11 is connected to corner 12 in sector 5.

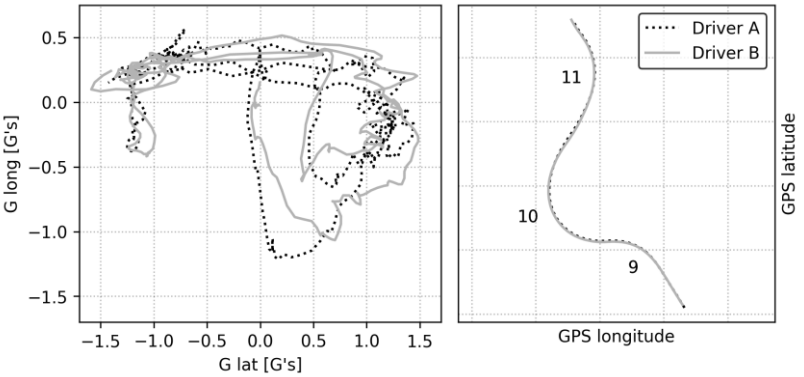

Figure A.15: G-G diagram and GPS coordinates of drivers A and B racing line.

In the G-G diagram, the left-hand corners 9 and 11 are on the right side of the plot. At corner 9, Driver B brakes with less intensity and turns in earlier than Driver A, who has a longer pure braking phase (seen on the diagram at ~0 G lateral). Except for the pure braking phase, where Driver A brakes with more intensity, Driver B has a larger performance envelope.

Figure A.16 presents a) time variance and b) vehicle speed data of sector 4.

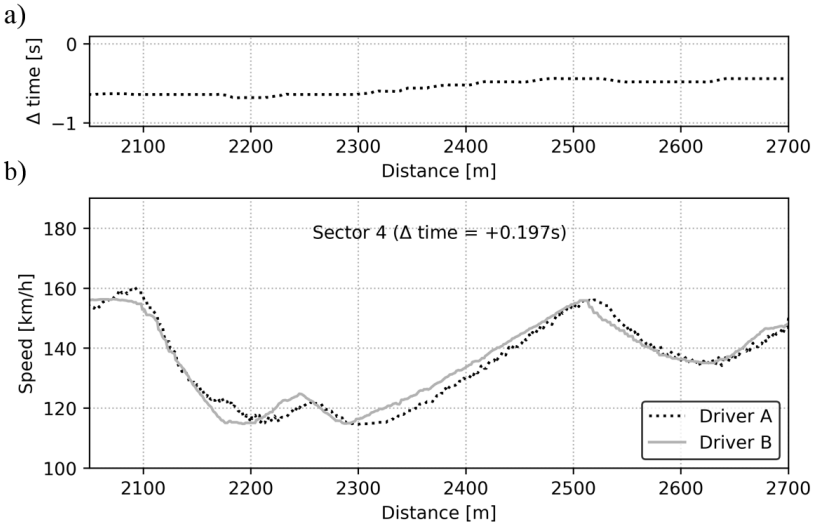

Figure A.16: Data comparison of a qualifying lap of two professional drivers in Sector 4. a) time variance - Δ time, b) vehicle speed. Driver A is 0.197s slower than Driver B.

According to the time variance in Figure A.16-a, Driver B is 0.197s faster than Driver A. Combined to the speed data in Figure A.16-b, time variance progressively increases from ~ 2300 m due the late apex approach of Driver B at corner 10.

The late apex was only possible because, at corner 9, slightly different racing lines were taken. Driver B takes the inside line of the racetrack to position the car for corner 10. Despite the time lost during the trail braking phase, throttle position data in Figure A.17, Driver B reaccelerates the car at ~2170 m; earlier than Driver A. Both approaches resulted in the same time spent to negotiate corner 9 (Figure A.16-a).

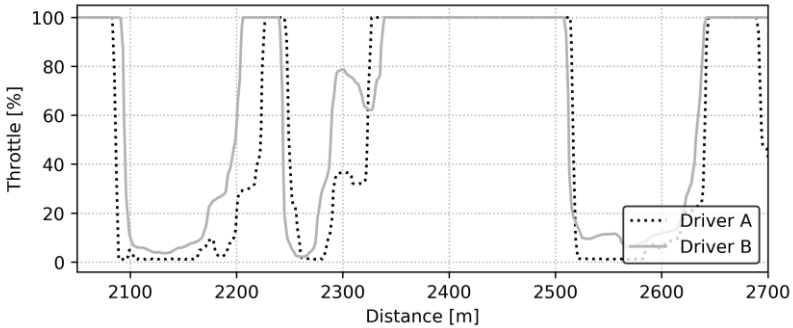

Figure A.17: Throttle position data of sector 4.

Although the time difference at corner 9 was negligible considering the different approaches taken, the late apex taken by Driver B in corner 10 was the primary cause of the time gain at sector 4. At corner 11, Driver B also takes a late apex. However, there was no time difference in comparison to the geometric line taken by Driver A.

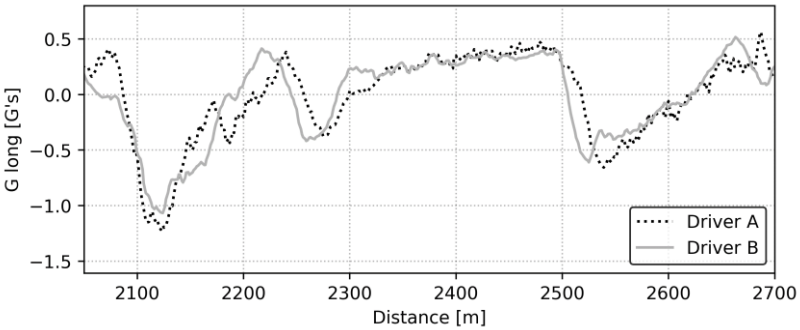

Figure A.18: Longitudinal acceleration data of sector 4.

From the longitudinal acceleration data in Figure A.18, at ~2280 m Driver B has higher acceleration along the corner exit. This approach was advantageous because the speed difference was carried all the way through the straight.

Gear shifting strategy is illustrated by the gear chart in Figure A.19.

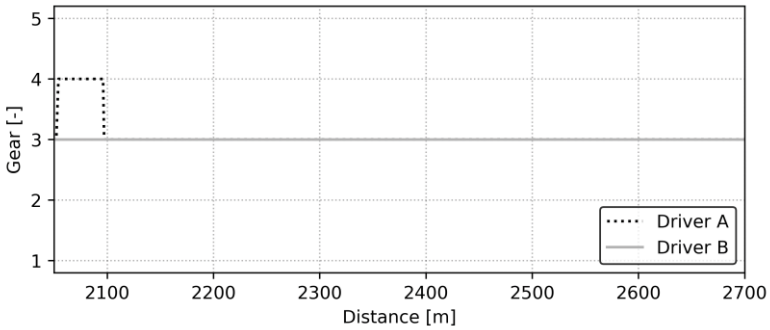

Figure A.19: Gear chart of sector 4.

Approaching corner 9, different gear shifting strategies were adopted. Driver B keeps the engine speed at the limiter while Driver A up shifts to fourth gear (~2050 m), which is about 0.05 seconds faster.

Metrics of sector 4 are shown in Figure A.20. Driver A has 20% higher aerodynamic grip factor and 10% higher braking grip, although cornering and overall grip factors are slightly lower in comparison to Driver B.

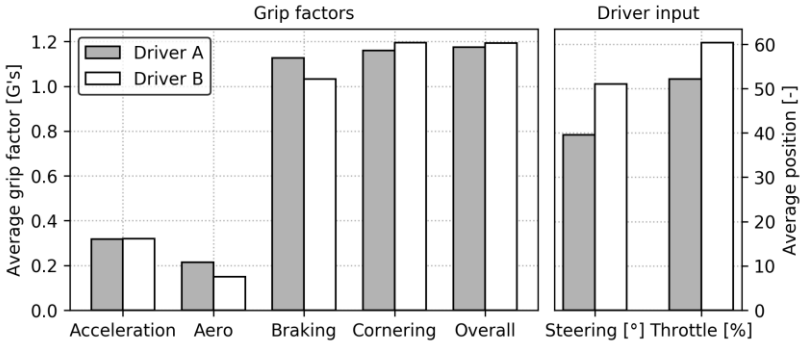

Figure A.20: Metrics of sector 4.

Metrics of drivers input reveals that the late apex approach of Driver B at sector 4 has risen average throttle position in about 17%. Driver B had 30% higher steering angle on average.

SECTOR 5

According to the GPS plot of Figure A.21 and the speed plot of Figure A.22, sector 5 is a sequence of mid and low-speed corners. Again, Drivers A and B takes distinct approaches to negotiate the corners.

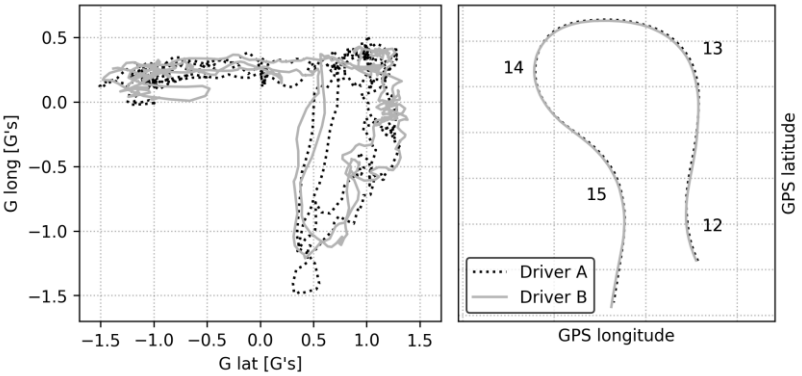

Figure A.21: G-G diagram and GPS coordinates of drivers A and B racing line.

From the G-G diagram of Figure 7.14, boundaries of the performance envelope of drivers A and B are close except for the higher negative G longitudinal of Driver A (bottom part of the diagram).

Data acquired at sector 5 is presented in Figure A.22: a) presents the time variance and b) the vehicle speed. In this sector, Driver B is 0.210 seconds faster than Driver A.

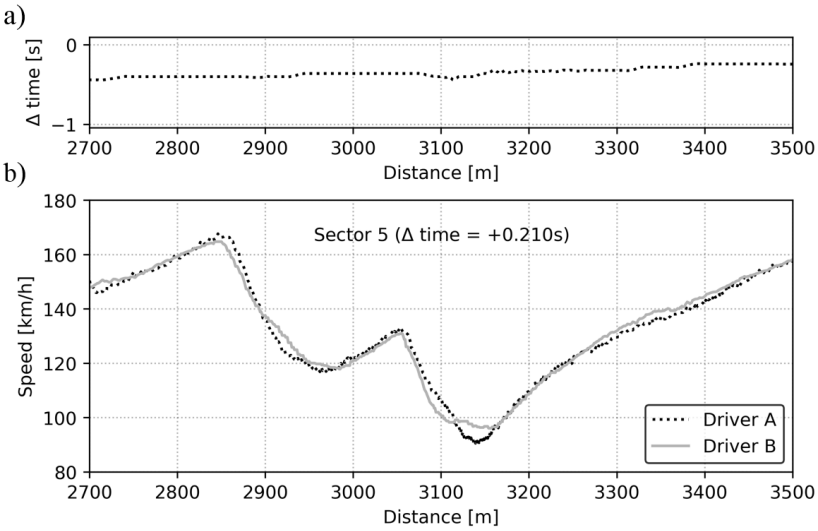

Figure A.22: Data comparison of a qualifying lap of two professional drivers in Sector 5. a) time variance - Δ time, b) vehicle speed. Driver A is 0.210 seconds slower than Driver B.

Throttle position data and the gear chart are presented in Figure A.23 and Figure A.24 respectively.

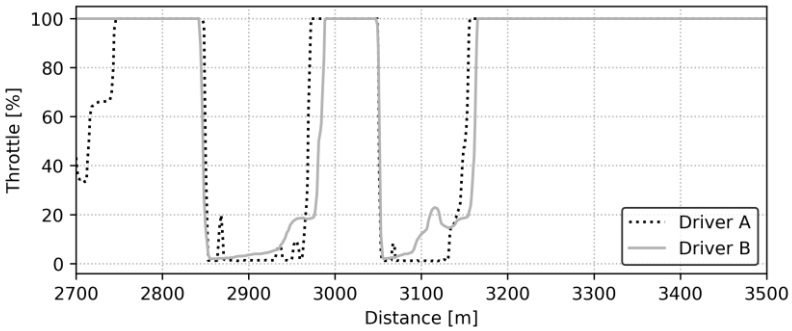

Figure A.23: Throttle position data of sector 5.

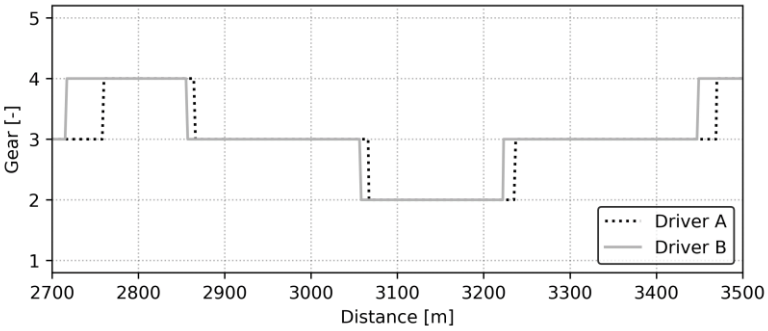

Figure A.24: Gear chart of sector 5.

At ~2700 m, Driver A negotiates corner 12 with part throttle application (Figure A.23). Driver B carries more cornering speed at WOT but anticipate upshifting to fourth gear to avoid understeering at the corner exit phase (Figure A.24).

From G lateral plot (Figure A.1), Driver B achieves higher G lateral ~2800 m to take an early apex at corner 13.

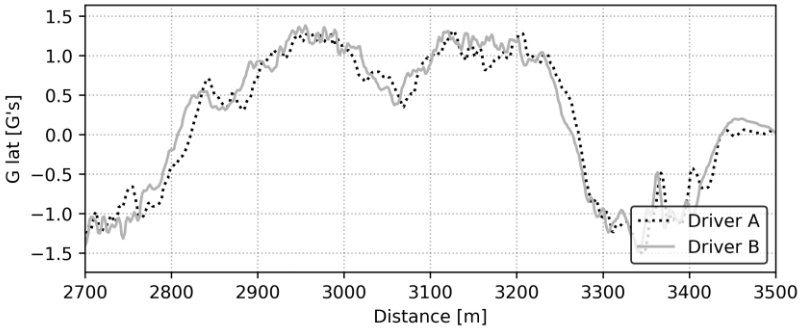

Figure A.1: Lateral acceleration data of sector 5.

From the longitudinal acceleration data (Figure A.1), from ~1850 m to ~2950 m, Driver A takes a geometric line, brakes with more intensity and in a shorter distance than Driver B, who trail brakes into the corner. Driver A is back at WOT before Driver B (~2960 m), however the link between corners 13 and 14 is not long enough to recover the time lost during the braking phase.

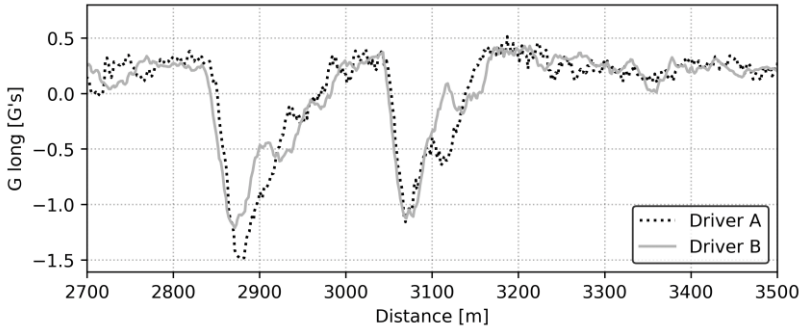

Figure A.1: Longitudinal acceleration data of sector 5.

At the low speed corner 14, both drivers brake with about the same intensity (seen in the G longitudinal plot at ~3070 m), however, driver A brakes for a longer distance while Driver B trail brakes into the corner (~3050 m to ~3150 m). Although Driver A is at WOT 10 m before, Driver B is at part throttle 50 m before and has higher momentum at corner exit.

Metrics of sector 5 are presented in Figure A.2. Driver A has 35% aerodynamic grip and 10% more braking grip. Overall grip factor is similar to both drivers.

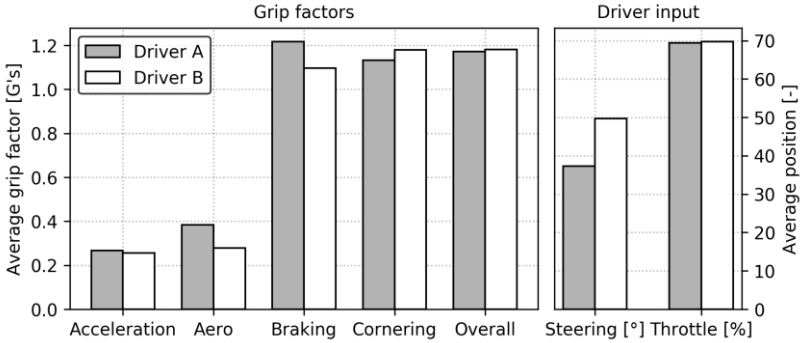

Figure A.2: Metrics of sector 5.

From the right side of the plot, although driver A accelerates earlier than Driver B at the exit phase of corners 13 and 14, average throttle position is similar because Driver B negotiates corner 12 at WOT.